Master's thesis

NTNU
Norwegian University of Science and Technology
Faculty of Engineering
Department of Energy and Process Engineering

Fredrik Schmidt

Large scale heat storage for district heating

Master's thesis in Mechanical Engineering
Supervisor: Erling Næss and Henrik Holmberg
June 2020

NTNU
Norwegian University of
Science and Technology

Fredrik Schmidt

Large scale heat storage for district heating

Master's thesis in Mechanical Engineering
Supervisor: Erling Næss and Henrik Holmberg
June 2020

Norwegian University of Science and Technology
Faculty of Engineering
Department of Energy and Process Engineering

NTNU
Norwegian University of
Science and Technology

NTNU | Norwegian University of Science and Technology

Master's Agreement – Problem Description

LARGE SCALE HEAT STORAGE FOR DISTRICT HEATING

Description

In industries with close to constant heat production throughout the year, but with large seasonal variations in demands, large amounts of excess heat are produced and lost. Storing the excess heat will increase the efficiency of the heat production, by utilizing the stored heat in high demand periods. Consequently, harmful emissions will be reduced, as will also the need for fossil fueled boilers for peak handling.

A borehole thermal energy storage utilizes the ground as a heat storage medium and can store large amounts of excess heat. Depending on the temperature of the excess heat supply, high temperatures (above ca 70^{o}C) can be achieved in the storage. This makes a high temperature borehole thermal energy storage (HT-BTES) an excellent candidate for seasonal storage of industrial waste heat. Particularly in district heating applications.

Goal

The goal of this master thesis is to gather knowledge regarding the potential of HT-BTES solutions and the thermal process in high temperature boreholes, and to use this knowledge to design and evaluate one or more HT-BTES system solutions.

The task will be solved through the following points:

1. Gather and present a summary of available information concerning existing HT-BTES, and collect and present key information on the potential of using HT-BTES for utilizing surplus heat from waste-to-energy plants in district heating applications.
2. Perform a thermal analysis of high temperature boreholes, evaluating their behavior during variations in heat injection and extraction. The methodology and the calculation results shall be presented and discussed.
3. A case analysis on one or more of the potential locations presented in Task 1 shall be performed. A HT-BTES will be the storage solution and the analysis will include an evaluation of different designs and operational strategies. Key parameters such as storage capacity, temperature development, heat loss and heat pump performance shall be defined and calculated.
4. Suggestions for further work shall be discussed.

Preface

This master thesis is written in the spring of 2020 for the Department of Energy and Process Engineering at the Norwegian University of Science and Technology (NTNU). The master thesis makes out 30 study points and is a continuation of the project report *Large scale heat storage* written during the autumn of 2019.

I would like to thank my supervisor Erling Næss and co-supervisor Henrik Holmberg for assisting and counseling me throughout this semester. They have given me motivation throughout my work and contributed with valuable input and informative discussions. I would also like to thank Randi Kalskin Ramstad for attending numerous counseling meetings. Lastly, I would like to thank the district heating companies who took interest and freely contributed with valuable data and information used in this master thesis.

Fredrik Schmidt
Trondheim, 10.06.2020

Abstract

This master thesis aims to gather knowledge on the potential of HT-BTES systems, the thermal process in HT-boreholes and apply this knowledge in a HT-BTES case analysis. The case analysis evaluated three different HT-BTES designs and a conceptual operational strategy (nightboosting). A HT-BTES system is an excellent seasonal storage system for industrial waste heat that both increases the energy efficiency of heat production and helps meet future energy demand.

The design of the three HT-BTES cases is based on information gathered from existing projects and a feasibility study targeting the waste-to-energy district heating sector in Norway. This resulted in the three cases having a storage capacity of 7.5 GWh, 60 GWh and 125 GWh, respectively. The load cycles for each HT-BTES case are based on monthly data acquired in the feasibility study.

Results in the thermal analysis showed that nightboosting caused a significant increase in the temperature of the heat carrier fluid. The MATLAB model used in the thermal analysis accounted for the borehole thermal capacity and was therefore used to calibrate a pre-pipe component in TRNSYS. The pre-pipe component accounts for the borehole thermal capacity and consequently improves short-time transient modeling in TRNSYS. Most accurate results were achieved by accounting for 50% of the total borehole thermal capacity in the TRNSYS-model.

The case analysis showed that increasing storage capacity affected the maximum average storage temperature. The maximum average temperatures were 85°C, 82.5°C and 75°C for case 1,2 and 3, respectively. With nightboosting operating with a charging rate of 60 W/m the temperature difference between the maximum and minimum average storage temperatures was decreased by 43.4%, 28.3%, and 24.9% for cases 1,2 and 3. A sensitivity analysis of case 2 evaluated four HT-BTES parameters. The sensitivity analysis pointed out top surface insulation and ground thermal conductivity to have the most significant impact on both the average storage temperature and heat carrier temperature.

It is found that there is a potential for HT-BTES systems in the waste-to-energy district heating sector in Norway. Previous projects show that design and operation are key factors in achieving well-performing systems. A more dynamic operation has shown to be able to increase the annual average storage temperature significantly. Assumptions have been made in the simulation models, and results should be reviewed with caution. The results still underline the potential and trends of HT-BTES system solutions.

Sammendrag

Denne oppgaven har som hensikt å øke kunnskap om HT-BTES (høytemperaturs borehullsbasert energilager) potensiale, utføre en termisk analyse av høytemperaturs borehull og anvende dette i en HT-BTES caseanalyse. Caseanalysen evaluerte tre forskjellige HT-BTES systemer samt én konseptuell styringsstrategi (nightboosting). HT-BTES er et utmerket sesonglagringssystem for industriell spillvarme, som både øker energieffektiviteten til varmeproduksjonen, i tillegg til at det bidrar til å møte fremtidens varmebehov.

Utformingen av de tre HT-BTES-casene er basert på kunnskap tilegnet fra eksisterende prosjekter, samt en mulighetsstudie rettet mot fjernvarmesektoren i Norge. Dette resulterte i en lagringskapasitet på henholdsvis 7,5 GWh, 60 GWh og 125 GWh for de tre casene. Lastesyklusene for hvert design er basert på månedlige data som ble innhentet i det aktuelle mulighetsstudiet.

Resultater fra den termiske analysen viste at nightboosting gav en betydelig økning i temperaturen til varmebærervæsken. MATLAB-modellen som ble brukt i den termiske analysen inkluderte den termiske kapasiteten til borehullet, og ble derfor brukt til å kalibrere en pre-pipe komponent. Denne komponenten ble anvendt i TRNSYS-modellen for å inkludere den termiske kapasiteten til borehullene og forbedre modelleringen av korte transienter. Mest samfallende resultater mellom MATLAB og TRNSYS ble oppnådd ved å ta hensyn til 50% av den totale termiske kapasiteten til borehullene.

Caseanalysen viste at en økning i lagringskapasitet påvirket den maksimale gjennomsnittlige lagertemperaturen. Den maksimale gjennomsnittlige lagertemperaturen var henholdsvis 85°C, 82.5°C og 75°C for case 1,2 og 3. Ved nightboosting, med en varmerate på 60 W/m, ble differansen mellom den årlige maksimale og minimale gjennomsnittstemperaturen i lagrene redusert med 43.4%, 28.3% og 24.9% for case 1,2 og 3. En parameteranalyse av case 2 evaluerte fire viktige brønnparkparametere. Parameteranalysen påpekte at overflateisolasjon og varmeledningsevnen til berggrunnen hadde størst påvirkning på både den gjennomsnittlige lagertemperaturen og temperaturen til varmebæreren.

Det er funnet et stort potensial for HT-BTES innen den norske fjernvarmesektoren. Etablerte prosjekter viser betydningen av designet, men også styringen av lageret for å oppnå et velfungerende system. En mer dynamisk styring av HT-BTES systemer har vist å kunne øke temperaturer betraktelig. I simuleringsmodellene presentert i oppgaven pekes det på antagelser, og det er derfor viktig med et kritisk blikk på resultatene. Resultatene vil likevel gi et godt bilde av potensialet og trendene vi finner blant HT-BTES systemer.

Abbreviations

BTES	Borehole thermal energy storage
BHE	Borehole heat exchanger
COP	Coefficient of performance
DH	District heating
DST	Duct Ground Heat Storage
DHW	Domestic hot water
DTRT	Distributed thermal response test
FLS	Finite line source
GWP	Global warming potential
HT	High temperature
HP	Heat pump
LT	Low temperature
LT-DH	Low temperature district heating
MATLAB	Matix laboratory
NGU	Norges Geologiske Undersøkelse
ODP	Ozone depletion potential
R717	Ammonia refrigerant
SCOP	Sesonal coefficient of performance
TRCM	Thermal resistance and capacity model
TRNSYS	Transient system simulation program
TRT	Thermal response test

Symbols

T_{in}	Incoming heat carrier fluid temperature	°C
T_{out}	Outgoing heat carrier fluid temperature	°C
T_f	Average temperature of the heat carrier fluid	°C
T_b	Average temperature of the borehole wall	°C
T_{am}	Average storage temperature	°C
T_m	Local average temperature	°C
T_0	Initial ground temperature	°C
R_b	Borehole thermal resistance	mK/W
R_b^*	Effective borehole thermal resistance	mK/W
R_g	Thermal resistance of the ground	mK/W
R_{sf}	Steady flux thermal resistance	mK/W
q	Heat transfer rate pr meter	W/m
Q	Heat transfer rate	W
E_{in}	Injected energy	Wh
E_{out}	Extracted energy	Wh
η_{BTES}	BTES efficiency	-
c_p	Specific heat capacity	J/kgK
k	Thermal conductivity	W/mk
f	friction factor	-
Nu	Nusselt number	-
h	heat transfer coefficient	W/m^2K
H	Total borehole depth	m
D_i	Vertical insulation depth	m
λ_i	Thermal conductivity of the total insulation layer	W/mK
d_i	Total thickness of the insulation layer	m
R	Radius of a cylindrical storage	m

V	Storage volume	m^3
d	Borehole spacing	m
N	Number of boreholes	-
A_b	Area occupied by one single borehole	m^2
A_s	Surface area of a geometry	m^2
L_{pp}	Pre-pipe length	m
R_{pp}	Pre-pipe radius	m
D_{pp}	Pre-pipe diameter	m
T_c	Condensing temperature	°C
T_e	Evaporation temperature	°C
Q_c	Heating power of a heat pump	W
f_q	Heat loss factor	-
η_{is}	Isentropic efficiency	-

Contents

List of Figures

List of Tables

Chapter 1

Introduction

With an increasing focus on energy efficiency and emission reduction, storage and utilization of excess heat will become increasingly relevant. In industries where demand varies seasonally, but production is close to constant, a large amount of excess heat will go to waste if not stored or used. By seasonally storing the excess heat and supplying it when the heating demand increases, the energy efficiency of the heat production will increase, and the operation of fossil-fueled peak handling equipment reduced.

A high-temperature borehole thermal energy storage (HT-BTES) uses the ground as the heat storage medium and can consequently store vast amounts of excess heat. With high-temperature (HT) waste heat, storage temperatures above 70°C can be achieved. A HT-BTES is therefore an excellent storage solution for the district heating sector.

1.1 Aim and objectives

The goal of this master thesis is to gather knowledge regarding the potential of HT-BTES solutions and the thermal process in high temperature boreholes, and to use this knowledge to design and evaluate one or more HT-BTES system solutions. The task will be solved through the following objectives:

1. Gather and present a summary of available information concerning existing HT-BTES, and collect and present key information on the potential of using HT-BTES for utilizing surplus heat from waste-to-energy plants in district heating applications.

2. Perform a thermal analysis of high temperature boreholes, evaluating their behavior during variations in heat injection and extraction. The methodology and the calculation results shall be presented and discussed.

3. A case analysis on one or more of the potential locations presented in Task 1 shall be performed. A HT-BTES will be the storage solution and the analysis will include an evaluation of different designs and operational strategies. Key parameters such as

storage capacity, temperature development, heat loss and heat pump performance shall be defined and calculated.

4. Suggestions for further work shall be discussed.

1.2 Outline

There will be ten chapters in this master thesis. Chapter One will give an introduction to the relevance, aim, and objectives of this master thesis. Chapter Two will be the first part of the literature review, presenting theory regarding the HT-BTES system and the thermal process in a HT-borehole and HT-BTES. Chapter Three will present a graphical summary of performance and design parameters from existing HT-BTES projects and is the second part of the literature review. Chapter Four is the final part of the literature review and will be a feasibility study gathering information on the potential of HT-BTES systems in the waste-to-energy district heating sector in Norway. In Chapter Five, a thermal analysis of HT-boreholes will be performed. In chapters Six a description of the case analysis is given. Chapter Seven presents the case analysis results as well as an evaluation of short-time transient modeling and a sensitivity analysis of case two. Chapter Eight will be the discussion, chapter Nine, the conclusion, and in chapter Ten, future work will be presented.

1.3 Scope

The theoretical evaluation of a HT-borehole and HT-BTES system solution was in focus during this master thesis. Practical limitations in the system solution are therefore not considered in this thesis. These practical limitations concern the growth of legionella in a LT-DH system and the practical installation and operation of an industrial heat pump. Groundwater flow inside the HT-BTES is also not accounted for both because of the complexity and unknown location of the HT-BTES cases. The load cycles developed for the case analysis are based on monthly data and the daily load cycles are therefore assumed equal over the duration of one month. Based on mentioned limitations, the presented results will still be representable for the thermal process in HT-boreholes and the potential of HT-BTES systems.

Chapter 2

Theory

This theory chapter will present HT-BTES and explain its principles regarding design and performance. In addition, the theory regarding the thermal resistance in boreholes will be presented, as well as theory on the local and global thermal process in a HT-BTES system.

Literature in this master thesis has been found by searching through the database Oria supplied by NTNU, google scholar and references used in credible literature. Literature was evaluated creditable based on the journal the content was published in, qualifications of the author or authors and neutrality of the literature. This was done to ensure the quality of the literature review and the credibility of the content presented. Information regarding excess heat production used in the feasibility study was acquired by contacting the relevant district heating companies.

2.1 The BTES system

A borehole thermal energy storage (BTES) system takes advantage of the large storage volume that is available in the ground. With the benefits of cost, accessibility, reasonable heat capacity and a non-toxic environment, the ground suits very well as a storage medium (Sibbitt and McClenahan, 2014). In order to transfer heat to the ground, a heat carrier fluid is circulated through a borehole heat exchanger (BHE), also called a collector. The BHE is located in a vertical borehole filled with groundwater or a grouting material (Gehlin, Spitler, and Hellström, 2016). The BHE exists in two fundamental designs, U-tube and coaxial (Malmberg, 2017).

A BTES consists of multiple boreholes in a certain pattern, all boreholes are installed with a BHE which injects heat into the ground during the summer and extract heat during the winter (see fig.2.1). Depending on the temperature level in the BTES the delivered heat can either supplied directly or through a heat pump (HP) or other auxillary heater. If the BTES temperature is low enough it can also be used for cooling purposes during the summer. Only HT-BTES systems will be addressed in this master thesis.

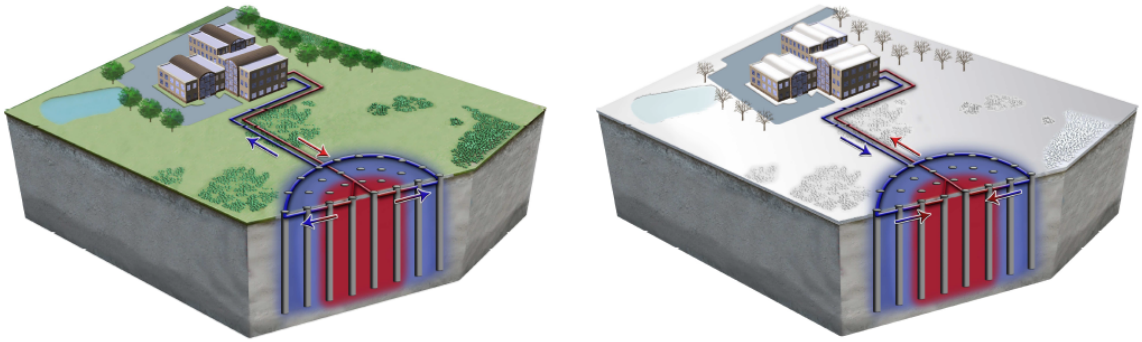

(a) Summer operation of the BTES **(b)** Winter operation of the BTES

Figure 2.1: Principle of seasonal heat storage using a BTES solution (Underground Energy, 2009).

2.1.1 Borehole heat exchanger (BHE)

A U-tube and coaxial BHE are based on different system principles, being closed and open (Nordell, 1994). In an open system, the heat carrier fluid is in direct contact with the borehole wall, which is typical for a coaxial design. For the U-tube design heat must be transferred through the BHE walls and the heat carrier is never in direct contact with the borehole wall.

The most commonly used BHE designs are the single and double U-tube designs (Gehlin, 2016). This is mainly due to the high reliability, low installation complexity and low cost of the U-tube design. The thermal resistance and pressure drop is however higher for the U-tube design compared to the coaxial (Gehlin, 2016). Thermal resistance and pressure drop in the U-tube BHE design can be reduced by increasing the number of U-tubes inside the borehole (Gehlin, 2002). Figure 2.2 shows a top view of the single U-tube and coaxial BHE design. The coaxial BHE in this figure is installed with a liner material along the borehole wall. A liner material can be installed if geochemical and geohydrological challenges are present.

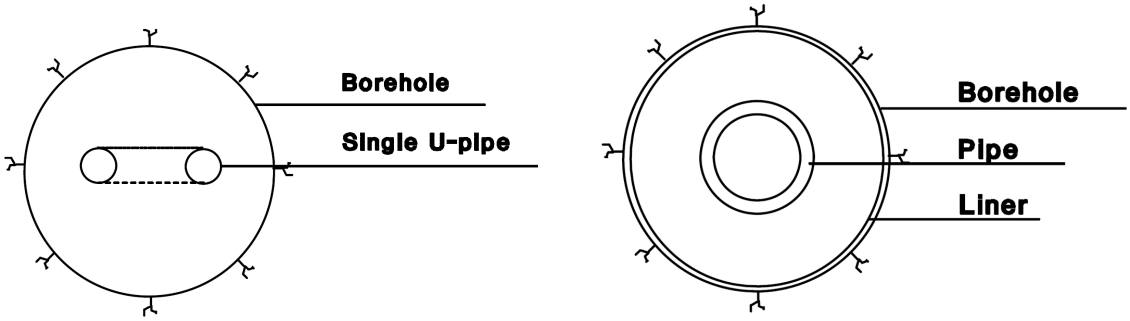

(a) Single U-tube BHE **(b)** Coaxial BHE

Figure 2.2: Top view of a single U-tube and coaxial BHE (Nordell, 1994)

2.1.2 Heat source

The available heat sources for a BTES can be many, but depending on the desired temperature level, the amount will be reduced. For existing HT-BTES systems, the two most commonly used heat sources are solar thermal collectors and industrial waste heat (Malmberg et al., 2018). The heat source will be a crucial component in the sizing of the HT-BTES. This is because the utilized heat source may limit the amount of available energy and temperature level of the storage. Due to restrictions of the BHE material, the highest possible charging temperature is 95°C (Reuss, 2015). Solar thermal collectors seldom produce these high temperatures, so this is mainly a restriction affecting systems with industrial waste heat as a heat source. The most important factor regarding the utilized heat source is that there is a seasonal variation in demand and supply. It is also essential for the reliability of the HT-BTES system that the heat source used for energy injection also is reliable.

2.1.3 Heat loss

Fourier's law (eq.2.1) explains the fundamental heat transfer due to conduction and highlights the most important factors in the heat loss of the HT-BTES. The main driving force for heat loss in the HT-BTES is the temperature difference between the storage and the undisturbed ground temperature and the temperature of the top surface. The conductivity of the surrounding ground and top layer will also be of significance since heat loss will be proportional to the conductivity (eq.2.1). Lastly, the size of the storage will determine the value of the surface area where heat is being conducted. The size will increase heat loss, but also increase the storage capacity. It is therefore desirable with a compact storage shape in order to minimize the surface area to volume ratio. This will result in large storage capacity with minimal surface area for heat loss.

$$Q = -A_s \cdot k \cdot \nabla T \tag{2.1}$$

Typical for the mentioned heat loss components is that they can be calculated or measured and consequently accounted for during the design of the HT-BTES. Groundwater flow is a more complex heat loss component to account for, as it can only be detected through test drilling. Since groundwater flow may introduce a significant heat loss, a geological investigation of the construction site should be performed.

2.2 Heat transport in the HT-BTES

Nordell (1994) defines the heat transport in the HT-BTES to be composed of three thermal processes. Each process has different characteristic behavior, and the processes are defined by the following definitions:

- The thermal process in each borehole between the heat carrier fluid and the borehole wall.
- The local process involving the borehole and the rock surrounding the borehole.
- The global process in the storage volume and surrounding ground.

Heat transfer from the heat carrier fluid to the HT-BTES and heat losses from the HT-BTES are the fundamental problems regarding the thermal analysis of a HT-BTES (Nordell, 1994). The thermal analysis begins with the thermal process in each borehole, where heat transfer is through both conduction and convection. This heat is then conducted into the surrounding rock, where the heat also interacts with surrounding boreholes and the average temperature inside the storage is increased. A heat loss from the storage boundary to the surrounding environment will then occur. This is caused by the elevated storage temperature and the lower temperature of the surrounding rock or environment.

In order to perform a thermal analysis on these thermal processes, two basic assumptions are made (Hellström, 1991):

- The heat transport in the ground takes place solely by heat conduction.
- The thermal properties in the ground, or in a subregion of the ground, can be represented by constant values.

A discussion of the validity of these assumptions is presented in Hellström (1991) chapter 5.

2.2.1 Thermal processes

Heat carrier fluid and borehole wall

This process is analyzed with a borehole thermal resistance. This resistance is explained more in-depth in section 2.3. An important remark is that the heat capacity of the materials involved is relatively small. Capacity effects are due to this only present during short-term variations, and the borehole thermal resistance is therefore analyzed during steady-state conditions (Nordell, 1994).

Borehole and surrounding rock

The thermal process from the borehole to the surrounding rock is defined as the local process, and it also includes the thermal interaction between adjacent boreholes (Nordell, 1994). The heat transfer rate is determined based on the temperature difference between the heat carrier fluid and the average temperature of the surrounding ground. This introduces a resistance in the surrounding ground in addition to the borehole thermal

resistance. Different methods can then be used in order to analyze this thermal process. This is explained more thoroughly in section 2.4.

Storage volume and surrounding ground

The large scale heat transfer between the storage volume and surrounding ground is defined as the global process. The primary objective of the global analysis is to calculate the heat loss at the storage boundary during a storage cycle (Nordell, 1994). The global process uses the average storage temperature and does not focus on small-scale temperature details. This is because heat loss depends on variations in the average storage temperature around the storage boundaries. After the transient thermal build-up of the HT-BTES, heat loss will be due to a periodic temperature variation and an annual average storage temperature. The net contribution of the periodic component is assumed zero, and the annual heat loss can therefore be calculated with the annual average storage temperature (Hellström, 1991).

2.3 Borehole thermal resistance

Heat transfer between the heat carrier fluid and the surrounding ground in a borehole will be dependant on the arrangement of the borehole heat exchangers, the convective heat transfer in the BHEs and the thermal properties of the materials involved in the thermal process (Hellström, 1991). These different parts will each have their own thermal resistance. These different resistances can however be united in order to form one total resistance. This is done for the resistance between the heat carrier fluid and the borehole wall, and this resistance is called the borehole thermal resistance (also called fluid to ground thermal resistance), denoted R_b (Nordell, 1994).

The relation between a heat rate q (W/m) and the temperature difference between the average heat carrier temperature (T_f)(see eq.2.3) and borehole wall temperature (T_b) is of main interests (Hellström, 1991). This relation can be expressed by the general equation 2.2, which is for N flow channels in a borehole. This equation can be solved through analytical methods. Two conventional methods are the finite line source (FLS) and the more advanced, multipole method (Hellström, 1991). Equation 2.2 can be solved analytically since the heat capacity of the materials in the borehole are relatively small compared to the thermal capacity of the entire storage. Capacity effects in the borehole can therefore be neglected, except for during short-term variations (Nordell, 1994).

$$T_{fm} - T_b = \sum_{n=1}^{N} R^o_{mn} \cdot q_n \qquad for\ m = 1, ..., N \tag{2.2}$$

$$T_f = \frac{1}{2}(T_{fin} + T_{fout}) \tag{2.3}$$

T_{in} is the incoming heat carrier fluid temperature to the HT-BTES, while T_{out} is the outgoing heat carrier fluid temperature from the HT-BTES.

2.3.1 Thermal resistance components

The borehole thermal resistance R_b will be dependant on the installed BHE in the borehole. Each BHE design consists of multiple thermal resistances, which in total make out the borehole thermal resistance. Nordell (1994) and Hellström (1991) present and explain the different resistance components for the coaxial BHE and U-tube BHE. The different resistance components for each BHE design are as follows:

Coaxial, with an outer liner

- R_{fc1} - Convective heat transfer resistance between the bulk fluid in the inner flow channel and the inner surface of the concentric pipe.
- R_{p1} - Thermal resistance of the pipe wall.
- R_{fai} - Convective heat transfer resistance between the bulk fluid in the outer annular flow channel and outer wall of the concentric pipe.
- R_{fao} - Convective heat transfer resistance between the bulk fluid in the outer annular flow channel and the borehole liner or borehole wall if no liner.
- R_{p2} - Thermal resistance of the liner material.
- R_{c2} - Contact resistance between the liner and the borehole wall.

These six resistances can be summed up into two different resistances. The first is the thermal resistance between the bulk fluid in the inner flow channel and bulk fluid in the annular flow channel, which consists of R_{fc1}, R_{p1} and R_{fai}. While the second thermal resistance is between the bulk fluid in the annular flow channel and the borehole wall, which consists of R_{fao}, R_{p2} and R_{c2} (Nordell, 1994).

U-tube

- R_{fc1} - Convective heat transfer resistance between the bulk fluid in the pipe and the pipe wall.
- R_{p1} - Thermal resistance of the pipe wall.
- R_{c1} - Contact resistance between the outer pipe wall and the grouting material in the borehole.

- R_{p3} - Heat transfer resistance of the grouting material.

The sum of R_{fc1}, R_{p1} and R_{c1} will make out the thermal resistance between the heat carrier fluid and the grouting material, while R_{p3} will be dependant on the grouting material used and is more complicated to calculate (Nordell, 1994).

The procedures on how to analytically calculate the borehole thermal resistance R_b for different BHE designs are thoroughly explained in Hellström (1991) chapter eight.

2.3.2 Effective borehole thermal resistance (R_b^*)

An effective borehole thermal resistance (R_b^*) has been derived for two different cases, uniform temperature and uniform heat flux along the borehole wall (Hellström, 1991). R_b^* accounts for the effect of varying fluid temperature along the borehole and the effect of heat transfer between the flow channels of the BHE (Nordell, 1994). Equation 2.4 defines the effective borehole thermal resistance for a BHE.

$$\bar{T}_f - \bar{T}_b = \bar{q} \cdot R_b^* \tag{2.4}$$

$\bar{T}_b$, $\bar{T}_f$ and $\bar{q}$ are averaged values along the borehole length. Formulas for the case of uniform temperature and uniform heat flux along the borehole wall are derived in (Hellström, 1991). In the case of uniform heat flux, the effective borehole resistance R_b^* is given by equation 2.5.

$$R_b^* = R_b + \frac{1}{3}\frac{1}{R_a}\left(\frac{H}{C_f \dot{V}_f}\right)^2 \tag{2.5}$$

R_a in the equation is the thermal resistance between the heat flow in the different flow channels of the BHE. C_f is the volumetric heat capacity of the heat carrier fluid, while $\dot{V}_f$ is the volumetric flow rate of the heat carrier, and H is the borehole depth (Hellström, 1991). One important observation is the influence of $\dot{V}_f$ in equation 2.5. If the flow is laminar, the flow dependant term in equation 2.5 will be of significance. In addition to this, there will also be a thermal short-circuiting between the different flow channels, which further increases the effective borehole thermal resistance (Nordell, 1994). This highlights that a turbulent flow inside the flow channels is to be preferred, although it will increase the total pressure loss of the piping system.

2.4 Local thermal process

The surrounding ground volume around the borehole in the local thermal process is dependant on the borehole pattern. Different patterns have different cross-sectional areas for the local ground region, denoted A_p. Figure 2.3 shows a hexagonal and rectangular

borehole pattern and the respective local ground region A_p. For the hexagonal borehole patter with a borehole spacing B, $A_p = B^2 \cdot \frac{\sqrt{3}}{2}$, while for the rectangular pattern with borehole spacing B and B1, $A_p = B \cdot B1$. The temperature in the region A_p is the local average temperature (T_m), and of main interest is the relation between the injection rate q and T_f - T_m. This relation will give the heat transfer capacity for the heat BHE system (Hellström, 1991). Different concepts can be used to analyze the local thermal process in order to calculate the injection rate q. Hellström (1991) presents an analysis based on step-pulses, an analysis for periodic components and the concept steady-flux regime. All these three different methods give a relation between the rate q and T_f - T_m.

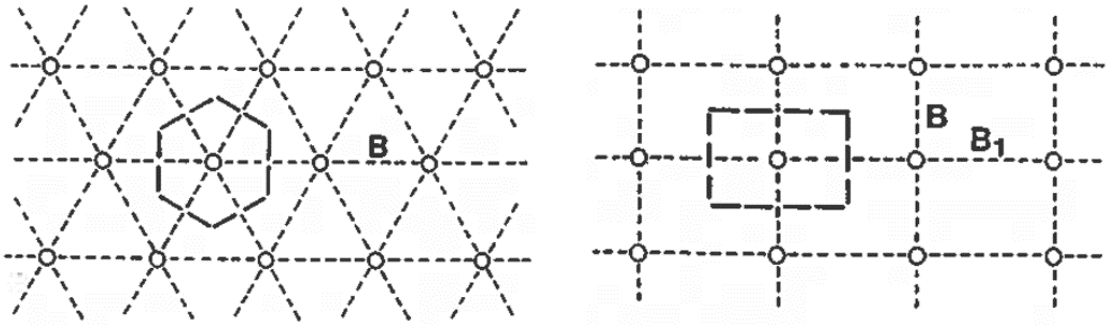

(a) Hexagonal borehole patter **(b)** Rectangular borehole pattern

Figure 2.3: Different borehole patter and local ground region (Hellström, 1991)

2.4.1 Steady-flux regime

A Steady-flux regime is obtained when an injection or extraction rate is constant for a more extended period of time. When the steady-flux regime is obtained, the temperature difference between the heat carrier fluid T_f and the local average temperature T_m is constant (Hellström, 1991). Due to the symmetry of the borehole pattern and local ground region (see fig.2.3), the heat flux through the outer boundary of the local ground region is zero (Hellström, 1991). The shape of the temperature field will therefore not change with time, after an initial transient period. As mentioned, the temperature difference T_f - T_m will be constant in the steady-flux regime, and it will be proportional to the heat transfer rate q, given by equation 2.6.

$$T_f - T_m = q \cdot R_{sf} \tag{2.6}$$

R_{sf} is the steady-flux thermal resistance and is composed of the borehole thermal resistance R_b and the ground thermal resistance R_g. The ground thermal resistance is the resistance between the borehole wall and the local ground region around the borehole. The steady-flux resistance is then the sum of these two resistances. Figure 2.4 shows the steady-flux thermal resistance map of the heat flow from the heat carrier fluid to the local ground region.

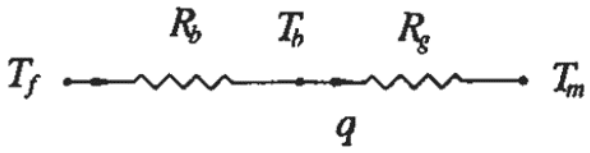

Figure 2.4: Thermal resistance map during the steady-flux regime for heat transfer from the heat carrier fluid to the local ground region (Hellström, 1991).

2.4.2 Step-pulse analysis

When heat injecting, or extraction rates vary with time q(t), they may be approximated by a step-wise constant values (Hellström, 1991). This is the underlying assumption for the step-pulse analysis. A short term variation will then become a superposition of step changes in the heat transfer rate q(t). The relation between the heat carrier temperature for a given step-pulse (q_1) and the local average temperature can then be expressed by equation 2.7.

$$T_f^q(t) - T_m = q_1 \cdot R_q(t) \tag{2.7}$$

R_q(t) will be a time dependant step pulse resistance. The step-pulse analysis is explained more thoroughly in (Hellström, 1991) chapter 10.

2.4.3 Periodic processes

Different methods can solve the thermal analysis of a BHE and the local ground region. A substitute for the step-pulse analysis is that the thermal process in the BHE and local ground region consists of a steady-flux component and a number of superposed periodical components (Hellström, 1991). This introduces the complex-valued ground resistance $\hat{R}_g$ of the local ground region. The periodic process is explained more thoroughly in (Hellström, 1991) chapter 11.

2.5 Global process

The global process concerns the heat transfer between the storage volume and the surrounding ground, and three different components define the global process of a HT-BTES system. These are the transient build-up phase, the periodic variation during an annual cycle and the steady-state component (Hellström, 1991). The three components are marked in figure 2.5. The transient build-up phase is required in order to heat the undisturbed ground temperature from its initial value to the operating temperature. During this preheating phase, heat will only be injected and not extracted. The transient thermal build-up phase can last from 3-6 years, depending on the capacity of the storage and annually injected energy(Skarphagen et al., 2019). The periodic variation is a result of the

annual charging and discharging cycle when the HT-BTES has reached its operating temperature. The periodic variations move along a steady-state component, shown in figure 2.5. This steady-state component is defined by the annual average storage temperature, and the annual storage heat loss is calculated with this temperature (Hellström, 1991).

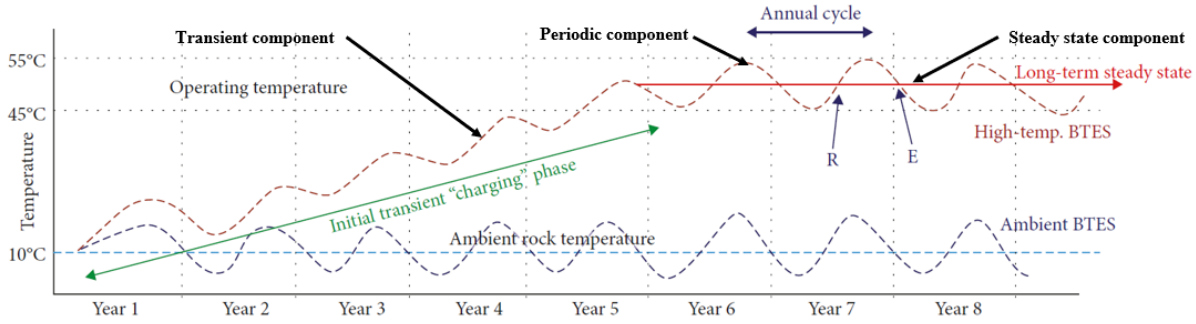

Figure 2.5: Global process and the respective heat loss components. R = recharge, E = extraction. The three different heat transfer components are indicated on their respective location (Skarphagen et al., 2019).

2.6 Duct ground heat storage (DST) model

A duct ground heat storage (DST) is defined as a system where heat is stored directly in the ground (Hellström, 1989). The DST model is a simulation model for such a system. Here the word duct is used as the name for the BHE. In the DST model, the storage volume is assumed to have a cylindrical shape with a vertical symmetry axis. Ducts are assumed to be uniformly placed in the storage, and there is a convective heat transfer in the ducts, and a conductive heat transfer in the ground (Hellström, 1989).

An essential feature of the DST model is that the temperature in the ground is calculated through superposition of three parts. These three parts are a global temperature, a local solution, and a steady-flux part. The global and local parts are solved with the explicit finite difference method (FDM), while the steady-flux part is calculated analytically (Hellström, 1989). Superposition of these three parts is then used to calculate the total temperature at specific locations in the HT-BTES. Hellström (1989) describes the DST model more in detail and how to incorporate the model into a computer code.

2.7 Low Temperature District Heating (LT-DH)

The information on this page is copied and only slightly modified from the project report leading up to his master thesis (Schmidt, 2019)

District heating has gone through a three-generation evolution since it first got introduced and now the fourth generation is starting to get established. The generations are characterized by transport media and the temperature level in the network. The different generations and their characterization are listed below (Dalla-Rosa et al., 2014):

- 1^{st} generation: Steam-based system
- 2^{nd} generation: Network supply temperature above 100 °C
- 3^{rd} generation: Network supply temperature between 80°C - 100°C
- 4^{th} generation: Consumer required supply temperatures, typically 45°C-60°C

The fourth-generation seeks to substitute the third generation DH systems as it is designed to improve the match between supply and demand. Dalla-Rosa et al. (2014) writes that with a well designed low-temperature district heating network, heat losses can be reduced up to 75% compared to existing DH networks. LT-DH systems are mainly applicable for low energy households or refurbished buildings (Brand et al., 2014). This is due to the heat loss requirements and low-temperature heating systems in these buildings.

The fourth-generation district heating network will possibly supply heat at temperatures as low as 50°C (Gadd and Werner, 2014). This will however require low-temperature space heating equipment in order to achieve thermal comfort for the end-user. Olsen et al. (2014) presents a system solution for hot water preparation at low temperatures and addresses the challenge of legionella. With a small piping volume between the taps and domestic hot water (DHW) system, DHW volume will be significantly reduced and consequently minimize the challenges with legionella (Lund et al., 2014). This enables supply temperatures at 40-50°C for DHW use in the household, which would require a supply temperature from the district heating network of as low as 45-55 °C (Lund et al., 2014). Challenges regarding legionella will not be addressed further in this master thesis.

In the article Nord et al. (2018), different LT-DH system solutions have been presented and analyzed. The lowest operational supply-/return temperatures are 55/25°C in the district heating network, supplying DHW at 50°C to the end-user. It is crucial to obtain low return temperatures and consequently, a high ΔT in the district heating network in order to avoid a substantial increase in volume flow and pumping costs (Gadd and Werner, 2014).

Chapter 3

Existing HT-BTES projects

In this chapter a graphical summary on existing HT-BTES will be presented, which is the second part of the literature review. The graphical summary will present and compare key parameters in the HT-BTES system and focus on the comparison between design and measured values. The graphical summary on existing HT-BTES projects is based on a study performed on HT-BTES projects in the project report leading up to this master thesis (Schmidt, 2019).

Table 3.1: Existing HT-BTES projects and overall system parameters, (Hellström, 1991)[1], (Lundh and Dalenbäck, 2008)[2], (Nordell et al., 2016)[3], (Plan Energi, 2013)[4], (Nussbicker, Heidemann, and Mueller-Steinhagen, 2006)[5], (Miedaner, Mangold, and Sørensen, 2015)[6], (Mesquita et al., 2017)[7].

Location	**Years of operation**	**Storage volume [m^3]**	**Max storage temp [°C]**	**Heat source**
Luleå, Sweden[1]	1983-1990	115 000	65	Industrial waste heat
Anneberg, Sweden[2]	2002-	60 000	47	Solar thermal
Emmaboda, Sweden[3]	2010-	323 000	45	Industrial waste heat
Brædstrup, Denmark[4]	2012-	19 000	50	Solar thermal
Neckarsulm, Germany[5]	1997-	63 360	63	Solar thermal
Crailsheim, Germany[6]	2008-	37 500	57	Solar thermal
Okotoks, Canada[7]	2007-	34 000	74	Solar thermal

There are in total 12 existing and planned HT-BTES projects, where nine are constructed, and three are only conceptual (Schmidt, 2019). The graphical summary will only include the constructed projects since data during operation is required for the summary. Seven of the existing projects will be included as two of the constructed HT-BTES projects lack relevant operational data. The seven HT-BTES projects that are included in the graphical summary are listed in table 3.1.

The following sections will present the graphical summary addressing design versus measured performance and other design parameters. Measured values are selected from the most representative operational year after the thermal build-up phase for the respective HT-BTES project.

3.1 HT-BTES efficiency (η_{BTES})

The efficiency of the HT-BTES projects is calculated with equation 3.1. The efficiency represents how much of the injected thermal energy that is extracted during an annual cycle for the HT-BTES. Figure 3.1 shows the design and measured efficiencies for the seven HT-BTES projects listed in table 3.1. The estimated annual average storage temperature is also included since it directly impacts the heat loss from the storage. The annual average storage temperature is estimated as the mean value between the measured maximum and minimum storage temperature.

$$\eta_{BTES} = \frac{E_{out}}{E_{in}} \tag{3.1}$$

From figure 3.1, it is observed that the measured efficiency is substantially lower than the desired design value for most of the HT-BTES projects. Only the HT-BTES in Okotoks has a measured value above the design value. The measured efficiencies are on average 17.42% lower than the design values, Emmaboda was excluded in the average value calculation. From HT-BTES theory, low storage temperature and large size should increase the efficiency, however figure 3.1 shows no clear correlation towards this.

From table 3.2, it is also observed that both Anneberg and Luelå did not have any top surface insulation, which would decrease the annual heat loss. Figure 3.1 shows that almost all projects have reasonably high design efficiencies, but that achieving the design efficiency can be challenging. The study on existing HT-BTES projects in Schmidt (2019) pointed out challenges during operation as one of the main factors causing the deviation from the design efficiency.

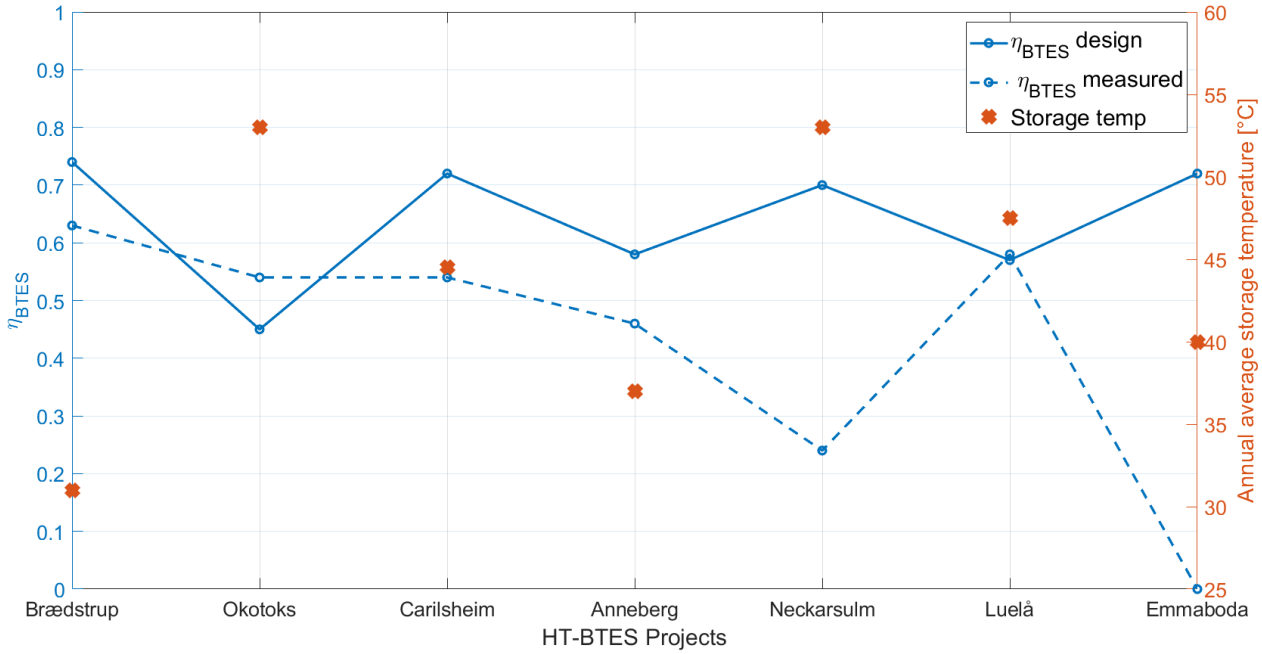

Figure 3.1: η_{BTES}, design and measured for existing HT-BTES projects. Projects are listed from smallest to largest on the x-axis.

3.2 Extracted thermal energy

The design and measured extracted thermal energy for the different HT-BTES projects are plotted in figure 3.2. Emmaboda is not included in this plot due to its extraction values not been representable for the real operation of the HT-BTES system (Nordell et al., 2016). Only two of the HT-BTES systems have small deviations between design and measured value, and the measured value is on average 25.66% lower than the design value. By comparing figure 3.1 and 3.2, a correlation between deviation regarding the efficiency and extracted thermal energy is observed. This is understandable because the η_{BTES} is a function of the extracted energy (E_{out}), seen in equation 3.1. For Luelå the injected and extracted energy during the presented operational year was less than their design values, which results in a deviation in extracted thermal energy, but not in the η_{BTES}.

Higher heat loss and lower charging temperatures than expected are two of the main driving factors for the deviation in extracted thermal energy (Schmidt, 2019). Lower charging temperature than designed for will result in lower annual storage temperature. If there are temperature requirements in the heating system, a lower annual storage temperature will consequently reduce the amount of usable heat stored in the HT-BTES. This will result in a lower amount of extracted thermal energy. This highlights the importance of both achieving and maintaining the desired storage temperature.

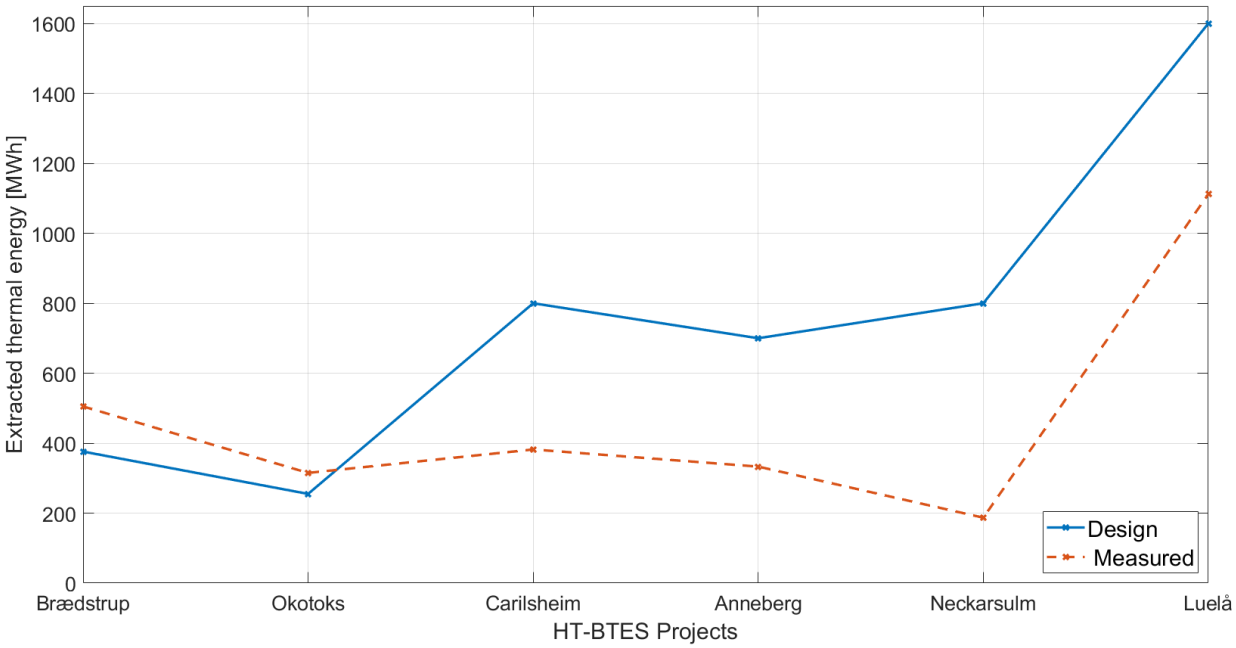

Figure 3.2: Extracted thermal energy, design and measured for existing HT-BTES projects. Projects are listed from smallest to largest on the x-axis.

3.3 Storage temperatures

The charging temperature will approximately represent the theoretically highest possible storage temperature that can be achieved. The deviation between charging temperature and maximum storage temperature should be as small as possible. This temperature difference will also be dependant on the borehole and ground thermal resistance, as explained in the theory chapter. Charging and storage temperatures for the HT-BTES projects are presented in 3.3. The results from figure 3.3 show that the charging temperature varies from 60°C to 84°C, the maximum storage temperature from 45°C to 74°C and the minimum storage temperature from 12°C to 40°C.

Two dimensionless parameters are defined in order to evaluate temperature relations in the HT-BTES system. These two dimensionless parameters, their average value, and the respective η_{BTES} for the HT-BTES projects, are presented in figure 3.4. For T_1^*, it is desirable to achieve a value as close as possible to 1. This indicates that the maximum storage temperature is close to the charging temperature. $\overline{T_1^*}$, which is the average value for all seven HT-BTES projects, is 1.26. If the storage is charged with 95°C the resulting maximum storage temperature would be 75°C. This is approximately a temperature difference of 20K, which is a reasonably high value.

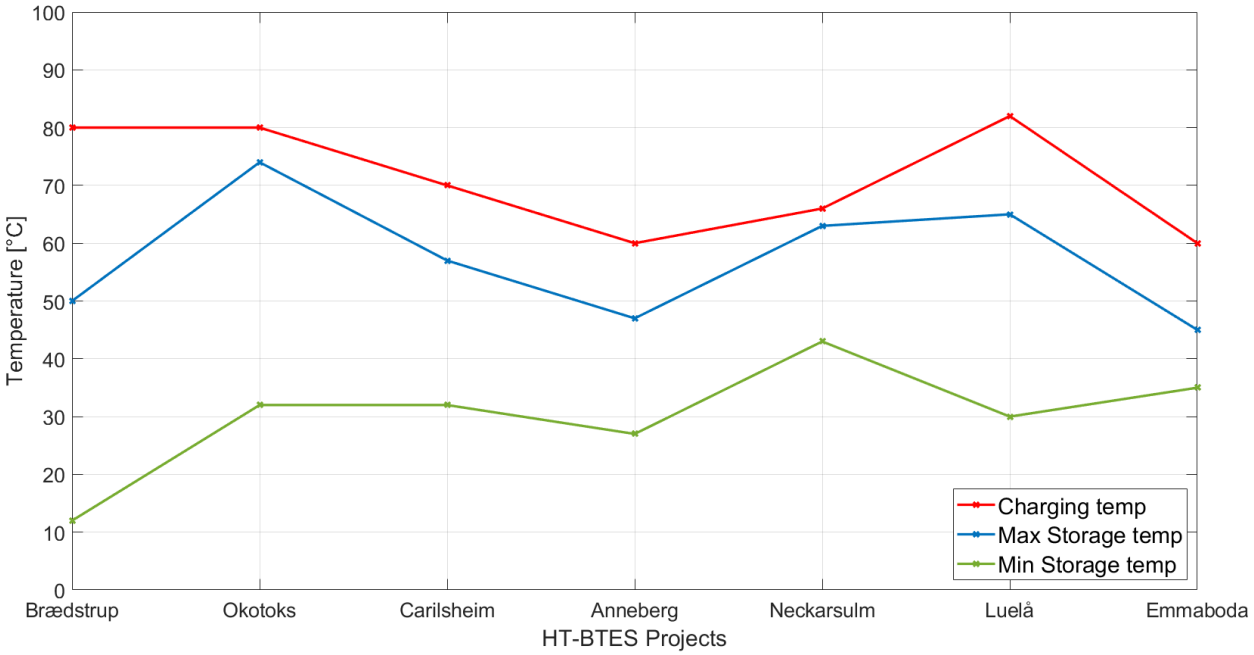

Figure 3.3: Storage temperatures and charging temperature for existing HT-BTES projects. Projects are listed from smallest to largest on the x-axis.

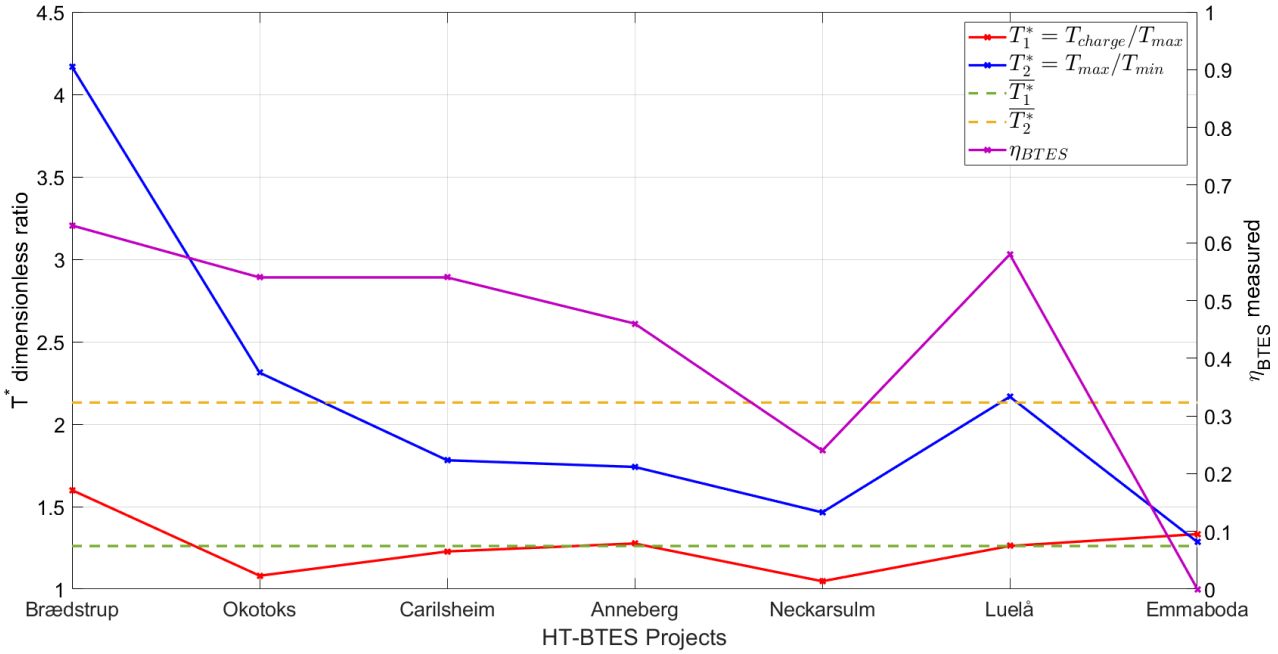

Figure 3.4: Dimensionless temperature ratios and measured BTES efficiency for existing HT-BTES projects. Projects are listed from smallest to largest on the x-axis.

T_2^* is the relation between the maximum and minimum storage temperature. From figure 3.4 the temperature difference seems to decrease with increase storage capacity. This must be evaluated in combination with the measured η_{BTES}. This is because a low efficiency indicates a lower amount of extracted energy than designed for and consequently increasing the minimum average storage temperature. The average value ($\overline{T_2^*}$) for the seven HT-BTES projects is 2.13. With a maximum storage temperature of 75°C the resulting minimum average ground temperature would be 35°C, resulting in a difference of 40K. This is a large temperature difference, and it is important to point out that Brædstrup significantly increases the average value. If Brædstrup is ignored in the average value of $\overline{T_2^*}$ becomes 1.80, and the temperature difference will be approximately 33K for a maximum storage temperature of 75°C.

3.4 Storage geometry and borehole configurations

Geometry will affect the heat loss of the HT-BTES. If considering heat loss only, the geometry should seek to minimize the surface area to volume ratio (Hellström, 1991). The most compact and construable storage geometry is therefore cylindrical storage with storage diameter and depth, aspect ratio = 1. The aspect ratio for the seven existing HT-BTES projects has been calculated and is plotted along with borehole spacing in figure 3.5. Based on this graph, it is observed that most of the HT-BTES projects have an aspect ratio between approximately 0.4-0.6. Okotoks is the only HT-BTES with an aspect ratio of exactly 1, and Neckarsulm is the only HT-BTES with an aspect ratio greater than 1. Neckarsulm was limited in borehole depth due to groundwater flow on the construction site (Nussbicker, Heidemann, and Mueller-Steinhagen, 2006).

From figure 3.5, it can be observed that borehole spacing trends to increase with storage capacity. The borehole spacing will however also be very dependant on the geological conditions of the construction site. With a constant storage volume, increasing the borehole spacing will reduce the number of boreholes and consequently the drilling cost. This cloud cause a significant cost reduction for the HT-BTES systems with large storage capacity, but it would also decrease the total borehole length of the system.

Depth of the boreholes in the HT-BTES typically increase when the capacity and size of the HT-BTES increases. This is observed in figure 3.6, except for the HT-BTES in Neckarsulm, which was limited in borehole depth due to geohydraulical conditions. A deeper borehole consequently increases the traveling length for the circulating heat carrier fluid and thereby increase the pressure loss pr borehole. Due to the increase in pressure loss number of boreholes connected in series will decline with increasing borehole depth. This correlation is also observed in figure 3.6, expect for the HT-BTES in Carilsheim, which only has two boreholes connected in series. Boreholes are connected in series in

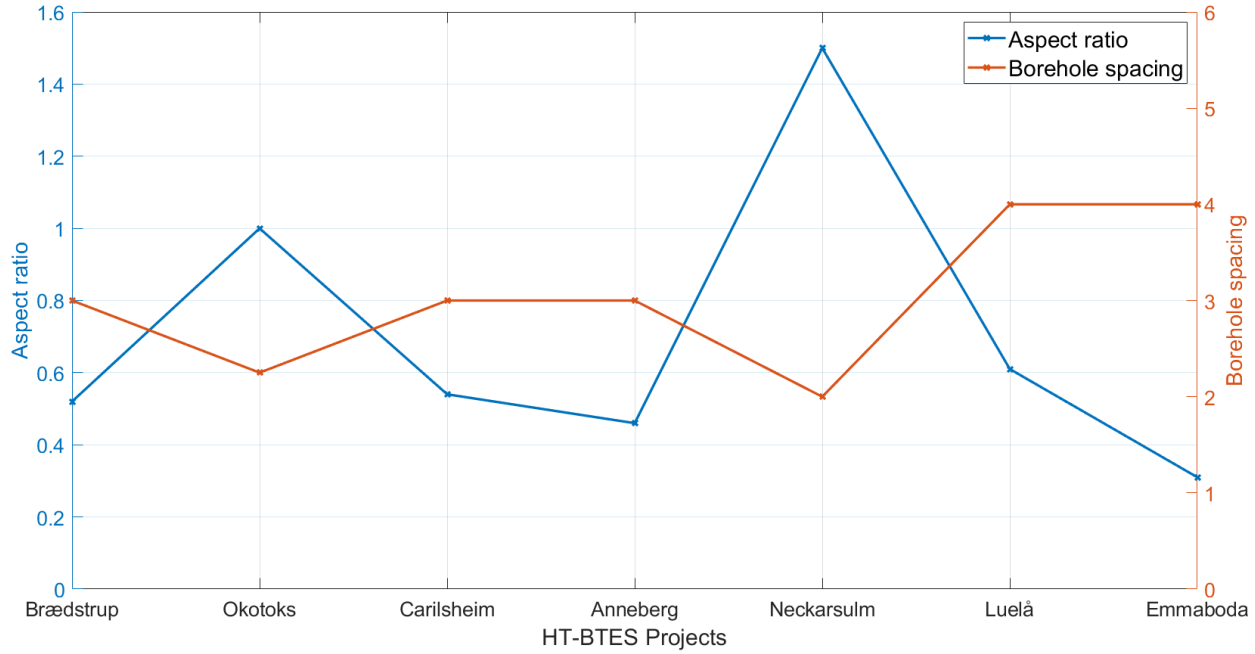

Figure 3.5: Aspect ratio and borehole spacing for existing HT-BTES projects. Projects are listed from smallest to largest on the x-axis.

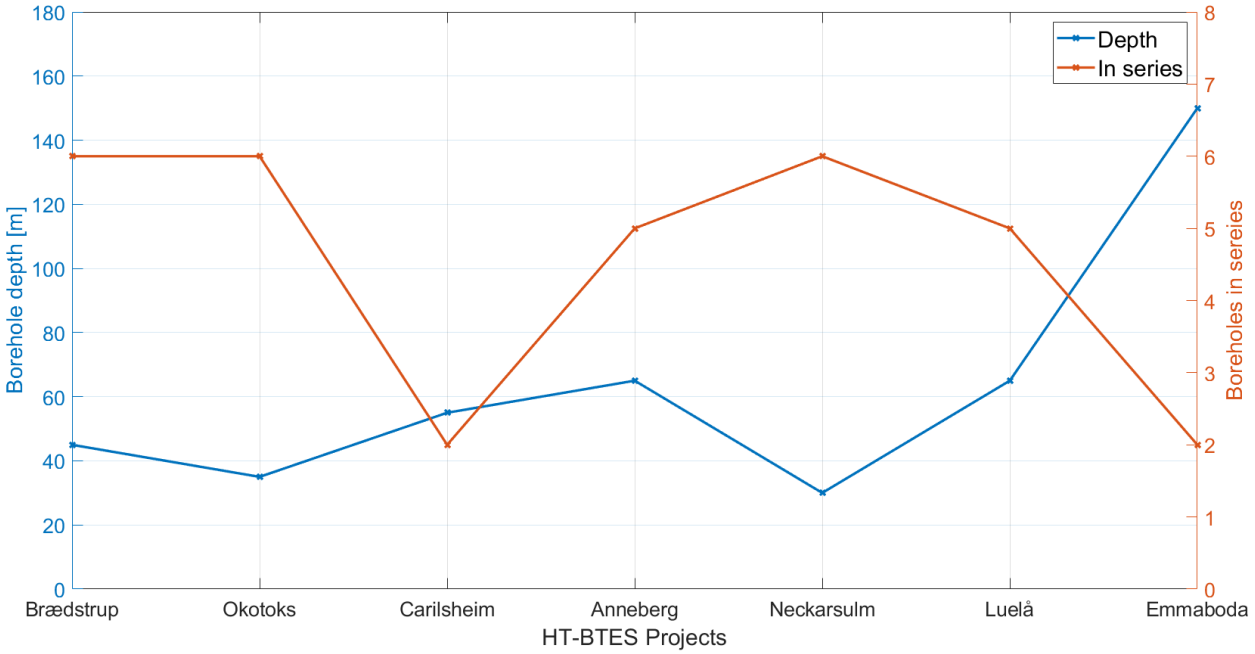

Figure 3.6: Borehole depth and number of boreholes connected in series for existing HT-BTES projects. Projects are listed from smallest to largest on the x-axis.

order to create a radial thermal stratification inside the HT-BTES.

3.5 System solution

Key parameters regarding the system solution for the seven HT-BTES projects are summarized in table 3.2. Only three out of seven projects have a heat pump installation. Whether a heat pump is required or not, is very dependant on the temperature requirements of the delivered heat. If the extracted heat from the HT-BTES is used to reheat return water in the existing DH network a heat pump or other auxiliary heater must be installed. If the HT-BTES is used to supply a LT-DH network or is used for space heating only, heat can be supplied directly from the HT-BTES.

Table 3.2 shows that most of the existing HT-BTES projects used insulation on the top surface. Most of the materials are synthetic and relatively expensive. The HT-BTES in Brædstrup did however use natural and low-cost material for their insulation (Plan Energi, 2013). The insulation on the top layer will decrease heat loss significantly, but it is important to evaluate the cost of heat loss reduction. Based on table 3.2 the typical insulation thickness varies from 0.2 - 0.5 meters.

The BHE design is an essential part of the HT-BTES. From table 3.2, U-tube BHE is the most commonly used design in existing projects. Only Luelå and Emmaboda used the coaxial design, which theoretically offers the best thermal performance. However, both these projects encountered challenges with the BHE design during operation, Emmaboda more than Luelå (Hellström, 1991) (Nordell et al., 2016). The U-tube is therefore based on experience, a more reliable design and it can increase its performance by adding more U-tubes (Reuss, 2015).

Table 3.2: Summary for the use of heat pump, top surface insulation and collector design.

HT-BTES project	Heat Pump	Insulation	Collector design
Brædstrup	1.3 MW	0.5m Mussels shells	Double U-tube
Okotoks	No	0.2m Extruded plystyrene	Single U-tube
Carilsheim	480 kW	0.2m Foam glass gravel	Double U-tube
Anneberg	No	No	Double U-tube
Neckarsulm	No	0.2m Polystyrene	Double U-tube
Luelå	2x200 kW	No	Open Coaxial
Emmaboda	No	0.4m Foam glass	Open Coaxial

Chapter 4

Feasibility study - waste to energy

With a growing population and growing consumption, more waste is being produced annually. Appropriate handling of this waste in terms of local and global environmental impacts is therefore essential. The three most common waste handling methods in Norway are recycling, incineration and landfill (SSB, 2019). Waste incineration creates large amounts of thermal energy and this has been utilized in the Norwegian DH sector. Heat production by waste incineration is therefore the largest heat source in Norwegian DH (Norsk Fjernvarme, 2019a). The development of waste incineration as a heat source in Norway can be viewed in figure 4.1. A law was enforced in 2009, which made it illegal to store most of the biodegradable waste at the landfill (Miljødirektoratet, 2019). This consequently led to an increase in waste incineration (see fig.4.1). Waste incineration substitutes the decomposition process of waste, which reduces emissions from waste significantly. This is because waste decomposition produces CH_4 (Methane) and waste incineration CO_2 (Carbon dioxide), and CH_4 has a global warming potential (GWP) 21-28 times larger than CO_2 (Pachauri et al., 2014).

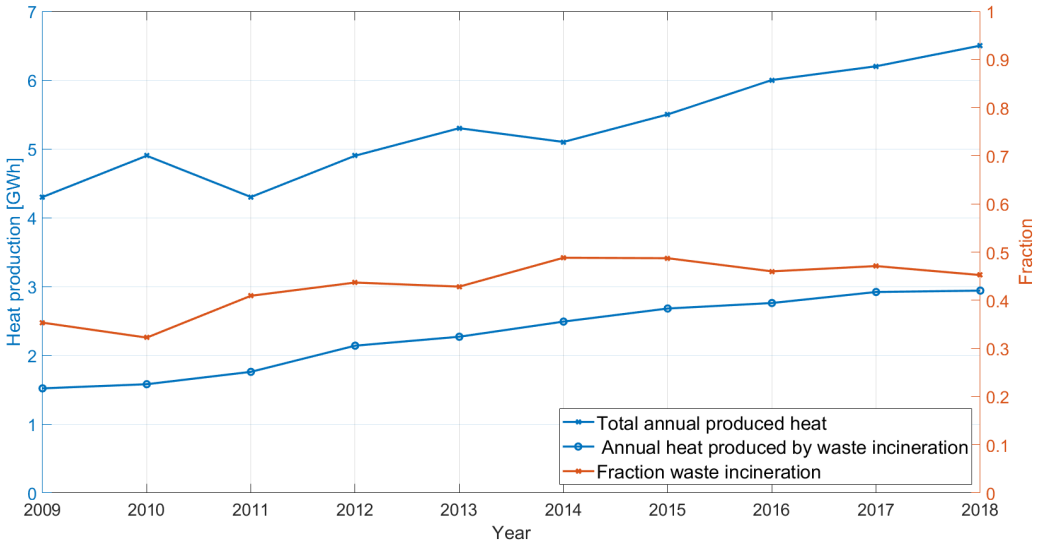

Figure 4.1: Annual values for heat production from 2009 - 2018 in the Norwegian DH sector (Norsk Fjernvarme, 2019a).

The combination of waste incineration as a waste handling method and as a heat source in the district heating sector can generate large amounts of excess heat. This is because the waste supply and incineration are more or less constant, while the heating demand in the DH network has significant seasonal variations. A feasibility study on the potential of using HT-BTES as seasonal storage for the excess heat produced by the waste-to-energy DH sector in Norway was therefore performed. Using a HT-BTES for seasonal storage of the excess heat will result in:

- Higher energy efficiency at the district heating plants.
- Peak load reduction due to seasonal storage.
- A low emission thermal energy station.

All graphs are generalized in order to keep the district heating plants who contributed with their data anonymous.

4.1 Heat storage potential

Ten district heating plants in Norway have waste incineration as a thermal energy source. In order to gather information for the feasibility study, all of these plants have been contacted. Nine out of the ten contacted DH plats replied with information regarding excess heat production and temperature of the supply water in the DH network. Based on this information, it was found that a total amount of 560 GWh excess heat is produced annually. This corresponds to almost 20% of thermal energy supplied by waste-to-energy DH plants in 2019 (Norsk Fjernvarme, 2019a). 560 GWh is a substations amount of thermal energy and shows that there is significant potential in terms of available excess heat.

The amount of available excess heat depends significantly on the capacity and size of the district heating plant. Figure 4.2 shows different ranges of produced excess heat and the percentage of district heating plants within this range. Based on figure 4.2, it is observed that most of the district heating plants produce between 40 - 80 GWh of excess heat annually.

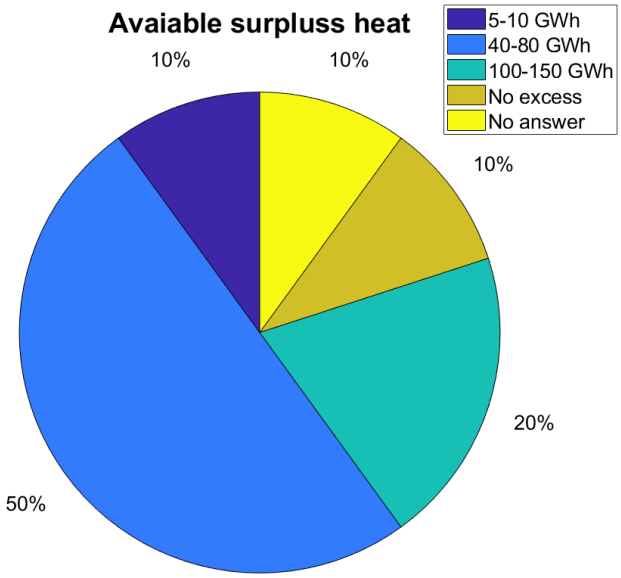

Figure 4.2: Percentage of district heating plants within a given range of available excess heat.

4.2 Excess heat production

From the survey, more detailed information regarding the monthly production of excess heat was received from five DH plants. The monthly distribution in each DH plant was normalized with respect to its maximum value (see eq.4.1). Two groups were formed due to differences in annual excess heat production. The district heating plants with 5 - 80 GWh are categorized "group 1" while the plants with 100 - 150 GWh are categorized "group 2". The results from the normalized excess heat production at each DH plant are presented in figure 4.3 for group 1 DH plants and 4.4 for group 2 DH plants.

$$E^* = \frac{E_{excess}}{E_{max-excess}} \tag{4.1}$$

Based on the acquired information presented in figure 4.3 and 4.4 average values where calculated. The average values were calculated based on the DH plants in group 1, group 2, and both groups combined. The distribution of the average values for group 1, group 2 and both groups combined are shown in figure 4.5. In order to create a more generalized graph, a polynomial curve fitting was performed for each distribution in figure 4.5. The resulting curves are shown in figure 4.6. For a comparison between the curve fitting and actual plot, see appendix A section A.1.

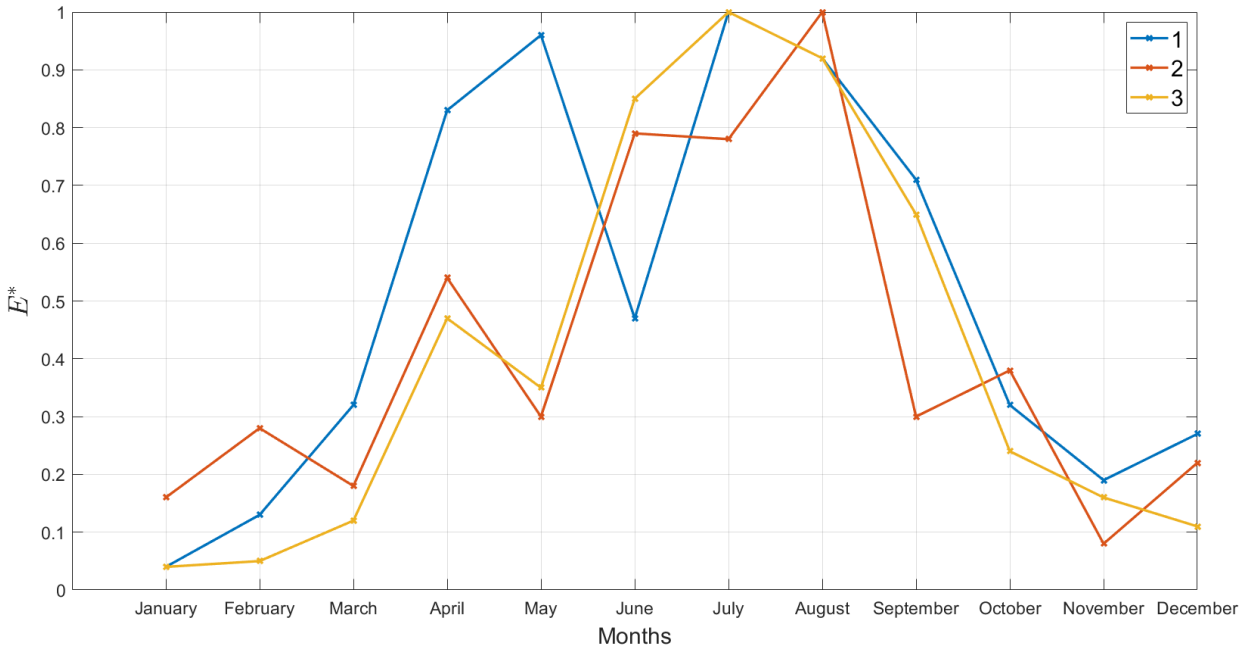

Figure 4.3: Normalized monthly excess heat production for district heating plants with available excess heat between 5 - 80 GWh/year.

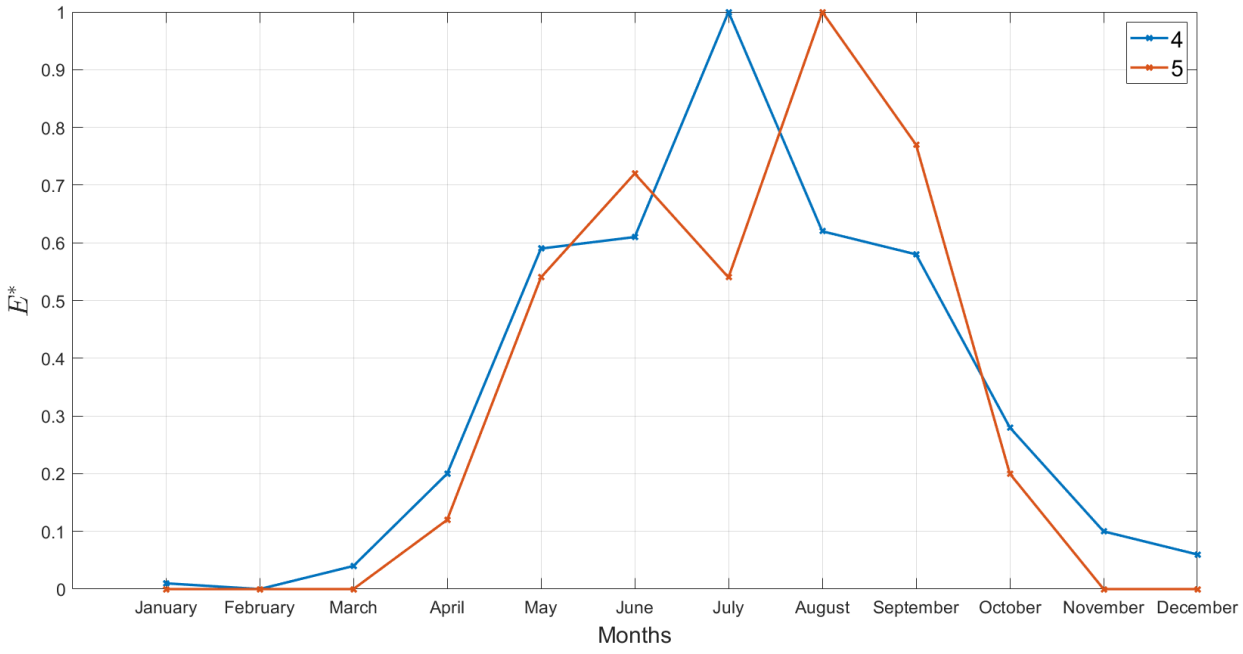

Figure 4.4: Normalized monthly excess heat production for district heating plants with available excess heat between 100 - 150 GWh/year.

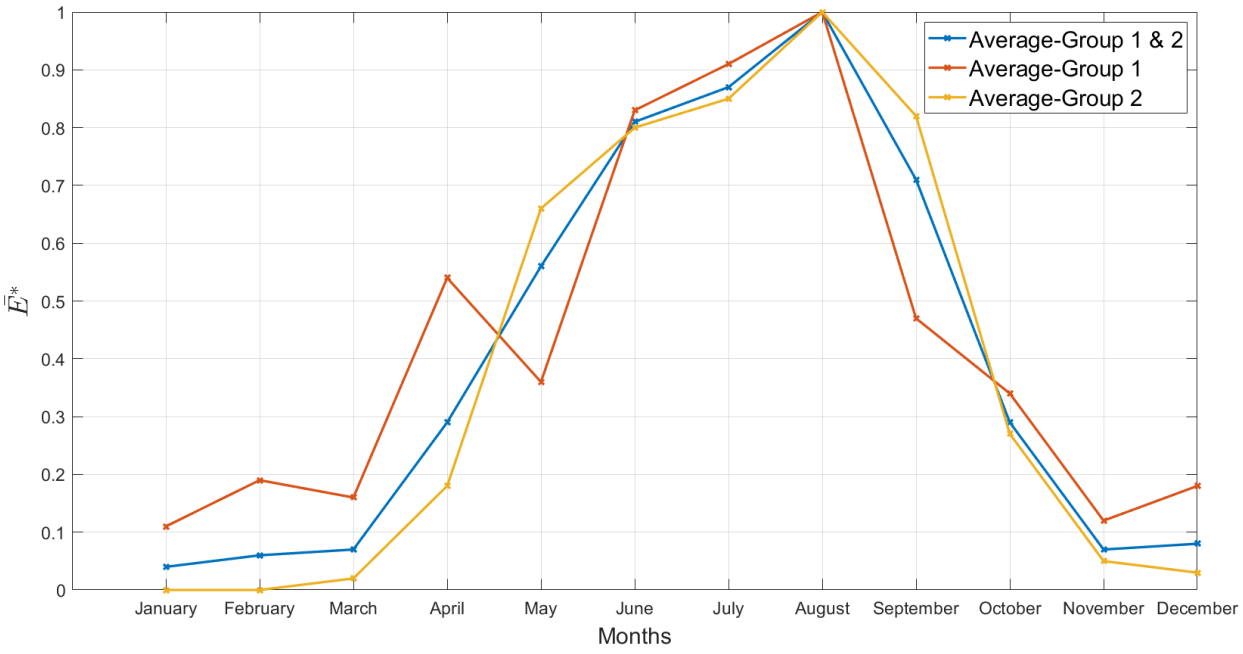

Figure 4.5: Average normalized monthly excess heat production for group 1, group 2 and group 1 & 2 combined.

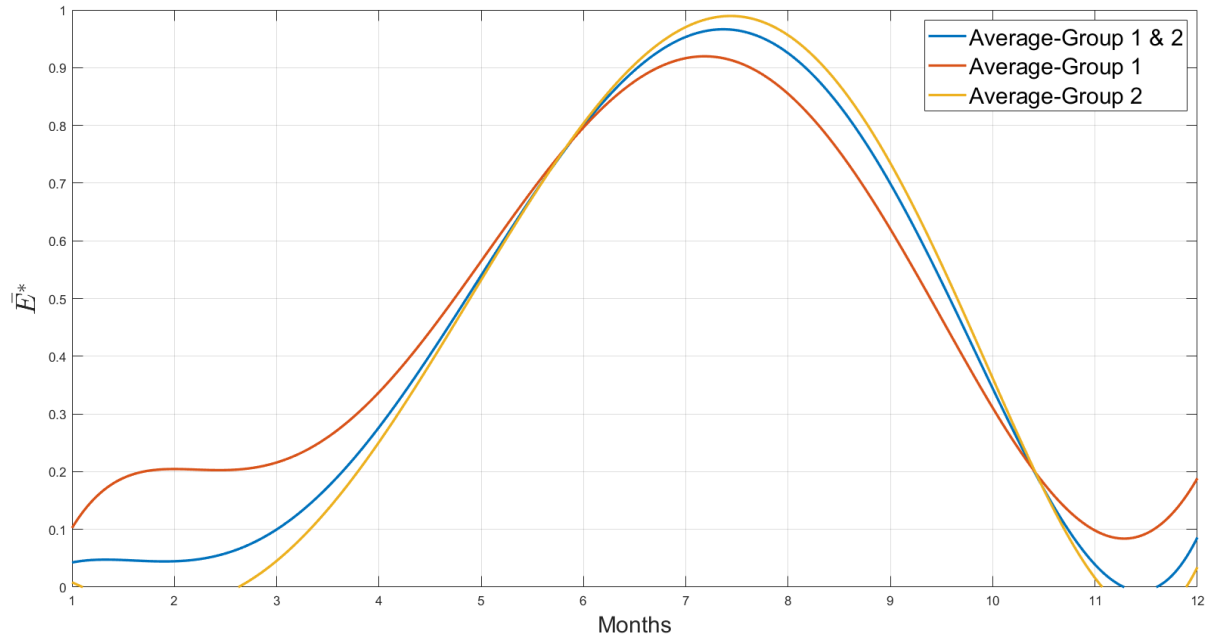

Figure 4.6: Polynomial fitted curves for the average normalized monthly excess heat production graphs in figure 4.5.

An important observation from figure 4.3 - 4.6 is that the group 1 DH plants have production of excess heat the entire year. In comparison, the group 2 DH plants have excess heat form approximately March to November. This indicates differences in excess heat production based on the size of the DH plant. Charging months could therefore not only be limited to the summer months for some DH plants, but include months during the winter when there also is excess heat available. This could result in a small temperature boost in the HT-BTES, which could be beneficial for its performance.

4.3 Generalized heat loss for HT-BTES systems

In order to give an understanding regarding heat loss from a conceptual HT-BTES, the steady-state heat loss will be evaluated and graphically presented in this section. The plots will show how temperature level, size and top surface insulation may impact the steady-state heat loss of a HT-BTES. The heat loss calculations will be in relevance with the presented data from the waste-to-energy DH plants in the previous section.

Figure 4.7 shows different ranges for the supply water in the DH network and the percentage of the contacted DH-plants within these ranges. These temperature ranges show that high charging temperatures are available at all of the DH-plants. This also implies that high storage temperatures can be achieved for all conceptual HT-BTES. As mentioned in the theory chapter, the maximum charging temperature will be 95°C due to material limitations in the BHE. And based on the presented information all DH plants should be able to charge a HT-BTES with water at approximately 95°C.

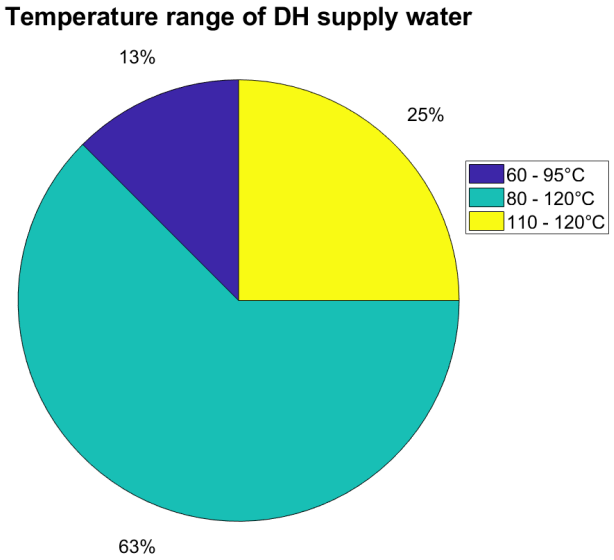

Figure 4.7: Temperature range of the supply water for contacted DH plants.

In order to calculate the storage capacity and respective steady state heat loss for theoretical HT-BTES systems, a few assumptions have to be made first. These assumptions concern the geometry of the storage, insulation, volumetric heat capacity of the ground, and the temperature difference between the maximum and minimum storage temperature (ΔT). These assumptions are presented in table 4.1.

Table 4.1: Assumptions concerning geometry, volumetric heat capacity of the ground and ΔT

Geometry	Aspect ratio = 1
Insulation	Insulation height fraction = 0.1
Volumetric Capacity	2.2 MJ/m^{3}K
ΔT	30 K

The assumption regarding the volumetric heat capacity of the ground is made in order to assume that the ground can hold 0.6 KWh/m^3 if heated 1°C (Gehlin, 2016). By assuming that the ground will be heated with a ΔT of 30K during an annual cycle, the resulting energy the storage can hold becomes 18 KWh/m^3. Based on the presented information in chapter three, a temperature difference between the maximum and minimum storage temperatures of ΔT = 30K is seen as valid. The steady-state heat loss is calculated based on the theory presented by Hellström (1991) in chapter 12 for cylindrical storage with D_i/H = 0.1 and H/R = 2. D_i is the vertical insulation depth (can also be placed horizontally), H is the borehole depth and R is the radius of the storage.

The heat loss will be presented as a dimensionless number Q^* calculated by $Q_{Loss}/Q_{Capacity}$. This is to illustrate how increasing storage capacity decreases the impact of steady-state heat loss. In addition, the components of the steady-state heat loss will be presented as a function of storage capacity and temperature level. The temperature used in the heat loss calculations is the annual local average temperature at the storage boundary, also denoted T_m.

In the calculations and presented figures in this section, the ground conductivity will be k_g = 3 W/mK and the soil conductivity k_{soil} = 1.5 W/mK. Mussel shells with a conductivity of 0.11 W/mK are assumed to be used as insulation material (Plan Energi, 2013). The soil depth is assumed to be 4 meters and the insulation thickness used is 0.5 meters. d_i represents the combined thickness of the soil and insulation material, while λ_i represents their combined thermal conductivity. Results from the steady-state heat loss calculations are presented in figure 4.8 - 4.12.

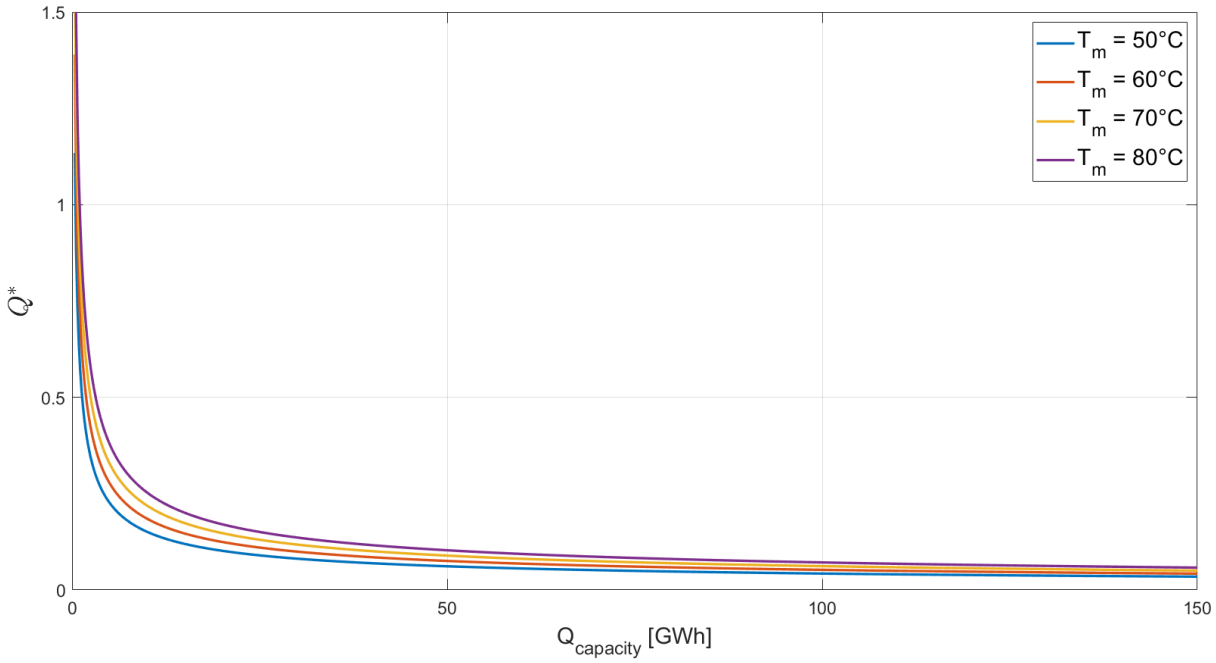

Figure 4.8: Dimensionless parameter Q* versus storage capacity. Results are with a top surface insulation material. $d_i = 4.5$m and $\lambda_i = 0.63$ W/mK.

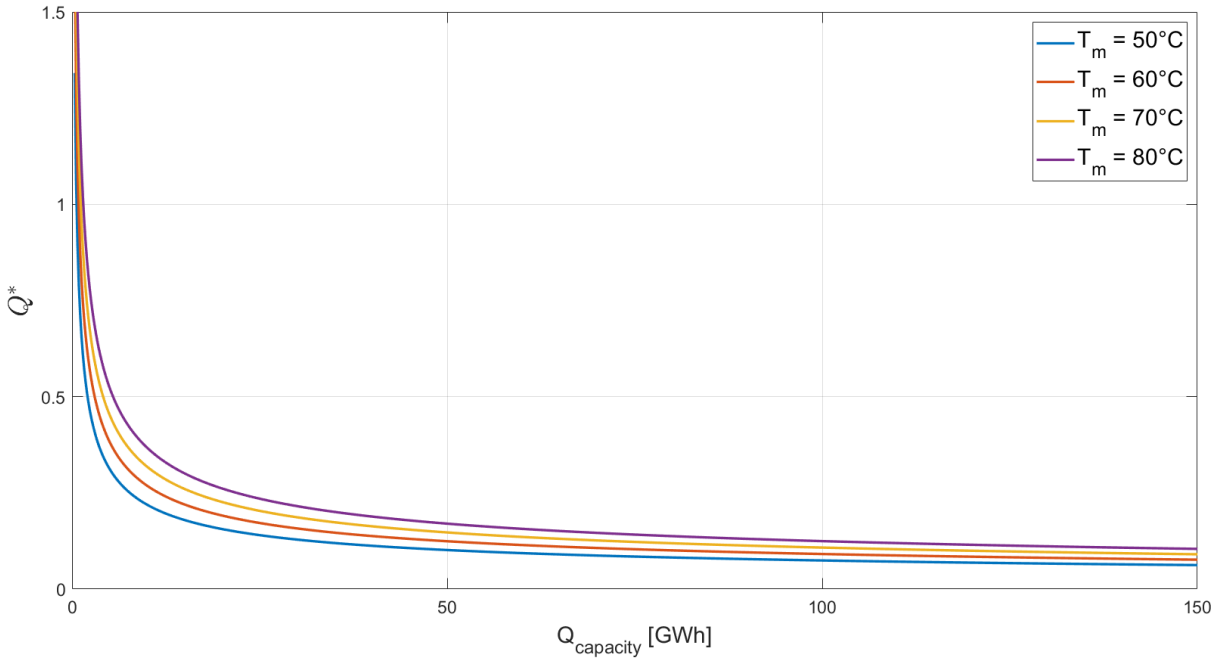

Figure 4.9: Dimensionless parameter Q* versus storage capacity. Results are without a top surface insulation material. $d_i = 4.0$m and $\lambda_i = 1.5$ W/mK.

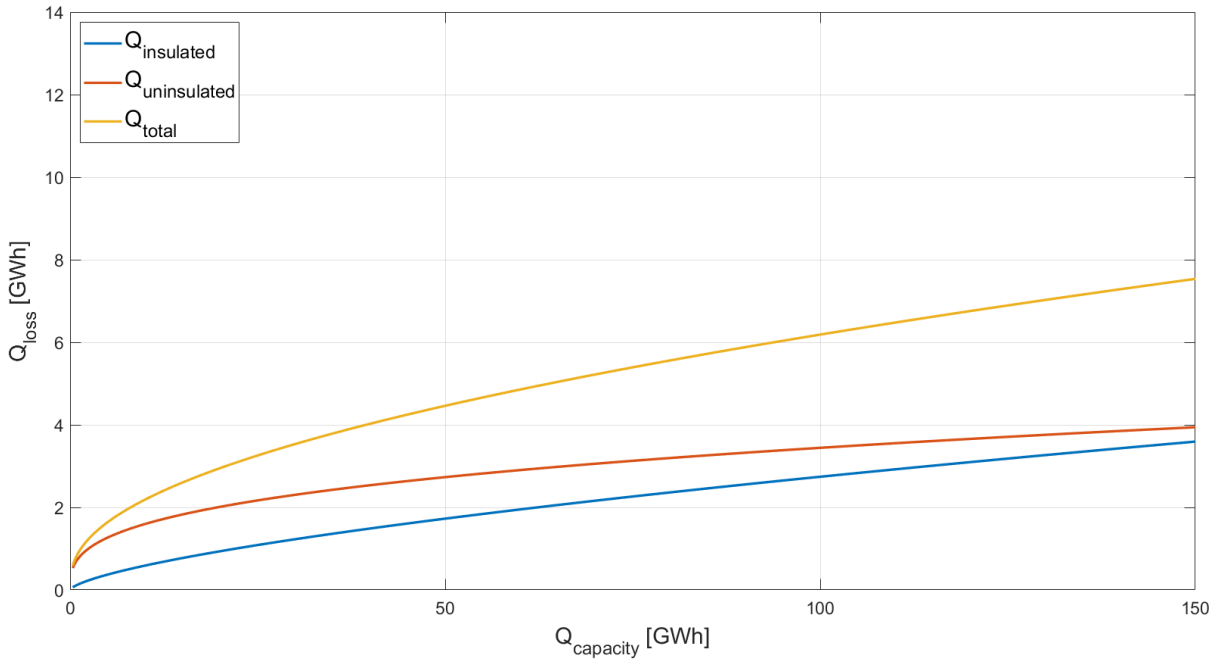

Figure 4.10: HT-BTES heat loss components and total heat loss versus storage capacity for $T_m = 70°C$, $d_i = 4.5m$ and $\lambda_i = 0.63$ W/mK.

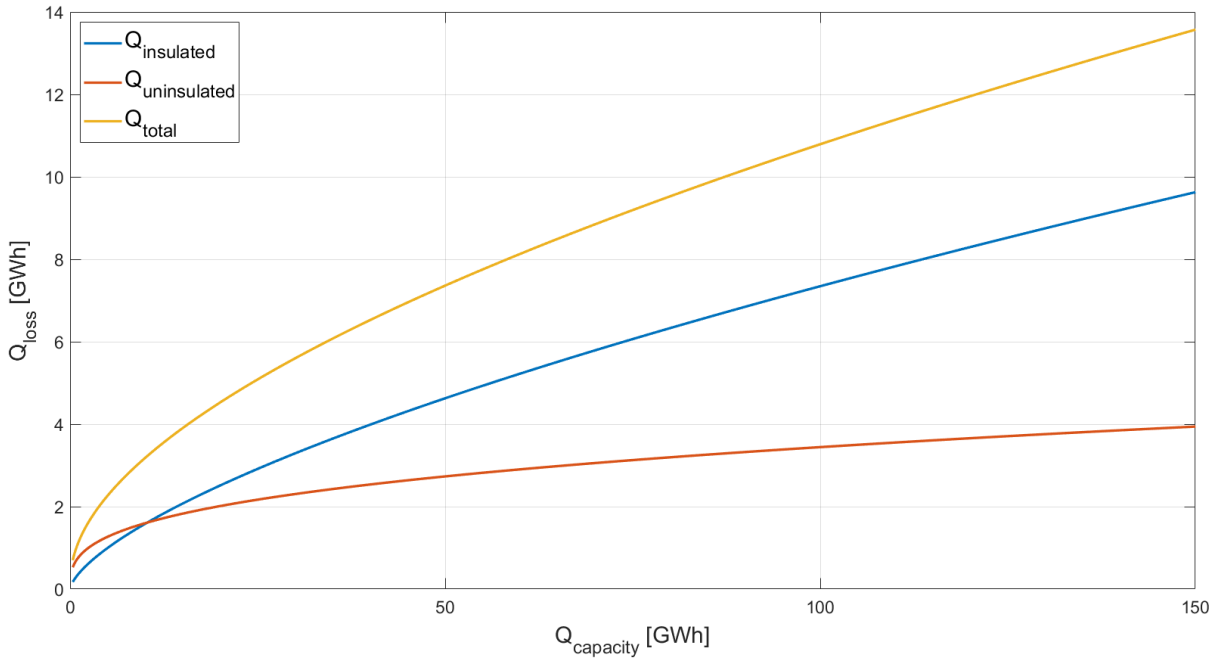

Figure 4.11: HT-BTES heat loss components and total heat loss versus storage capacity for $T_m = 70°C$, $d_i = 4.0m$ and $\lambda_i = 1.5$ W/mK.

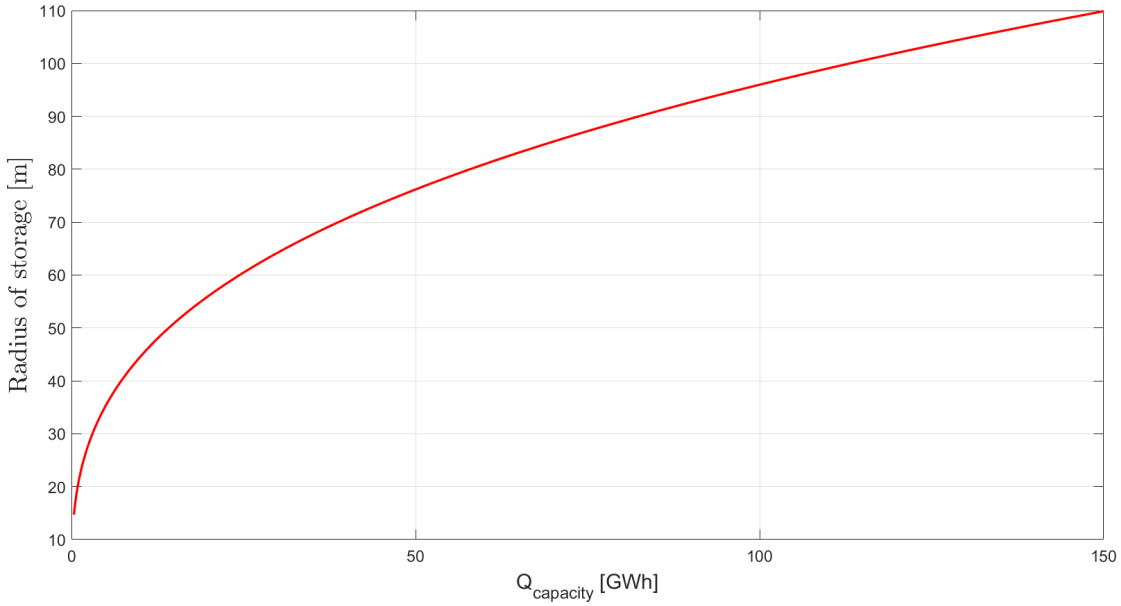

Figure 4.12: Storage radius versus storage capacity. Aspect ratio = 1 and ground volumetric heat capacity = 2.2 MJ/m^{3}K.

Figure 4.8 and 4.9 show that the dimensionless value Q* has a asymptotic behaviour. With an increased storage capacity, the importance of the steady-state heat loss decreases. In addition to this, the impact of higher T$_m$ on the steady-state heat loss also significantly decreases with increasing storage capacity. Figure 4.8 and 4.9 also show the impact of not using an insulation material on the top surface. Figure 4.9 shows the uninsulated results and it can be observed that the graph moves upwards to a higher asymptotic value and has a greater difference between each temperature level.

The total steady-state heat loss will be composed of two components, the uninsulated part and the insulated part of the storage. The uninsulated is only in contact with the surrounding ground, while the insulated part is in contact with the ambient air. Figure 4.10 and 4.11 show the importance of the insulation material on these two components. The figures show that there is a significant difference in the insulated heat loss component and consequently, also total heat loss. However by evaluating figure 4.8 to 4.11 simultaneously it is exposed that the impact of using an insulation material is most significant for lower capacity HT-BTES systems.

Figure 4.12 shows how the radius of the storage increases with the storage capacity. This graph is for a HT-BTES with aspect ratio = 1, which means that the depth of the borehole will be 2 × R. The radius increases rapidly to approximately 25 GWh before it increases more linearly. This is the development of a cubic root (x$^{1/3}$). This is because the capacity is a function of the volume and for an aspect ratio = 1, the radius is calculated as R = $(\frac{V}{2\cdot\pi})^{1/3}$.

4.4 Insulation alternative

Insulation of the top surface is an important parameter to consider for the HT-BTES system. The economy plays a crucial role and both insulation material and its thickness will increase the investment cost of the project. It is there essential to evaluate different technical possibilities that can reduce the investment cost of the project.

The purpose of the insulation material is to add a significant thermal resistance with a minimal impact on the thickness of the top layer. Small material thickness can only be achieved by using materials with low thermal conductivity. Equation 4.2 shows how conductive thermal resistance is calculated for a plane wall. R [m^2K/W] is the resistance, t [m] is the thickness, A is the contact area and k [W/mK] is the thermal conductivity.

$$R_{cond} = \frac{t}{kA} \tag{4.2}$$

Equation 4.2 show that thermal resistance also can be increased by increasing the thickness of the material. This highlights the possibility of utilizing the rock in the ground as insulation material. The HT-BTES will then have a depth of insulating rock volume before the actual storage and heat exchange begins, also called the header depth. Figure 4.13 shows the equivalent rock depth if the rock is used to insulate instead of mussel shells. The drilling cost of a few extra meters can be lower than the cost of the insulation material and then making this a more economically feasible solution. Figure 4.13 also shows that for higher ground/rock thermal conductivity values, the equivalent rock depth increases.

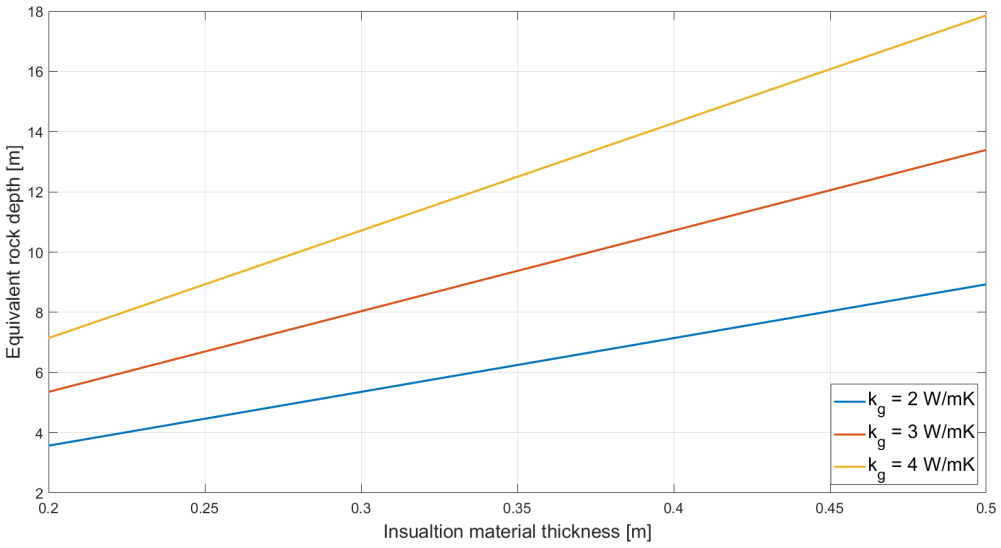

Figure 4.13: Equivalent rock depth for variable ground conductivity (k_g).

Chapter 5

Thermal Analysis

In this chapter, a thermal analysis of a non-grouted HT-borehole will be performed in order to gain more knowledge regarding the thermal process in HT-boreholes. The thermal analysis will be in combination with an analysis of the conceptual operational strategy, named "nightboosting" in this thesis. The nightboosting operational strategy is a more dynamic operation of the HT-BTES, making it a seasonal and short term thermal energy storage. Nightboosting is an operational measure, which could increase the HT-BTES system performance and storage and heat carrier temperatures. Sensitivities for the nightboosting concept will be simulated and evaluated in order better to understand the concept and its behaviour during different circumstances.

5.1 Nightboosting

Nightboosting is a conceptual operational strategy found of interest, based on the findings presented in chapter three and four. Chapter three show that the design of the HT-BTES is important, but that the operation of the HT-BTES system can significantly influence the actual performance of the HT-BTES system solution. Chapter four pointed out that excess heat was available during the entire year for some of the waste-to-energy DH plants. Nightboosting is an operational measure seeking to improve the operation of HT-BTES systems and utilizing excess heat or available heat all year round.

Figure 4.6 shows that excess heat for some of the district heating plants is available almost the entire year. This heat should be stored during the winter months, and this can give a slight boost to the storage temperature. Nightboosting concerns energy storage during the night and excess or available heat during this period was not outsourced in the feasibility study. The concept could therefore be applicable for all DH plants analyzed in chapter four.

Nightboosting intends to charge the HT-BTES for a certain amount of time during the night, both during the discharging and charging season. This is to give a short term temperature boost of the borehole its surrounding ground. With this boost, the HT-

BTES system could possibly contribute greater to peak loads during the day and operate at higher temperature levels longer. The impact of nightboosting could therefore improve the performance of the HT-BTES system solution.

5.2 Simulation model

In order to accurately model the transient behavior of a non-grouted BHE during a short time interval, a numerical model has to be used. Since the simulation time will be between 24 and 168 hours, it is reasonable to assume that there will be no thermal interaction between adjacent boreholes (Nordell, 1994). Based on this time limitation it will be sufficient to simulate only one HT-borehole in thermal analysis in order to evaluate the short-time effect of nightboosting on HT-boreholes.

The simulation model used in the thermal analysis is a numerical model for non-grouted boreholes and is developed by Holmberg (2016) in the software MATLAB. The model is developed specifically for non-grouted boreholes, where heat transfer by natural convection is essential. A simplified numerical model is used, and the model can be categorized as a thermal resistance and capacity model (TRCM) (Holmberg, 2016). In the thermal resistance and capacity model the thermal resistance within the borehole is described by applying an analogy to electric networks. Also, a geometrical simplification is made where the different parts inside the borehole are described by single nodes (Holmberg, 2016). A numerical grid describes the bedrock around the borehole in two or three dimensions, and the borehole, BHE, and heat carrier fluid are simulated as one-dimensional features. The model developed by Holmberg (2016) uses the TRCM concept and finite difference method. The benefit of this is that it enables transient simulations of the non-grouted borehole with a high level of accuracy.

An advantage of the model is that it is accurate on a timescale of minutes while being fast enough to allow parameter studies of the transient behavior of the borehole (Holmberg, 2016). The simulation model was validated by comparing its simulation results with detailed measurements from both a distributed thermal response test (DTRT) and heat pump operation (Holmberg, 2016). The was performed by varying different parameters and for both injection and extraction scenarios. The results and shows that the numerical model can accurately capture the transient behavior of a non-grouted borehole down to a timescale of minutes (Holmberg, 2016). The numerical simulation model uses the conventional single U-tube BHE, but can be altered in order to use both the double U-tube and coaxial design. A more detailed review of the TRCM models and the evaluation of the developed simulation model is presented in Holmberg (2016).

5.2.1 Software

MATLAB (Matix laboratory) is a mathematical software used for numerical calculation, simulation, and visualization. It is a high-performance language and is programmed in an easy to use environment with familiar mathematical notations. One of the main benefits of MATLAB is the computation time, especially for problems with matrix and vector formulations. MATLAB also offers a high degree of flexibility and transparency, and the non-grouted borehole model was therefore developed in MATLAB (Holmberg, 2016).

5.2.2 Heat transfer

In this subsection, the heat transfer circuit and equations used in the simulation model will be briefly explained and introduced. This is in order to give a general understanding of the heat transfer process in the simulation model. It is important to specify that some of the symbols used in this subsection differ from the previously used symbols.

Figure 5.1 shows the thermal Y-circuit in the simulation model, where two nodes represent the heat carrier fluid, and one node represents the groundwater in the borehole (Holmberg, 2016). Assumed in the model is that there is no direct contact between the BHE pipes, or between the BHE and borehole wall. The position of the BHE inside the borehole is not explicitly defined in the model, and heat transfer is expressed as a resistance between heat carrier temperature (T_f) and temperature of groundwater (T_w) in the borehole. Also, the thermal capacity of the BHE wall is neglected since its impact will be minimal on the transient behavior of the model (Holmberg, 2016).

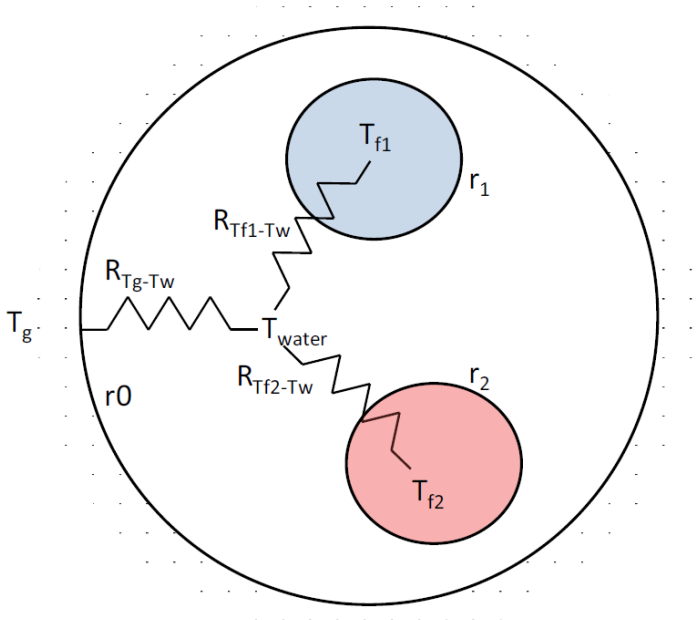

Figure 5.1: Thermal resistance circuit of the numerical simulation model (Holmberg, 2016).

The expression for the borehole resistance R_b can be expressed based on the Y-circuit given in figure 5.1. This results in the following equation:

$$R_b = R_{T_g - T_w} + \frac{1}{\frac{1}{R_{T_{f1}-T_w}} + \frac{1}{R_{T_{f2}-T_w}}} \tag{5.1}$$

Where the three other resistances are defined as:

$$R_{T_{f1}-T_w} = \frac{1}{2\pi r_{11} h_{c11}} + \frac{\ln(r_{12}/r_{11})}{2\pi k_c} + \frac{1}{2\pi r_{12} h_{c21}} \tag{5.2}$$

$$R_{T_{f2}-T_w} = \frac{1}{2\pi r_{21} h_{c12}} + \frac{\ln(r_{22}/r_{21})}{2\pi k_c} + \frac{1}{2\pi r_{22} h_{c22}} \tag{5.3}$$

$$R_{T_g-T_w} = \frac{1}{2\pi r_0 h_0} \tag{5.4}$$

The two first terms in $R_{T_{f1}-T_w}$ and $R_{T_{f2}-T_w}$ represent the internal thermal resistance within each BHE tube. The last terms represent the influence of natural convection along with the resistance $R_{T_g-T_w}$, T_g represents the temperature of the borehole wall. The natural convection resistance terms are calculated based on geometrical values and the heat transfer coefficient; h_0, h_{c21}, h_{c22}. These three coefficients are determined by the Nusselt correlation derived in (Holmberg, 2016). It is desirable to have a slightly turbulent flow within the U-tube BHE since it will result in a higher heat transfer coefficient compared to laminar flow. For the turbulent flow, the following equations are used to calculate the Nusselt number and heat transfer coefficients.

$$Nu = \frac{(f/8)(Re - 1000)Pr}{1 + 12.7(f/8)^{0.5}(Pr^{2/3} - 1)} \tag{5.5}$$

$$f = (0.790 \ln(Re) - 1.64)^{-2} \tag{5.6}$$

$$h = \frac{Nu \cdot D}{k} \tag{5.7}$$

With the one dimensional simplification of the borehole, BHE and heat carrier fluid as well as assuming that the heat carrier fluid is incompressible, the borehole can be accurately represented using only the energy equation in one dimension (Holmberg, 2016). The one-dimensional energy equation is given by equation 5.8.

$$\pi r^2 \rho \frac{\partial u}{\partial t} + \pi r^2 \rho V \frac{\partial u}{\partial z} = S \tag{5.8}$$

u is the internal energy of the fluid, r is the inner radius of the BHE tube, V is the bulk velocity and S is a source term for convective heat transfer. Equation 5.8 can be rewritten to equation 5.9:

$$\pi r^2 \rho C \frac{\partial T}{\partial t} + \pi r^2 \rho V C \frac{\partial T}{\partial z} = S = \frac{\Delta T}{R} \tag{5.9}$$

In equation 5.9, C is the specific heat capacity of the heat carrier fluid while ΔT represents the temperature difference between the average fluid temperature and groundwater or borehole wall. R is the respective resistance, calculated with equation 5.2 - 5.4. The ground surrounding the borehole is as mentioned discretized with an axis-symmetric cylindrical grid so that heat is transferred in the radial direction, see figure 5.2. Heat in the ground is only transferred through conduction, and a coupling between the thermal process in the borehole and the ground is made through a heat flux boundary condition on the borehole wall (Holmberg, 2016). By combining the respective thermal process with equation 5.9, the heat transfer in the borehole can be summarized by the following equations:

$$\pi {r_0}^2 \rho_w C_w \frac{\partial T_w}{\partial t} + \pi {r_0}^2 \rho_w V_w C_w \frac{\partial T_w}{\partial z} = \frac{\Delta T_{T_g - T_w}}{R_{T_g - T_w}} + \frac{\Delta T_{T_{f1} - T_w}}{R_{T_{f1} - T_w}} + \frac{\Delta T_{T_{f2} - T_w}}{R_{T_{f2} - T_w}} \tag{5.10}$$

$$\pi {r_1}^2 \rho_f C_f \frac{\partial T_{f1}}{\partial t} + \pi {r_1}^2 \rho_f V_{f1} C_f \frac{\partial T_{f1}}{\partial z} = \frac{\Delta T_{T_{f1} - T_w}}{R_{T_{f1} - T_w}} \tag{5.11}$$

$$\pi {r_2}^2 \rho_f C_f \frac{\partial T_{f2}}{\partial t} + \pi {r_2}^2 \rho_f V_{f2} C_f \frac{\partial T_{f2}}{\partial z} = \frac{\Delta T_{T_{f2} - T_w}}{R_{T_{f2} - T_w}} \tag{5.12}$$

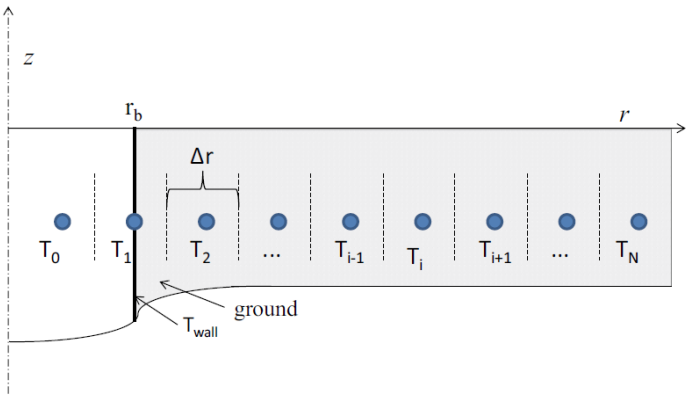

Figure 5.2: Section of the cylindrical grid and an illustration of the coupling between the thermal process in the borehole and surrounding ground. T_0 is a ghost node used in the implementation of the heat flux boundary condition (Holmberg, 2016).

5.2.3 Model adaptions

In order to simulate a HT-borehole some adaptions had to be made in the simulation model. Since the temperature of the heat carrier is well above 0 °C, the heat carrier was changed from being an alcohol/water mixture to pure water. This will increase the thermal properties of the heat carrier fluid slightly. In addition to this, the temperature of the surrounding ground was assigned higher temperatures values, ranging from 20°C to 90°C. This was in order to simulate the scenario of a HT-borehole in a HT-BTES at different temperature levels. A new load cycle is also implemented in order to simulate the effect of nightboosting and different heating loads. This is explained more in subsection 5.2.5.

5.2.4 Simulation Parameters

The parameters listed in table 5.1 are the key parameters for the simulated HT-borehole. These values are set initially before the simulation and not calculated during the simulation. Nightboosting sensitivity is analyzed by altering a specific parameter and comparing the results. Parameters investigated are the ground temperature, q_{charge}, borehole depth, ground conductivity, and mass flow. This is performed in order to increase the understanding of both nightboosting and the thermal process in HT-boreholes.

In the simulation model, ground temperatures are prescribed a constant value at the top of the surface and increases linearly due to the temperature vertical ground gradient in the ground. For a 100 meter deep borehole, the temperature on the top and bottom of the borehole will consequently be 60°C and 62°C, if prescribed a ground temperature of 60°C. There is no heat loss during the simulations, and this is assumed reasonable for simulations with only one week simulation time or less. The vertical ground gradient is used since a vertical stratification can occur in a HT-BTES.

5.2.5 Load cycle

Table 5.2 shows the daily load cycle used in the simulation model. Both the morning peak and mid-day peak load are included in order to observe the temperature effect on both. Charging is assumed to be possible from 00.00 - 06.00 based on the user profile in NS 3031:2014 (Standard Norge, 2014). This load cycle is implemented in the simulation model, and the daily load cycle will be repeated for simulations with a simulation time of one week. The peak, base and charging loads are general values used to analyze the HT-borehole and illustrate the effect of nightboosting. Actual loads may differ from those used during this thermal analysis.

Table 5.1: Parameter values for the initial benchmark simulations.

Parameter	Value	Unit
Massflow	0.5	kg/s
Borehole depth	100	m
Borehole diameter	0.140	m
Collector type	Single U-tube	n/a
Collector inner radius	0.0176	m
Collector outer radius	0.020	m
Collector material conductivity	0.42	W/mK
Ground conductivity	3	W/mK
Ground temperature(top surface)	60	°C
Temperature gradient	0.02	°C/m
$q_{Baseload}$	-40	W/m
$q_{Peakload}$	-80	W/m
q_{Charge}	40	W/m

Table 5.2: Daily load cycle with and without nightboosting

Time	Load
00.00 - 06.00	0 or q_{charge}
06.00 - 08.00	$q_{Peakload}$
08.00 - 16.00	$q_{Baseload}$
16.00 - 18.00	$q_{Peakload}$
18.00 - 24.00	$q_{Baseload}$

5.3 Nightboosting evaluation

In the following section, nightboosting and the resulting thermal process in a HT-borehole will be evaluated. The evaluation will be done through multiple simulations assessing nightboosting as a concept and its parameter sensitivity. The evaluation has the purpose of increasing knowledge concerning the conceptual operational strategy nightboosting, and the thermal process in a HT-borehole.

The parameters for the simulation setup and the main load cycles are described in the two previous subsections. These values are used to simulate two base cases, one with and one without nightboosting. The resulting temperature development for the outgoing heat carrier temperature (T_{out}) in both base cases is plotted in figure 5.3 and 5.4. From the results, it is observed that nightboosting has the most significant impact on the morning peak load. The temperature difference after 6 hours is 4.4°C and 1.49°C after 8 hours. The results in figure 5.4 shows that the temperature difference between the load cycle

with and without nightboosting increases throughout the week. After 150 hours the temperature difference is 5.11°C and 2.18°C after 152 hours.

These results show that nightboosting has a reasonable effect on T_{out}. Nightboosting could therefore increase the amount of usable heat supplied directly or increase the seasonal coefficient of performance (SCOP) of a heat pump using T_{out} as a heat source. The sensitivity analysis will map further characteristics of nightboosting and visualize the influence on the temperature development of the outgoing heat carrier temperature.

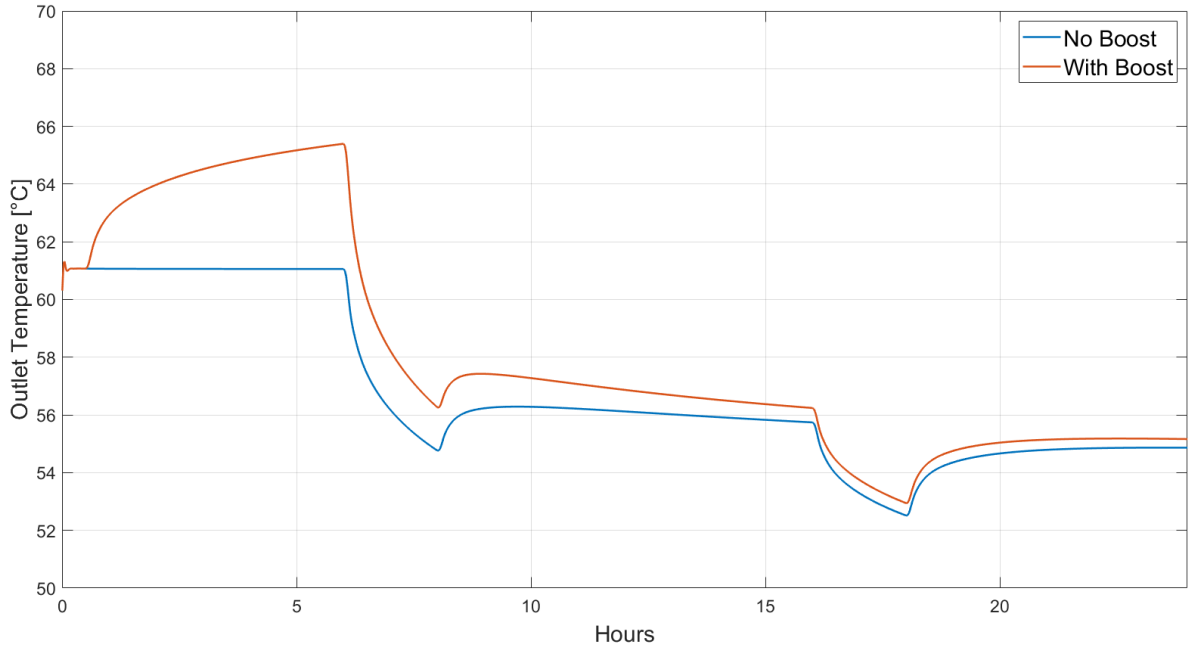

Figure 5.3: Temperature development for T_{out} in a single HT-borehole over 24 hours.

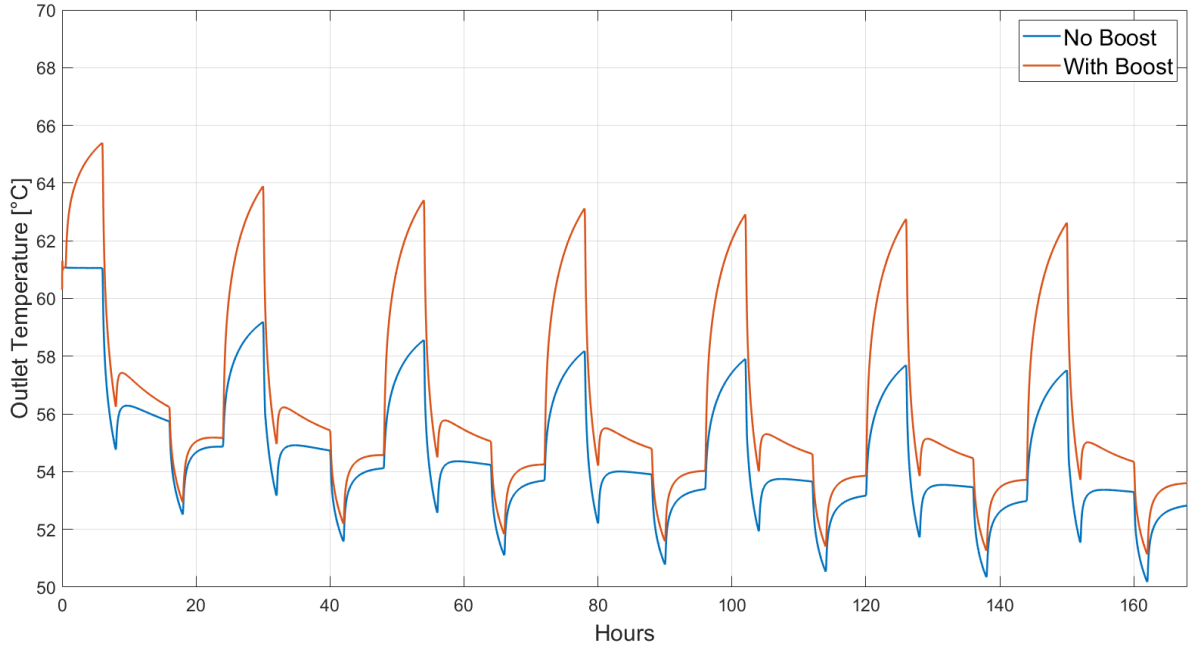

Figure 5.4: Temperature development for T_{out} in a single HT-borehole over 168 hours.

5.3.1 Ground temperature

In figure 5.5 the temperature of the surrounding ground has been varied in order to analyze its effect. The results presented in figure 5.5 show that the effect of nightboosting seems to be independent of the temperature of the surrounding ground. However, a closer look at the results shows that there are small differences caused by the ground temperature. The temperature difference between nightboosting and no nightboosting increases slightly for lower ground temperatures. The difference is however only visible during the last 3 hours of nightboosting and in a magnitude of 0.05 - 0.2 kelvin.

The results in figure 5.5 shows that the use of nightboosting affects almost independent of the ground temperature. Even at high ground temperatures, a boost of the surrounding ground could be desirable in order to reduce the temperature decline in the borehole. It must also be specified that if the ground temperature is too high, no nightboosting will be possible. This is because of the borehole thermal resistance, which requires an absolute temperature difference between T_f and T_b to transfer the desired amount of heat. At high ground temperature T_f will consequently be limited by the temperature limitation in the BHE material.

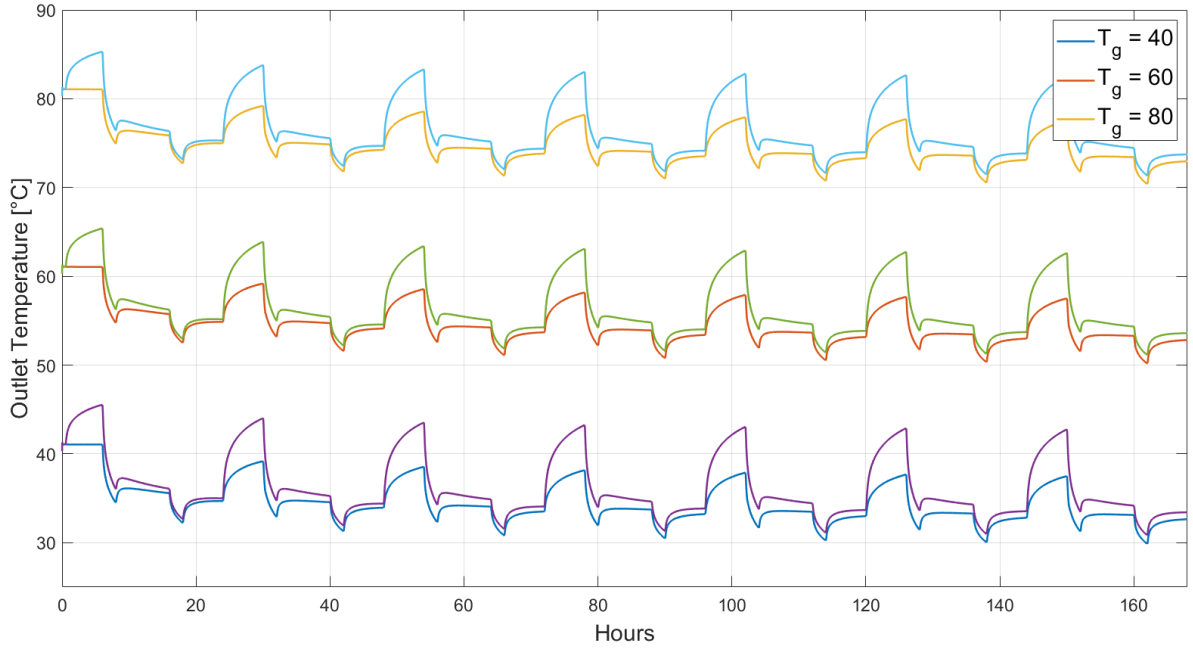

Figure 5.5: Temperature development for T_{out} in a HT-borehole at different ground temperatures.

5.3.2 Charging rates

Perhaps the most important parameter in the nightboosting concept is the charging rate q(W/m). This parameter determines the amount of energy that injected into the ground during nightboosting. Figure 5.6 and 5.7 shows the temperature development for different charging rates. The results show that increasing the charging rate increases the effect of nightboosting. This is understandable since more energy is injected into the ground. The charging rates are simulated in increments of 20 W/m, and the effect of increasing the charging rate is close to equal for each increment. Figure 5.6 also shows that the effect of nightboosting is most significant for the first 0 - 15 hours.

Figure 5.7 shows that the impact of nightboosting increases throughout the week. With a charging rate of 80 W/m the temperature difference between a load cycle with nightboosting and without nightboosting after 150 and 152 hours is 9.97°C and 4.32°C respectively. The results consequently show that there is a significant potential regarding nightboosting, but that it also is very dependant on the available energy during the hours of nightboosting. With increasing amounts of available energy and consequently increasing charging, a more significant effect from nightboosting is possible to achieve.

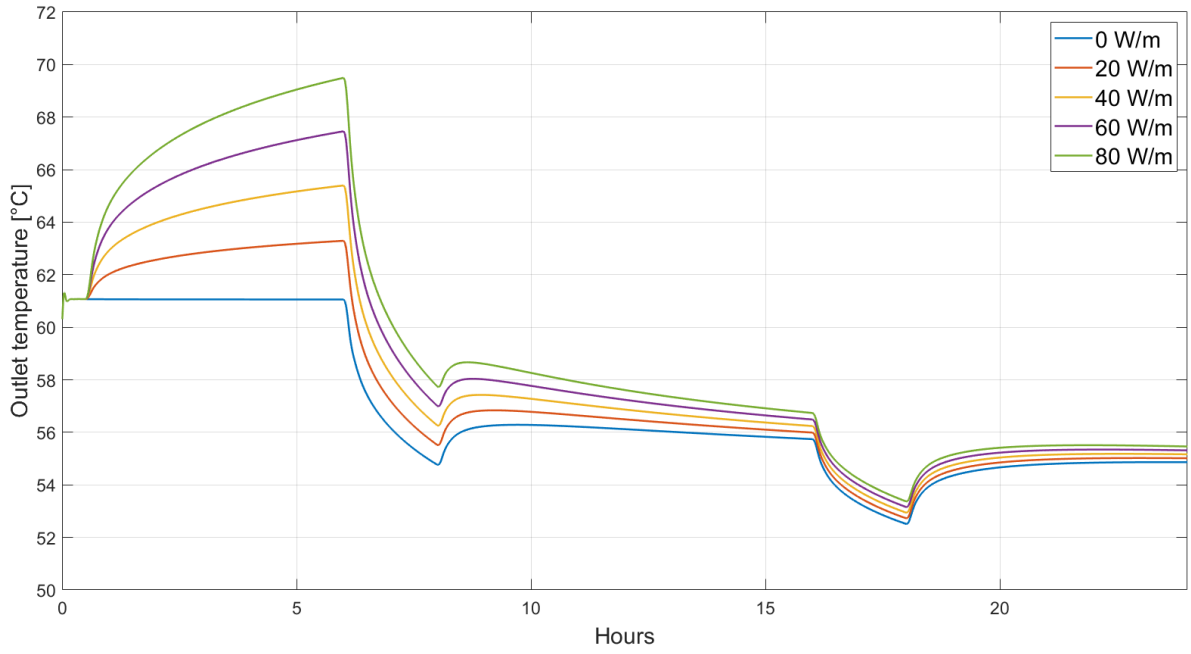

Figure 5.6: Temperature development for T_{out} during a daily cycle with different charging rates.

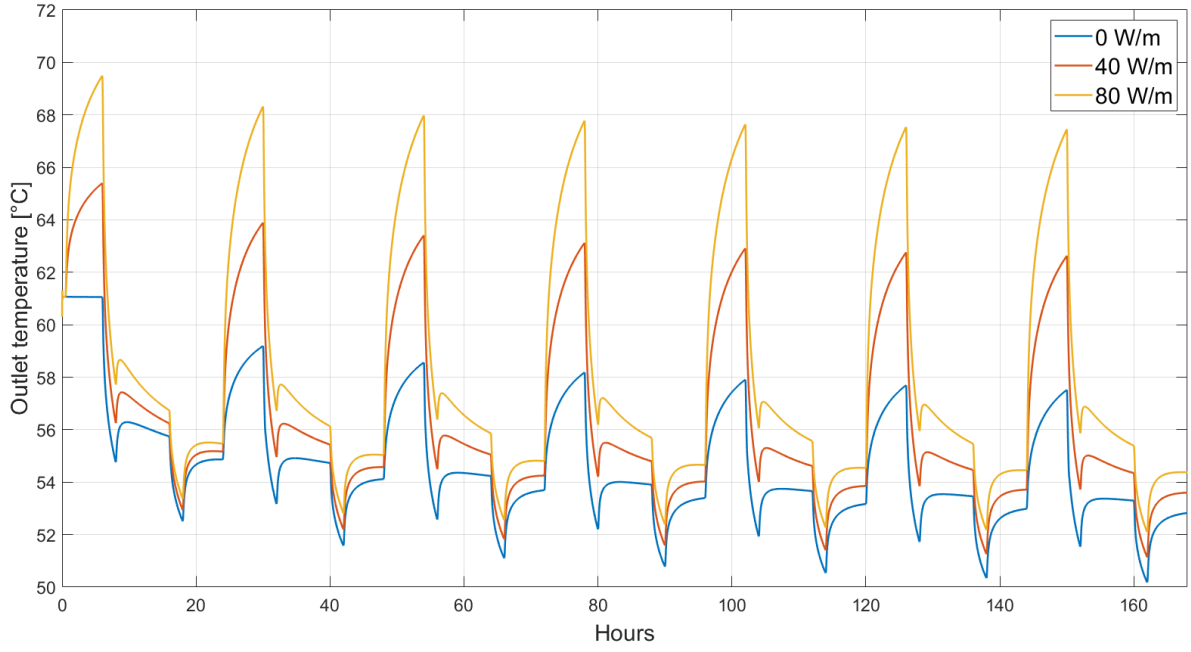

Figure 5.7: Temperature development for T_{out} during a weekly cycle with different charging rates.

5.3.3 Borehole depth

The results presented in figure 5.8 shows the effect of increasing borehole depth. The injection and extraction rates (W/m) are equal, therefore with increasing borehole depth, more heat (W) is extracted from or injected into the HT-borehole. Since more heat is extracted or injected for deeper boreholes, and mass flow and specific heat capacity are constant values, the absolute value of the temperature difference T_{in} - T_{out} increases with increasing borehole depth. If an equal amount of heat is to be extracted or injected, deeper boreholes would be beneficial since the heating rate (W/m) would be lower.

Figure 5.8 shows that T_{out} increases significantly with increasing borehole depth. Simulations with and without a ground gradient reveal that this is mostly due to the ground gradient. The ground gradient increases the average ground temperature for increasing borehole depths, which consequently increases T_{out}. By analyzing the effect of increasing borehole depth, but without a ground gradient, the effect of increasing borehole depth is far less significant. For 200 and 300 meters, no temperature difference is observed, while a close to constant difference of approximately 0.33 K is observed between 100 and 200-meter borehole depth. By comparing the results with and without the ground gradient, it is found that the effect of the ground gradient increases with increasing borehole depth. The temperature difference between the results after 168 hours is 0.11K, 1.50K and 3K for 100, 200 and 300-meter borehole depth, respectively.

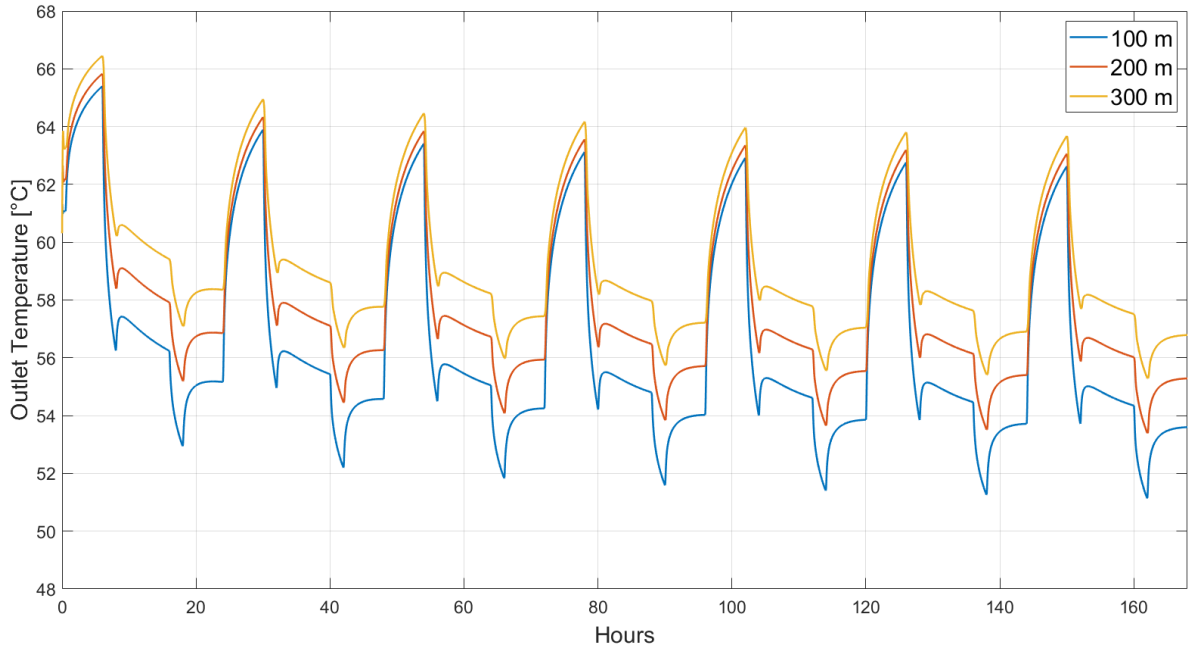

Figure 5.8: Temperature development for T_{out} with different borehole depths. Ground gradient = 0.02 °C/m.

5.3.4 Ground conductivity

The conductivity of the ground is an important parameter in the heat transfer processes in the HT-BTES and the ground surrounding a HT-borehole. A low ground conductivity implies a higher thermal resistance than for a higher ground thermal conductivity value. Equation 2.7 shows that a higher total resistance will increase the temperature difference T_f - T_m. This is observed in figure 5.9. Since the average ground temperature is close to equal for each k_g value, T_f will be lower with decreasing k_g. As a consequence of this so will T_{out} also, observed in figure 5.9.

The presented results are however only over a week, so heat loss and thermal interaction between boreholes are therefore not accounted for in the simulations. A lower ground thermal conductivity will result in a lower heat loss for a single HT-borehole and HT-BTES, while a higher conductivity will decrease the ground resistance. This implies that low ground thermal conductivity could be desirable in a longer time perspective and high ground thermal conductivity for shorter time perspectives. An annual evaluation must therefore be performed in order to understand better the impact of higher and lower values over a longer time interval.

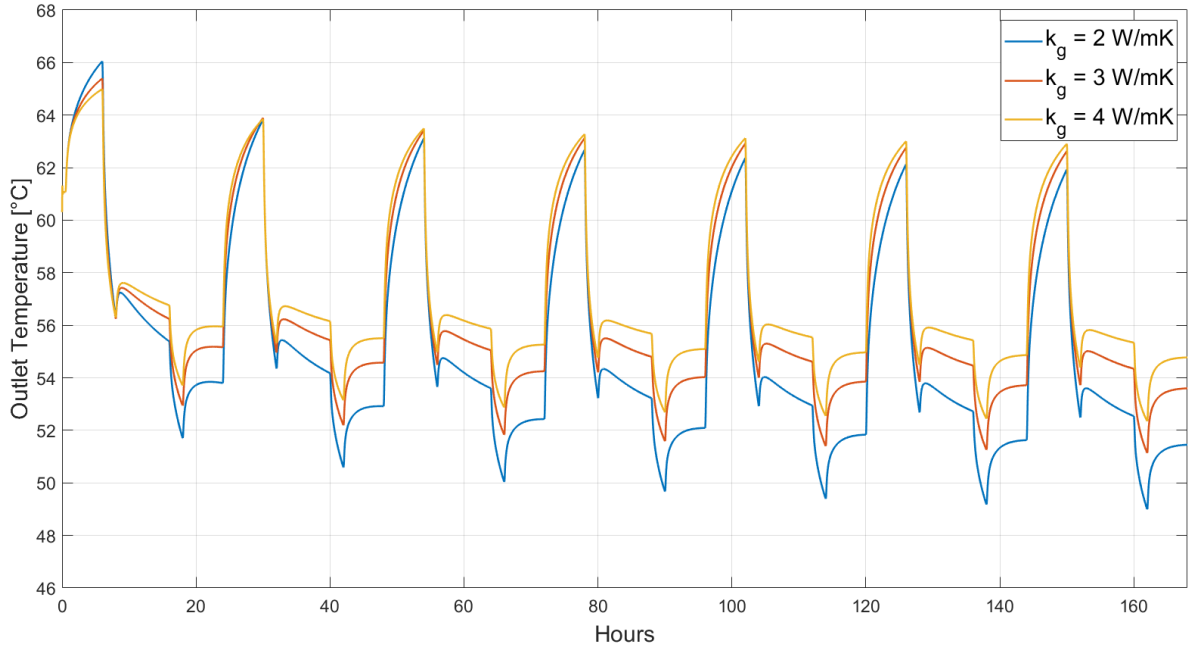

Figure 5.9: Temperature development for T_{out} with different ground thermal conductivity.

5.3.5 Massflow

The mass flow can be altered in order to vary the heat transfer in a single HT-borehole or HT-BTES system. Described by equation 5.13, where $\dot{m}$ is the mass flow, c_p is the specific heat capacity of the heat carrier fluid and ΔT is the heat carrier temperature difference (T_{in} - T_{out}). If the heat transfer rate Q is kept constant, but the mass flow increased, then ΔT will decrease and visa versa if the mass flow decreases. Simulation results are presented in figure 5.10 and 5.11 for 0.5 kg/s and 1.5 kg/s respectively. The reduction in ΔT is clearly observed from 0.5 kg/s to 1.5 kg/s, and another important observation is that T_{out} increases due to the reduction in ΔT.

The mass flow will also directly influence the velocity of the heat carrier fluid inside the pipes of the BHE and consequently also impact the pressure loss, see eq. 5.14. It is important to note that the heat transfer rate develops proportionally with the mass flow rate while the pressure loss develops quadratic. Pressure loss can have a significant impact on the operational cost of the HT-BTES system since increasing pressure loss requires increasing pumping power.

The mass flow rate will also impact the convective heat transfer coefficient since mass flow and fluid velocity is directly correlated. The correlation is observed through equation 5.5 as the nusselt number is dependant on the Reynolds number, which again is dependant on the fluid velocity. Higher mass flow rates therefore result in higher convective heat transfer coefficients, which reduces the convective thermal resistance in the BHE.

$$Q = \dot{m} \cdot c_p \cdot \Delta T \tag{5.13}$$

$$\Delta P = f \cdot \frac{L \cdot \rho \cdot V^2}{D_h \cdot 2} \tag{5.14}$$

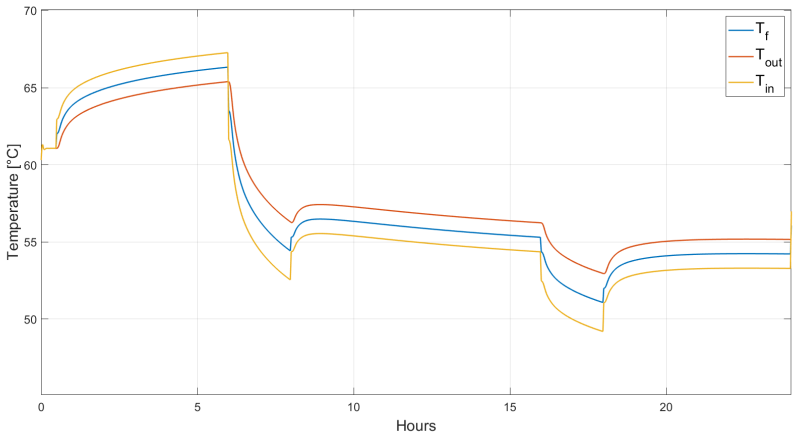

Figure 5.10: T_{in}, T_{out} and T_f development with mass flow = 0.5 kg/s.

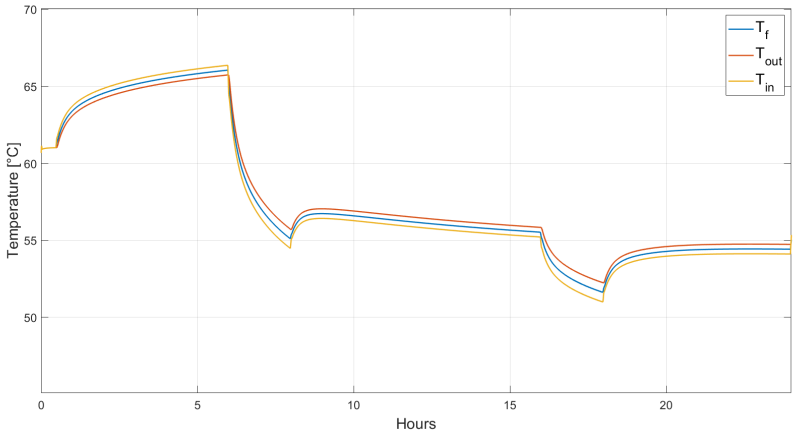

Figure 5.11: T_{in}, T_{out} and T_f development with mass flow = 1.5 kg/s.

5.3.6 Gradient development

Three different scenarios were simulated in order to visualize the lasting effect of nightboosting on the temperature development of T_{out}. These three scenarios had different nightboosting charging loads for the first six hours, while for the remaining 162 hours, all three had a constant extraction load of 40 W/m. Figure 5.12 shows the temperature development of T_{out} for all three scenarios. The results show that the temperature development is close to equal after approximately 60-80 hours. The temperature development again shows the significant effect of nightboosting on the thermal process inside the borehole. Simulations performed for lower and higher extraction loads showed that the value of the extraction load did not influence the duration of time for which nightboosting affected the development of T_{out}. The charging rate is therefore solely responsible for the difference observed in figure 5.12.

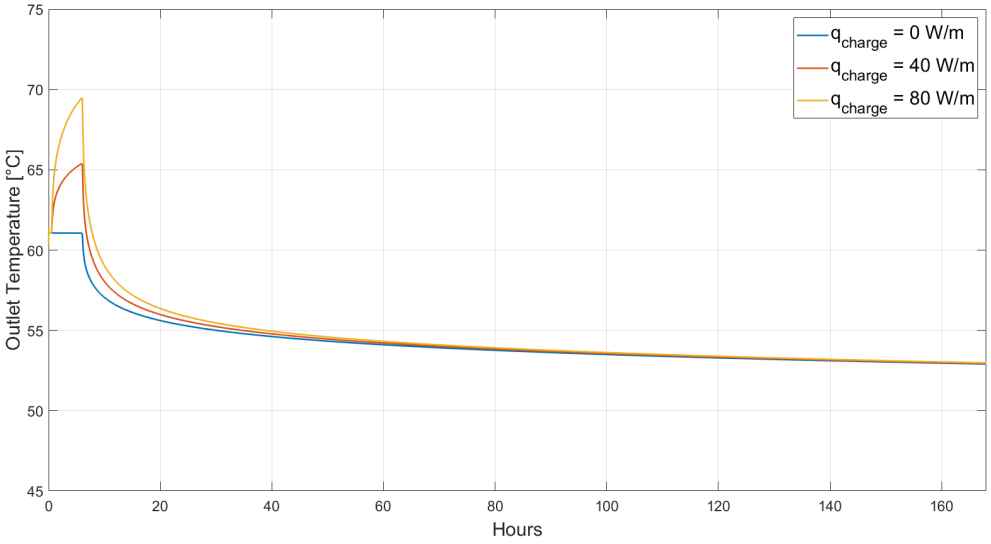

Figure 5.12: T_{out} for three cases with different charging rates and equal discharging rate.

5.4 Software evaluation

A comparison between simulation software is performed in order to evaluate the modeling of short time transients in TRNSYS 17(Transient system simulation program). This evaluation was also performed in order to compare results from the MATLAB model with other simulation software. Low-temperature results from the modified MATLAB model were compared with results from the unmodified model in order to evaluate its validity. The comparison gave similar results, and the modified model is therefore assumed to have the most accurate results compared to TRNSYS.

The simulation setup will be equal for each simulation software as far as parameter restrictions allow. The ground will have an initial top surface temperature of 60°C and a ground gradient of 0.02°C/m. The MATLAB model simulates non-grouted boreholes, which is not possible in TRNSYS. This is accounted for through the fluid to ground thermal resistance and will be further explained in subsection 5.4.1.

5.4.1 TRNSYS model

TRNSYS is a software used to simulate the behavior of transient systems (TRNSYS, 2020a). The software consists of multiple components found in thermal and electrical energy systems. The user then specifies which components that build up their system and determines the correct layout by connecting the respective components. In order to acquire the correct BHE component, an additional component library must be bought from TESS-libraries, "Geothermal Heat Pump (GHP) Components" (TRNSYS, 2020b). The layout of the simulation model in TRNSYS is presented in figure 5.13 and shows the system components and their connections. The equation component is uses equation 5.13 to calculated T_{in} based on T_{out} and the load input Q. The temperature T_{in} is then supplied to the circulation pump as an input parameter. Table 5.3 summarizes the components used in the model.

The Type 557 BHE component in TRNSYS can model a U-tube (557a,557b) or coaxial (557c,557d) BHE design and the Type 557 BHE uses the DST model (Pärisch et al., 2015). The type 557 does not include the thermal capacity of the borehole or the heat carrier fluid. However, for type 557b and 557d, the thermal capacity of the fluid can be accounted for since the fluid to ground thermal resistance is assumed to be a known value, often measured during a thermal response test (TRT) (Thorén, 2016). Short time transients are not modeled accurately with the type 557 BHE component, which is a consequence of neglecting the borehole thermal capacity (Pärisch et al., 2015). Pärisch et al. (2015) and Bertram (2015) purposes a pre-pipe solution in TRNSYS in order to account for the thermal capacity of the borehole and improve the short-time transient modeling.

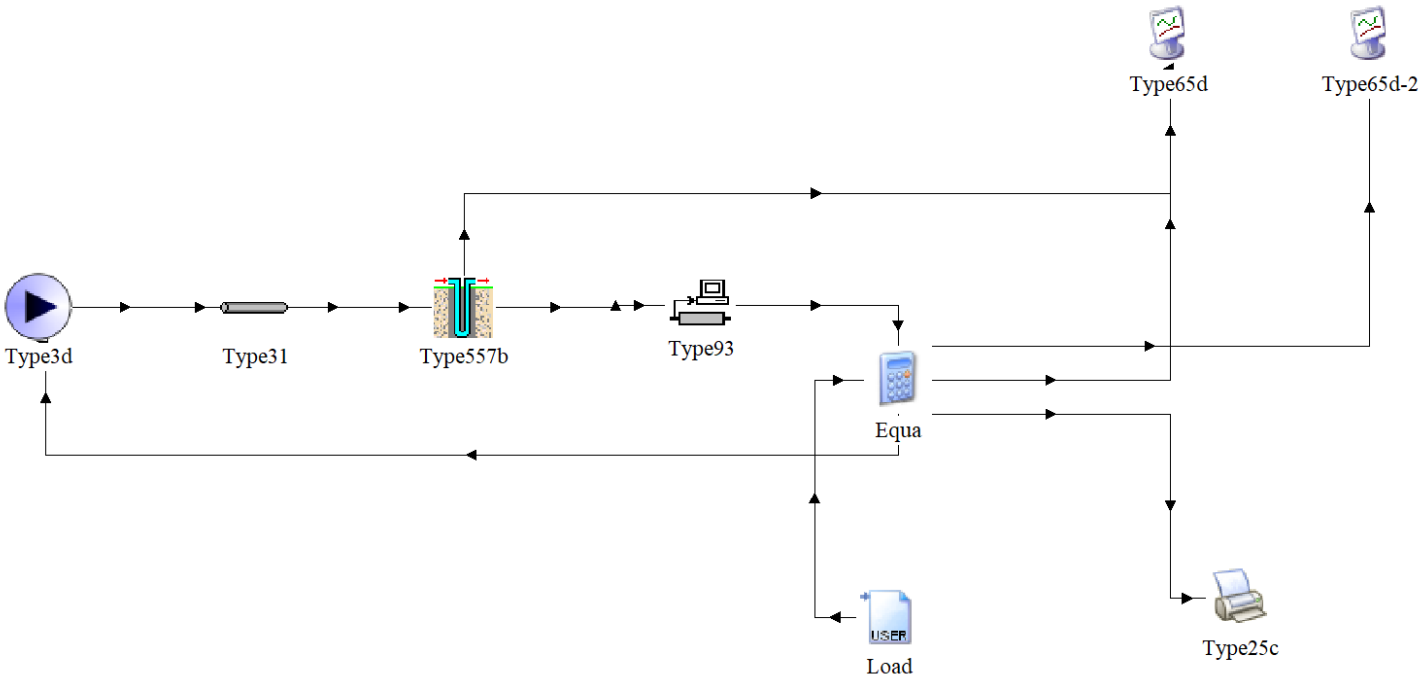

Figure 5.13: System layout in TRNSYS for a model simulating a single HT-borehole.

Figure 5.13 shows the system layout of the simulation model in TRNSYS. The time step used in the simulations is 0.1 hours (360 seconds). The type 557b BHE component is used since the fluid to ground thermal resistance can be determined for this component and consequently give the best resemblance to a non-grouted borehole. The value of the fluid to ground thermal resistance/borehole thermal resistance for the type557b component is calculated with the MATLAB model, which resulted in a resistance of 0.0684 mK/W.

Table 5.3: Short description of the components in the TRNSYS thermal analysis model.

Component	Description
Type3d	Circulation pump
Type31	Pipe/Duct
Type557b	Ground heat exchanger
Type93	Input Value Recall
Type25c	Printer
Type65d	Online Plotter
Type9a(load)	Data reader
Equa	Custom equations

5.4.2 Pre-pipe component

The pre-pipe concept presented in Pärisch et al. (2015) and Bertram (2015) accounts for the thermal capacity of the borehole with the type 604 pipe component in TRNSYS. The type 604 component is found in one of the additional TESS libraries (TRNSYS, 2020b). Since the type 604 component was not available in this master thesis, the standard library component type31 was used. The boreholes analyzed in this study are non-grouted, and the thermal capacity of the borehole is therefore the thermal capacity of the groundwater in the borehole.

Pärisch et al. (2015) and Bertram (2015) present how the geometrical parameters of the type 604 pre-pipe are calculated. Bertram (2015) specifies that the material properties of pipe mass are equal to the material properties of the filling material. For the type 31 component, the properties of the circulating fluid are assumed equal to the groundwater properties, which again are assumed equal to the heat carrier properties. The length of the pre-pipe (L_{pp}) is set equal to the borehole depth (Pärisch et al., 2015). The radius of the pre-pipe (R_{pp}) is calculated with the derived equation 5.15. Equation 5.15 is derived by setting the thermal capacity of the fluid in the pre-pipe equal to the thermal capacity of the groundwater in the borehole. The borehole and BHE radius are listed in table 5.1.

$$r_{pp} = \sqrt{r_b^2 - 2r_{BHE}^2} \tag{5.15}$$

The resulting r_{pp} is the radius of the pre-pipe, while r_b is the borehole radius, and r_{BHE} is the BHE radius. With the values listed in table 5.1 the calculated pre-pipe radius becomes 0.064m. This value is altered and the resulting fluid temperature profile compared in order to investigate the influence of the pre-pipe diameter and consequently, also the amount of borehole thermal capacity accounted for.

5.4.3 TRNSYS pre-pipe evaluation

Two different load cases will be analyzed in order to evaluate the performance of the TRNSYS model and pre-pipe solution. The fist load case is a constant extraction load of 40 W/m while the second is a daily load cycle with nightboosting, see table 5.2. The results from the pre-pipe evaluation are presented in figure 5.14 - 5.17.

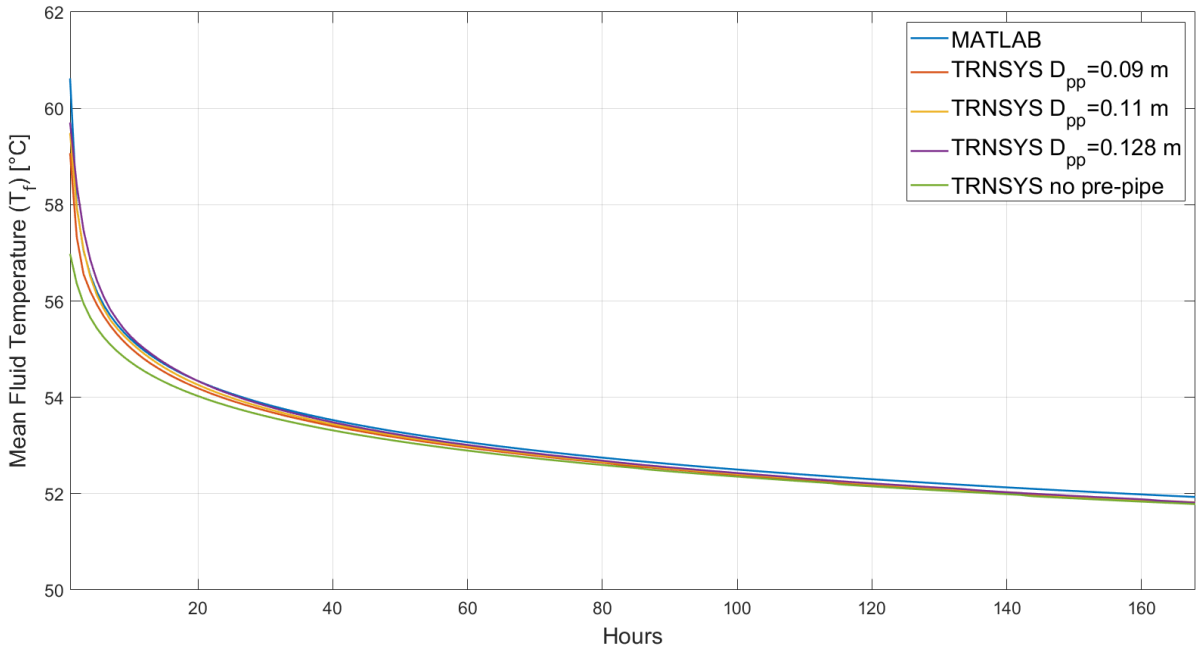

Figure 5.14: Resulting T_f for all investigated pre-pipe diameters and the MATLAB model during a constant load cycle with timescale = 168 h.

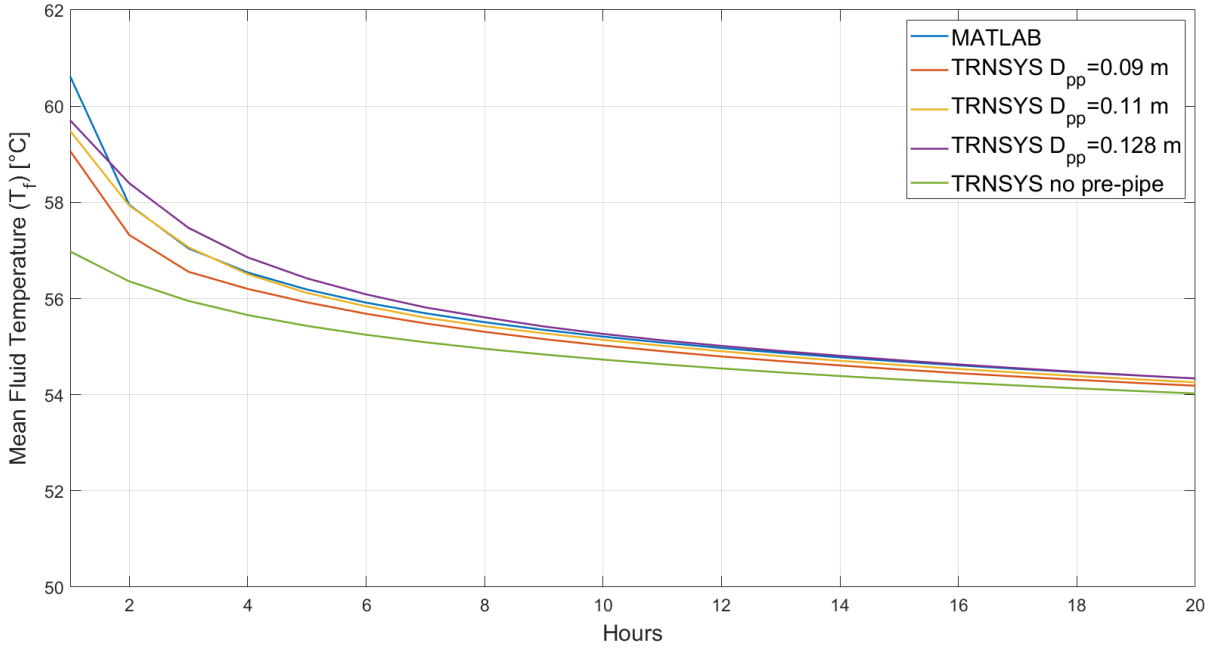

Figure 5.15: Resulting T_f for all investigated pre-pipe diameters and the MATLAB model during a constant load cycle with timescale = 20 h.

Figure 5.14 shows that the pre-pipe component has a substantial effect on the early hours of the simulation results. Figure 5.15 shows the same load, but for the first 20 hours were the effect of the pre-pipe is more visible. The results show that all pre-pipe diameters have the highest deviation from the MATLAB results during the first two hours of the simulation. After this, a pre-pipe diameter of 0.11 m gives the best resemblance to the MATLAB results.

The resemblance during a daily load cycle was also investigated. The results for all the investigated pre-pipe diameters are presented in figure 5.16. The results show that with increasing pre-pipe diameter discontinuities seem to occur. Also, the results with higher diameter trends to overestimate the average fluid temperature. A pre-pipe diameter of 0.09 m results in the best resemblance to the MATLAB results. Figure 5.17 shows the MATLAB result, the results without a pre-pipe component, and the results with a pre-pipe component with $D_{pp} = 0.09$ m. Both figure 5.16 and 5.17 shows that the pre-pipe component greatly improves the short-time transient modeling.

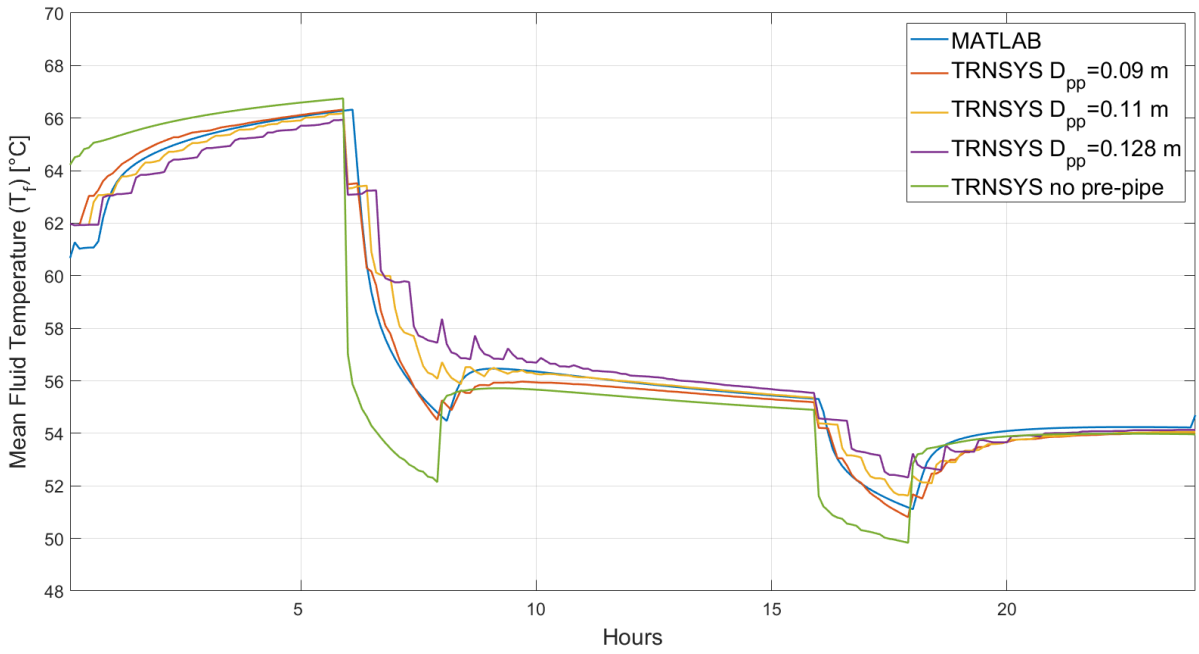

Figure 5.16: Resulting T_f for all investigated pre-pipe diameters and the MATLAB model during a daily load cycle.

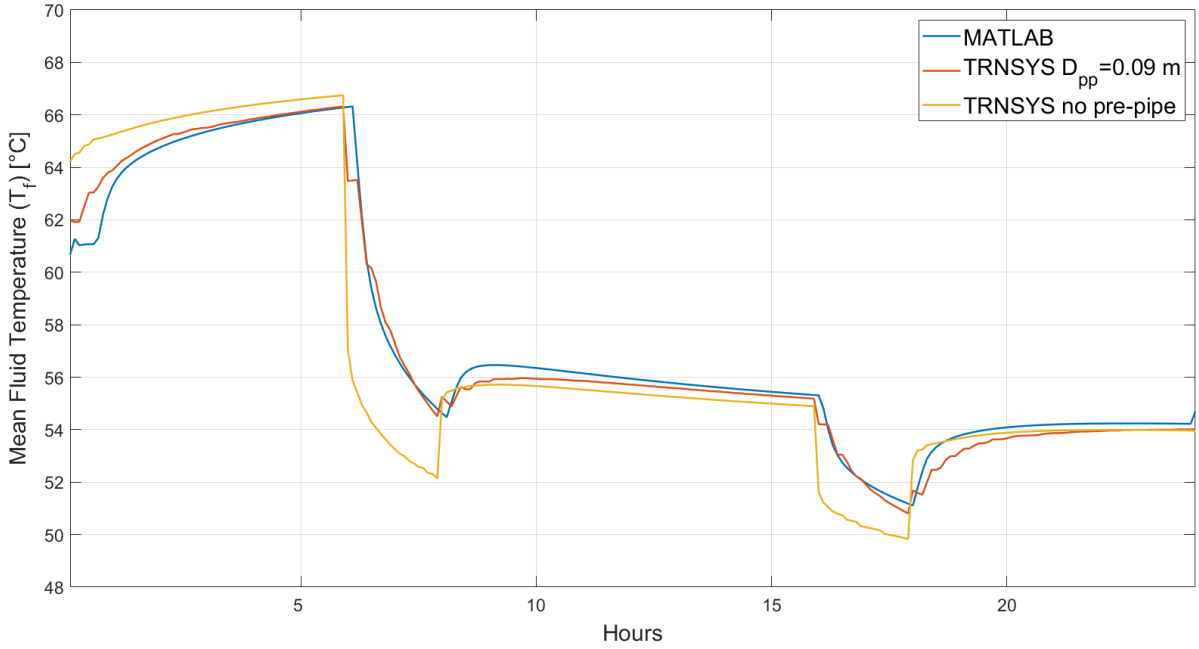

Figure 5.17: Resulting T_f for $D_{pp} = 0.09$ m, no pre-pipe and MATLAB model during a daily load cycle.

The results presented in figure 5.14 to 5.17 highlight the impact of the borehole thermal capacity during short-time transients. Without the borehole thermal capacity, the heat carrier temperature is underestimated during short-time discharging loads and overestimated during short-time charging loads. The pre-pipe solution improves the short-time transient modeling in TRNSYS, but varies in accuracy depending on the pre-pipe diameter. A pre-pipe diameter of 0.09 m will only include 50% of the borehole thermal capacity but gave the best resemblance to the MATLAB results during a daily load cycle.

Chapter 6

Case Analysis Description

6.1 Introduction

Approximately 45% of the heat supplied in the Norwegian district heating sector is through waste incineration (Norsk Fjernvarme, 2019a). Waste incineration as a waste handling method is a more environmentally friendly solution compared to having waste on landfills (Norsk Fjernvarme, 2019b). With an increasing focus on reducing emissions while keeping up with increasing heating demand, it is desirable to increase the amount of heat supplied by waste-to-energy DH plants.

In this master thesis, a HT-BTES system is proposed as a storage solution for the excess heat produced by the waste-to-energy DH sector. In order to evaluate the HT-BTES system as a potential solution, a case analysis of three HT-BTES cases will be performed. The HT-BTES capacity and respective load cycle will be based on the findings presented in chapter four. This is in order to make the case analysis and the presented results relevant for the waste-to-energy DH plants analyzed in chapter four. The three analyzed HT-BTES system solutions will supply heat to a LT-DH network. The extracted heat will either be supplied directly from the HT-BTES or through a heat pump installation.

Based on the findings presented in chapter five, the effect of nightboosting and the use of a pre-pipe component will be further evaluated in the case analysis. Nightboosting will be evaluated in order to assess its effect over a longer time scale and on a HT-BTES. The pre-pipe component will also be analyzed to evaluate its effect when used in a TRNSYS model for a HT-BTES. Lastly, a sensitivity analysis of one of the presented HT-BTES cases will be performed in order to give an understanding of the importance and influence of different HT-BTES parameters.

6.2 HT-BTES cases

Three storage capacities will be defined based on the gathered information presented in chapter four. These three different capacities will reflect the amount of excess heat produced by waste-to-energy DH plants in Norway. The capacity of the storage will be defined in GWh and assumes a 30K difference between the annual minimum and maximum average storage temperature. The three cases and their respective storage capacity are listed in table 6.1.

Table 6.1: Capacity in GWh for the three different HT-BTES cases.

Case	**Storage Capacity [GWh]**
Small - Case 1	7.5
Medium - Case 2	60
Large - Case 3	125

6.3 Base case design

The information and assumptions presented in section 4.3 are used when designing the base case design for each of the three cases given in table 6.1. The assumptions presented in table 4.1 are therefore assumed valid for each case. Since the storage capacities are known for each case, figure 4.8 can be used to calculate the expected steady-state heat loss and figure 4.12 to calculate the storage radius. Since all three cases have an aspect ratio of 1, the borehole depth will be two times the storage radius. The three storages are assumed to have a cylindrical shape.

The storage volume for each case is calculated by dividing the storage capacity with the expected energy pr volume, which is 18 KWh/m^3. The borehole spacing is determined based on the empirical findings presented in chapter three. With the storage volume, radius, borehole depth, and borehole spacing known for each case, equation 6.1 is used to calculate the resulting number of boreholes. Equation 6.1 is the storage volume formula used in TRNSYS for the Type 557 component (Malmberg, 2017).

$$Storage\,volume = \pi \cdot H \cdot N \cdot (0.525 \cdot d)^2 \tag{6.1}$$

H is the borehole depth, N the number of boreholes and d the borehole spacing.

Dragvoll in Trondheim, Norway, is used as location when gathering data on the ground conditions from (NGU, 1858b) and (NGU, 1858a). Weather data is also from a weather station located in Trondheim. Colder climates would therefore have a slightly higher top surface heat loss and warmer climates a slightly lower top surface heat loss. An initial ground gradient of 0.02°C/m is used in each case. The HT-BTES base case design parameters, as well as ground, soil, insulation and heat carrier properties, are listed in table 6.2 for each of the three cases.

Table 6.2: HT-BTES design parameters for case 1, 2 and 3 as well as ground, soil, heat carrier and insulation properties.

Parameter	**Case 1**	**Case 2**	**Case 3**	**Unit**
HT-BTES characteristics				
Storage Volume	416 667	3 333 333	6 944 444	m^3
Storage radius	40.6	81	103.4	m
Borehole depth	81.2	162	206.8	m
Number of boreholes	484	1485	1915	n/a
Boreholes in series	5	3	2	n/a
Borehole spacing	3.5	4	4.5	m
Header Depth	1			m
Borehole radius	0.07			m
Collector design	Single U-tube			n/a
Fluid to ground thermal resistance	0.0684			mK/W
Rock properties				
Thermal conductivity	3			W/mK
Heat capacity	2200			kJ/m^3K
Soil properties				
Thermal conductivity	1.5			W/mK
Heat capacity	2200			kJ/m^3K
Soil thickness	4			m
Top surface insulation				
Thermal conductivity	0.11			W/mK
Insulation thickness	0.5			m
Insulation height fraction	0.1			n/a
Heat carrier fluid (Water @ 60°C)				
Fluid density	985			kg/m^3
Specific heat	4.183			kJ/kgK

The top surface insulation material for each case is assumed to be mussel shells. Mussel shell is a low cost and natural insulation material, which also was used for the HT-BTES in Brædstrup (Plan Energi, 2013). Crushed mussel shells have a higher thermal conductivity than conventional synthetic insulation materials (e.g. foam glass gravel), but the price of the mussel shells is significantly lower (Plan Energi, 2013).

6.4 Load cycle

When determining the load cycle of a HT-BTES, a charging and discharging period have to be defined. These two periods depend on whether there is excess heat available or not. Based on the excess heat information presented in figure 4.6, the charging and discharging period for all three cases were determined. The resulting charging and discharging periods are listed in table 6.3.

Table 6.3: Charging and discharging period and hours for case 1, 2 and 3.

Case	**Charging**	**Discharging**
Case 1	15.April-15.Oct	16.Oct-14.April
Case 2	15.April-15.Oct	16.Oct-14.April
Case 3	1.Mai-31.Sep	1.Oct-31.April

Assumed for each case is that the storage capacity equals the amount of available excess heat during the respective charging period. The annually discharged energy is calculated by subtracting the calculated steady-state heat loss from the storage capacity. In order to consider monthly variation, a monthly fraction has been calculated for each month, for charging and discharging individually. The monthly fractions are calculated based on the excess heat production graphs in figure 4.6. The resulting monthly injected or extracted energy is calculated by multiplying the total injected or extracted amount with the respective fraction. Resulting monthly energy amounts are listed in table 6.4 for each of the three cases. For cases 1 and 2, energy is both injected and extracted during April and October.

Table 6.4: Monthly energy distribution during the charging and discharging period for each case.(+ injection, - extraction). All values are given in GWh.

Month	Case 1	Case 2	Case 3
Jan	-1.01	-9.71	-18.31
Feb	-0.90	-8.65	-18.42
Mar	-0.88	-8.54	-17.61
Apr	+0.30 / -0.37	+2.4 / -3.61	-13.67
May	+1.05	+8.40	+16.25
Jun	+1.50	+12.00	+25.00
Jul	+1.73	+13.80	+30.00
Aug	+1.58	+12.60	+31.25
Sep	+1.13	9.00	+22.5
Oct	+0.23 / -0.40	+1.80 / -3.87	-11.82
Nov	-1.02	-9.82	-18.19
Dec	-0.92	-8.86	-17.84
Summation of charging and discharging energy			
Charging	7.50	60	125.00
Discharging	5.49	53.07	115.86

An hourly heating rate is calculated for both charging and discharging of the storages. The rates depend on the respective month and hour of the day. Charging is assumed to be possible 24 hours of the day for the entire charging seasons. For the discharging season, a daily load cycle is determined. This load cycle is presented in table 6.5 and consists of one peak load in the morning and a base load after that. From 00.00 - 06.00, it is assumed no heat is extracted from the HT-BTES, and that this time can be used for nightboosting. Based on the results presented in chapter five, the only peak load included in the case analysis daily load cycle is the morning peak load. The transient behavior of the TRNSYS model evaluated in the thermal analysis is seen as sufficient, allowing for a two hour long peak load.

Table 6.5: Daily load cycle with and without nightboosting for the case analysis.

Time	Load
00.00 - 06.00	0 or q_{charge}
06.00 - 08.00	$q_{Peakload}$
08.00 - 24.00	$q_{Baseload}$

The monthly extracted energy in table 6.4, monthly peak and base load hours and total borehole length is used to calculate the daily peak and base load rates (W/m), for each of the three HT-BTES cases. The peak and base load rates will therefore be constant during the respective month, but vary monthly depending on the amount of extracted energy. When calculating the peak and base load rates, the peak load is assumed to be twice the base load. The resulting rates during both the discharging and charging period for each case are listed in table 6.6 and 6.7. Charging rates are calculated based on the monthly injected energy, total hours of the month and the total borehole length of the particular case. Resulting in constant monthly rates.

During nightboosting a rate (q_{charge}) of 60 W/m will be used for all three cases. With nightboosting operation, the total energy injected during the charging season will be subtracted from the amount injected by nightboosting. This results in equal annually charged and discharged energy for the load cycle with and without nightboosting. Since less energy is being injected during the charging season for the load cycle with nightboosting, a constant charging rate will be used. There will be no discharging of the HT-BTES during the pre-heating years in each case. Nightboosting will however also take place during the pre-heating years, which increases the amount of available energy used for pre-heating of the HT-BTES.

Table 6.6: Monthly peak and base loads during the discharging season. Unit is W/m and values are given as absolute value.

Month	**Case 1**	**Case 2**	**Case 3**
Oct	$q_{Base} = 31.9$ $q_{Peak} = 63.8$	$q_{Base} = 50.3$ $q_{Peak} = 100.6$	$q_{Base} = 48.1$ $q_{Peak} = 96.2$
Nov	$q_{Base} = 43.1$ $q_{Peak} = 86.2$	$q_{Base} = 68$ $q_{Peak} = 136$	$q_{Base} = 76.6$ $q_{Peak} = 153.2$
Dec	$q_{Base} = 37.6$ $q_{Peak} = 75.2$	$q_{Base} = 59.4$ $q_{Peak} = 118.8$	$q_{Base} = 72.7$ $q_{Peak} = 145.4$
Jan	$q_{Base} = 41.3$ $q_{Peak} = 82.6$	$q_{Base} = 65.1$ $q_{Peak} = 130.2$	$q_{Base} = 74.6$ $q_{Peak} = 149.2$
Feb	$q_{Base} = 40.7$ $q_{Peak} = 81.4$	$q_{Base} = 64.2$ $q_{Peak} = 128.4$	$q_{Base} = 83.1$ $q_{Peak} = 166.2$
Mar	$q_{Base} = 36.3$ $q_{Peak} = 72.6$	$q_{Base} = 57.3$ $q_{Peak} = 114.6$	$q_{Base} = 71.7$ $q_{Peak} = 143.4$
Apr	$q_{Base} = 31.7$ $q_{Peak} = 63.4$	$q_{Base} = 50$ $q_{Peak} = 100$	$q_{Base} = 57.5$ $q_{Peak} = 115$

Table 6.7: Monthly charging rates during the charging season. Unit is W/m and all values are given as absolute value.

Month	Case 1	Case 2	Case 3
Apr	21	28	-
May	36	47	55
Jun	53	69	88
Jul	59	77	102
Aug	54	70	106
Sep	40	52	79
Oct	16	21	-

From table 6.6, the highest base and peak load for cases 1 and 2 occur during November and during February for case 3. By multiplying the rates with the total borehole length of the respective case the highest base and peak heating demand (W) can be calculated.

- Case 1 - Q_{Base} = 1.70 MW & Q_{Peak} = 3.4 MW
- Case 2 - Q_{Base} = 16.40 MW & Q_{Peak} = 32.8 MW
- Case 3 - Q_{Base} = 32.90 MW & Q_{Peak} = 65.8 MW

6.5 System solution

In the case analysis, heat will be delivered to a LT-DH network. The system solution must however also be able to maintain a sufficient temperature during the entire discharging season and have a heat source during the charging season. A principle sketch of the conceptual system solution is presented in figure 6.1.

Figure 6.1a shows the operation of the system solution during the discharging season. Heat can either be supplied directly from the HT-BTES (1), from a R717(Ammonia) heat pump (2), or through the existing DH network (3). It is desirable to supply the entire heating demand directly from the HT-BTES in order to avoid the investment cost of a heat pump. It must however first be validated through simulations that the outgoing temperature from the HT-BTES stays above the temperature limit of 60°C during the entire discharging season (see subsec.6.5.1). If T_{out} goes below 60°C, T_{out} will be the heat source for a R717 HP heating the water in the LT-DH to the desired temperature.

The LT-DH network can heat exchange with the existing DH-network (see fig. 6.1b). This connection is established to have a reliable system and to be able to supply heat to the LT-DH network during the charging of the HT-BTES. Figure 6.1b also sketches how nightboosting could be performed.

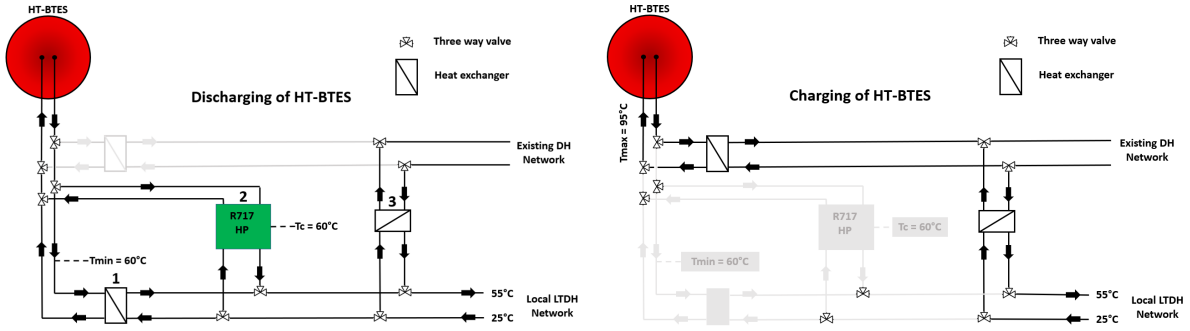

(a) Discharging operation **(b)** Charging operation

Figure 6.1: Principle sketch of the system solution during discharging and charging operation.

6.5.1 LT-DH network

A LT-DH network will allow lower supply temperatures compared to the existing DH-network. The lower temperature will increase the amount of heat that can be supplied directly from the HT-BTES or potentially make it possible to cover the entire heating demand directly with the HT-BTES. Based on the theory presented in section 2.7, a LT-DH network with a supply temperature of 55°C and return temperature of 25°C is assumed for this case analysis. The heat exchanger between the HT-BTES and LT-DH network is assumed to have a pinch point temperature difference of 5K. This results in 60°C being the minimum temperature limit for T_{out} from the HT-BTES in order to supply heat directly. If temperatures go below 60°C, T_{out} will be used as a heat source for the HP installation, which then will heat the return water in the LT-DH network.

6.5.2 Ammonia (R717) - Heat pump

R717 is a natural working fluid with global warming potential (GWP) and ozone depletion potential (ODP) of 0. In addition to this, R717 also offers excellent thermodynamic properties, and a R717 HP can achieve a high coefficient of performance (COP) if operated correctly (Stene, 2019). One of the challenges with R717 as working fluid is its level of toxicity, which must be accounted for at the installation site. In addition to this high discharge temperatures can become a problem if the HP is not designed and operated correctly (Stene, 2019).

The HP system will consist of two R717 HP installations with equal heating power (Q_c). The installations are connected in parallel in order to ensure system redundancy and the capability to handle peak loads if both HP installations are operated simultaneously. The heating power of each HP installation will therefore be equal to the highest base load in each case. One HP installation may consist of multiple heat pumps connected in parallel in order to reduce the required heating power per HP. The heating power of the HP installations in cases 2 and 3 are very high compared to commercial products, and

a custom made solution must be constructed for such specifications (Malmberg, 2017). The maximum heating power, as well as other key parameters for one of the two HP installation in cases 1, 2 and 3, are listed in table 6.8.

Table 6.8: Specifications for one heat pump installations in case 1, 2 and 3.

Parameter	**Case 1**	**Case 2**	**Case 3**	**Unit**
Heating Power (Q_c)	1.70	16.40	32.90	MW
Condensing temperature (T_c)	60			°C
Isentropic efficiency (λ_{is})	0.75			n/a
Heat loss factor (f_Q)	0.1			n/a

6.6 Simulation model

The TRNSYS model presented in subsection 5.4.1 is developed further in order to simulate not only one borehole, but an entire HT-BTES. TRNSYS was used as simulation software for the case analysis because of its ability to model a dynamic thermal process and the component flexibility in the simulation studio. The components used in the case analysis TRNSYS model are presented in table 6.9, and the system model is presented in figure 6.2.

The system model receives hourly input information through pre-made text files, which are processed by three data readers (Type9a). The weather, thermal stratification control value, and heating load are given as input information to the simulation model. The connection between the data readers and the component receiving the information is colored green in the system model. The "Temperature" equation component calculates T_{in} based on the heating load from the input information, the total mass-flow, c_p and T_{out} from the HT-BTES (Type557b)(see eq.5.13). The average temperature T_f is also calculated in the "Temperature" equation component. Each simulated year lasts from the beginning of the charging season to the end of the discharging season (see tab.6.3)

The main loop, which is the connections creating the loop for the heat carrier fluid, is colored black. The purple connections are data that is being plotted during the simulation, while the light blue connections are data stored in external documents. The "Heat transfer" custom equation changes the unit of the heat transfer data from the Type557b from [kJ/h] to [W], before sending it to the printegrator component(Type46a) which integrates and stores the information.

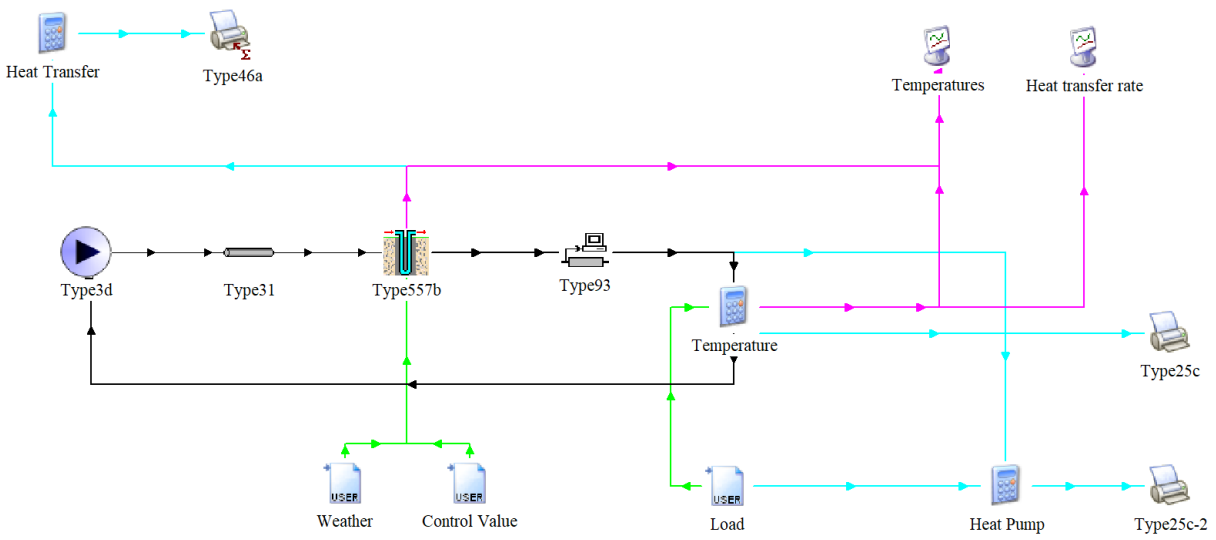

Figure 6.2: System layout in TRNSYS for the case analysis simulation model.

Table 6.9: Short description of the components in the TRNSYS case analysis model.

Component	Description
Type3d	Circulation pump
Type31	Pipe/Duct
Type557b	Ground heat exchanger
Type93	Input Value Recall
Type25c	Printer
Type46a	Printegrator
Type65d	Online Plotter
Type9a (Load, Weather, Control Value)	Data reader
Equation (Temperature, Heat Transfer)	Custom equations

The simulation model will have a simulation period of 15 years. This is in order to include a sufficient amount of operation years when analyzing the HT-BTES cases. The simulation period will include the preheating phase of the storage.

6.6.1 Thermal stratification

The "Control Value" data reader gives an input value to the type557b component. This input value can either be 1 and -1 and controls how the heat carrier fluid is circulated through the boreholes. If the control value is equal to 1, the heat carrier fluid is circulated from the center to the outer border, and if the control value equals -1 from the outer border to the center. This control is only relevant for HT-BTES having two or more boreholes coupled in series. The control value equals 1 when energy is injected and -1 when energy is extracted from the HT-BTES. This control system will induce a radial stratification inside the HT-BTES.

6.6.2 Heat pump modeling

CoolPack is used as simulation software for the heat pump simulations in this master thesis. This is a user-friendly freeware made for energy analysis and optimization of refrigeration systems (CoolPack, 1999). It is also well suited for analyzing heat pump heating systems. With the parameters presented in table 6.8 the remaining key parameter is the evaporation temperature(T_e). The evaporation temperature will be a function of T_{out} from the HT-BTES and is assumed to be 5K lower than T_{out}. Due to a low-temperature difference between T_c and T_e, a one-stage flooded evaporator R717 HP will be modeled in *CoolPack*. The discharge gas temperature is below its critical value due to the low-temperature lift in the heat pump (Stene, 2019).

A potential function for the COP of the HP installation as a function of T_c - T_e is made by curve fitting simulation results from CoolPack. The curve fitted results and potential function is presented in figure 6.3. T_c - T_e is represented by x in the potential function, and by incorporating this function in TRNSYS, hourly COP values for the HP installation are calculated as a function of T_c - T_e. This is implemented in the TRNSYS model through the "Heat Pump" equation component. It is assumed that the COP function presented in figure 6.3 is representable for all three cases.

It is essential to specify that the heat pump model is theoretical. Changes in compressor efficiency during part-load operation and variable source temperatures are therefore not accounted for in the model. The calculated theoretical COP values can therefore become notably high since the temperature difference between T_c - T_e will be very low when T_{out} is 60°C or close below. It is therefore important to evaluate the COP results by their trend and not exact value.

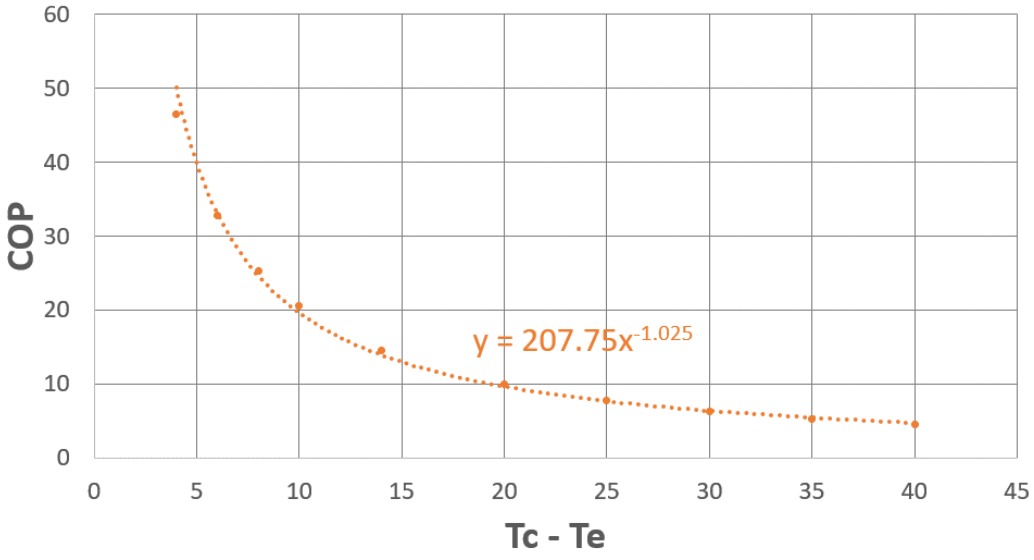

Figure 6.3: Curve fitted potential function for simulated COP values in CoolPack.

Chapter 7

Case Analysis Results

The results presented in this chapter are intended to give an understanding of the HT-BTES system, the influence of nightboosting, and the influence of key HT-BTES parameters. A continuation of the pre-pipe analysis in chapter five will be presented first in order to understand and highlight the impact of the pre-pipe on HT-BTES simulation results. After the pre-pipe evaluation, the three cases are analyzed. The analysis focuses on the influence of storage capacity, nightboosting, and how these two factors affect the performance of a heat pump installation. At the end of this chapter, a sensitivity analysis of case 2 is presented. The sensitivity analysis will evaluate how different parameters influence the development of the average storage temperature (T_{am}).

Results are presented over a period of 15 years, but in some figures also for other specified periods due to visualization of the desired results.

7.1 Pre-pipe evaluation

Based on the findings presented in subsection 5.4.3, a pre-pipe diameter of 0.09m will be used in the case analysis simulation models. This is assumed a valid diameter for all three cases since cases 1,2 and 3 have the same borehole size as the investigated borehole in subsection 5.4.3. The pre-pipe length will be equal to the total borehole length of the particular case. Approximately 50% of the total borehole thermal capacity is therefore accounted for in cases 1, 2 and 3. Figure 7.1 shows the development of T_f for cases 1, 2 and 3 with nightboosting during the last discharging week in year 15. The temperature development of the models with and without pre-pipe have the same distinction in figure 7.1, as previously observed in figure 5.16. In order to evaluate this difference more in-depth two dimensionless parameters are defined. T_f^* and T_{am}^*. These parameters are calculated by dividing simulation results with pre-pipe by the results without a pre-pipe.

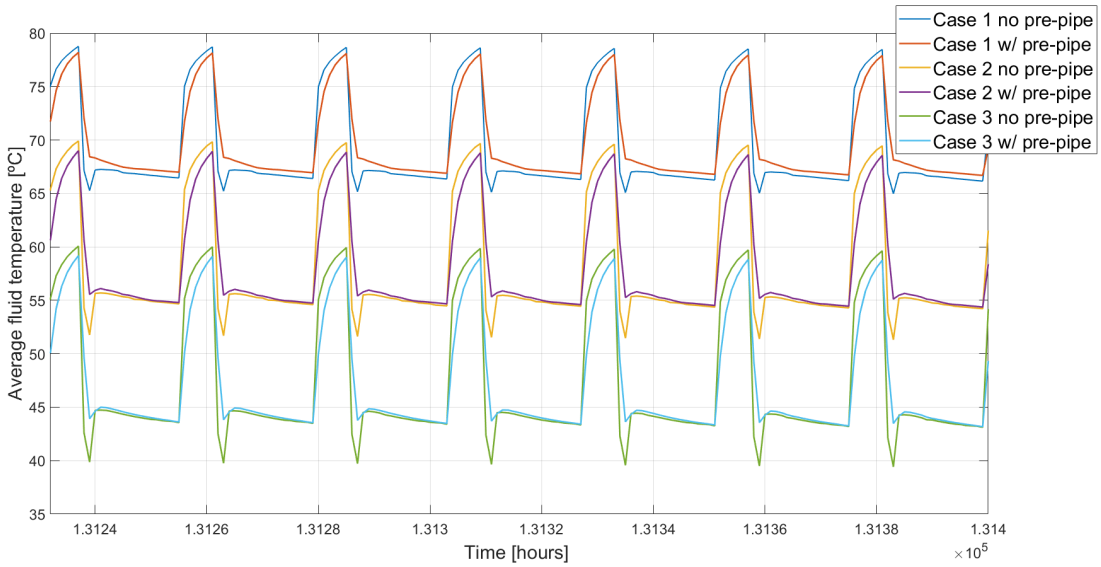

Figure 7.1: Average fluid temperature development for results with and without pre-pipe for case 1-3. Simulations are with nightboosting.

Figure 7.2 shows the dimensionless temperature parameters, along with the average storage temperature for case 1 without nightboosting. The same graph was also made for case 1 with nightboosting, and for case 2 and 3 with and without nightboosting. The graphs showed that the temperature deviation significantly increased with nightboosting. This can be observed by comparing figure 7.2 with figure 7.3 during the same discharging year. An interesting observation viewed in figure 7.2 - 7.5 is that T^*_{am} is close to 1 for case 1,2 and 3. The value of T^*_{am} indicates that accounting for the borehole thermal capacity mainly affects the thermal process in the borehole and the heat carrier temperature.

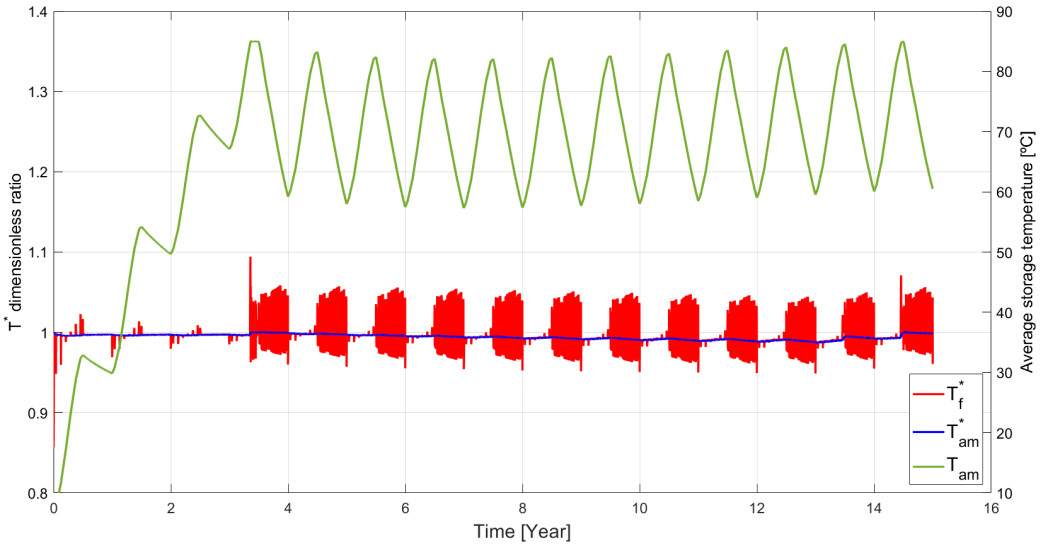

Figure 7.2: Dimensionless temperature parameters and average storage temperature for case 1. Results are without nightboosting and shown for the entire time period of 15 years.

A closer analysis of each case was performed in order to investigate other effects that might increase the temperature deviation. Figure 7.3,7.4 and 7.5 shows the dimensionless temperatures and average storage temperature for case 1,2 and 3 with nightboosting. A significant increase in the deviation can be observed from case 1 to case 3. Table 6.6 shows that peak rates also significantly increase from case 1 to case 3, which could be responsible for the increase in T_f^*. T_f^* also increases with declining average storage temperature, observed by the linear increase of T_f^* in each discharging month in figure 7.5.

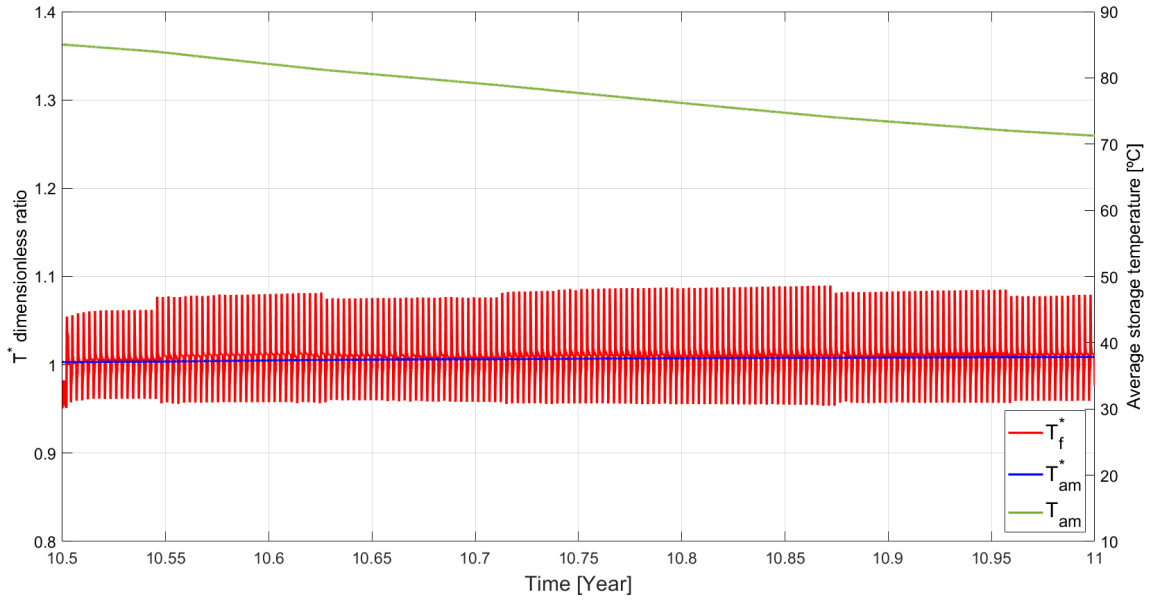

Figure 7.3: Dimensionless temperature parameters and average storage temperature for case 1. Results are with nightboosting and shown for the discharging season in year 10.

The deviations observed in figure 7.2-7.5 can be explained by figure 7.1. T_f^* below 1 indicates nightboosting while T_f^* above 1 indicates a peak load. During base load the temperature profiles match more closely and T_f^* is close to 1. The size of the charging and discharging rate q (W/m) is observed to increase the temperature deviation most significantly. The effect of increasing storage capacity on T_f^* is analyzed by comparing the last discharging month in figure 7.4 with the first in figure 7.5. A larger deviation is observed for case 2, although the load cycle rates are close to equal. The average storage temperature is however lower for case 2, but these results indicates that storage capacity has a minimal or negligible effect on T_f^*.

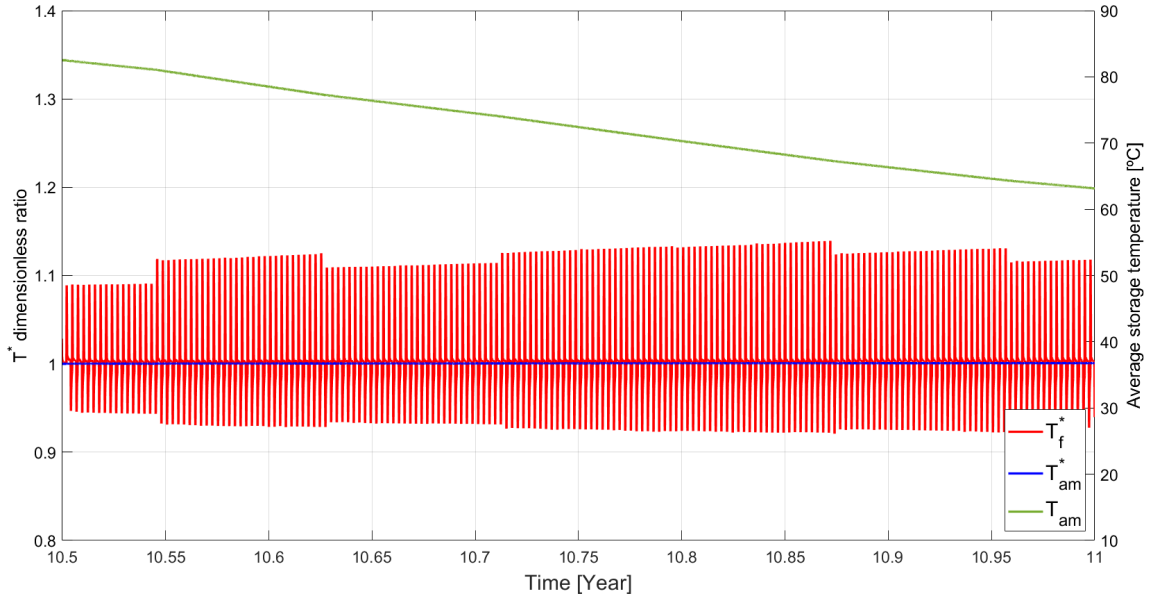

Figure 7.4: Dimensionless temperature parameters and average storage temperature for case 2. Results are with nightboosting and shown for the discharging season in year 10.

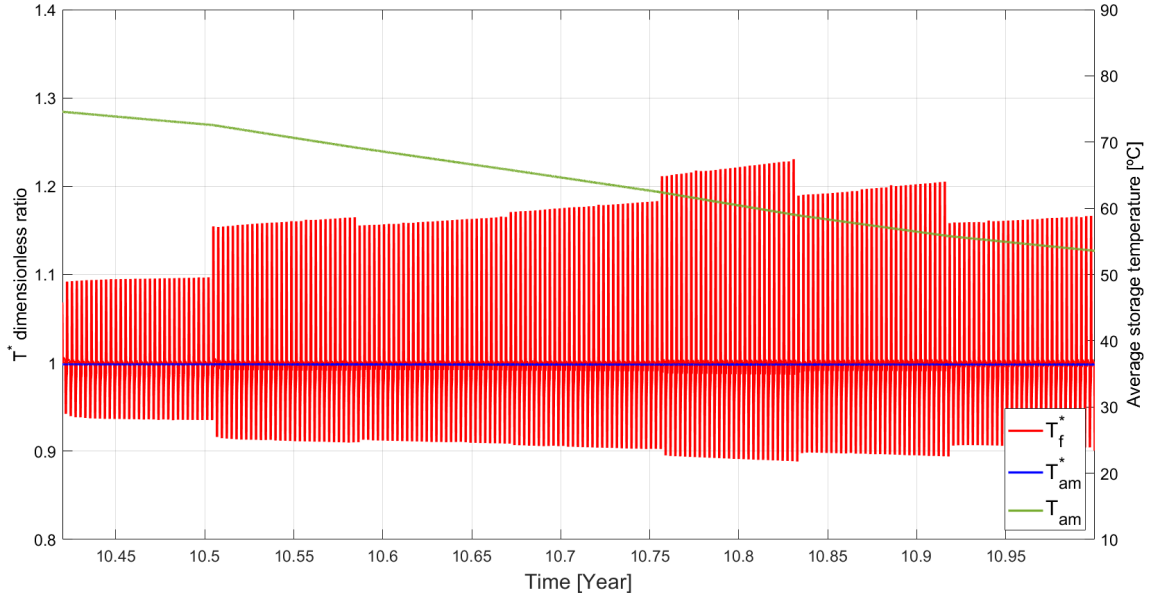

Figure 7.5: Dimensionless temperature parameters and average storage temperature for case 3. Results are with nightboosting and shown for the discharging season in year 10.

7.2 Case results

Results from cases 1, 2 and 3 with a load cycle both with and without nightboosting will be presented in this section. Due to the findings presented in the pre-pipe analysis, results will be presented with and without the pre-pipe component.

7.2.1 Load cycle without nightboosting

Temperature results for case 1 are presented in figure 7.6. By analyzing the development of the average storage temperature, it is observed that the maximum storage temperature of 85°C is achieved again after the preheating phase, in year 12. After year 12, the annual average storage temperature will be close to constant. Year 12 can therefore be viewed as the point where the HT-BTES in case 1 reaches steady-state operation with the annually charged and discharged energy amounts, listed in table 7.1. T_{out} goes below 60°C in the end of January for results without pre-pipe and mid-February for results with pre-pipe. The HT-BTES in case 1 would therefore not be able to supply the entire heating demand directly to the LT-DH network. The results in figure 7.6 also show that four charging seasons are required in the preheating phase before the HT-BTES can be discharged.

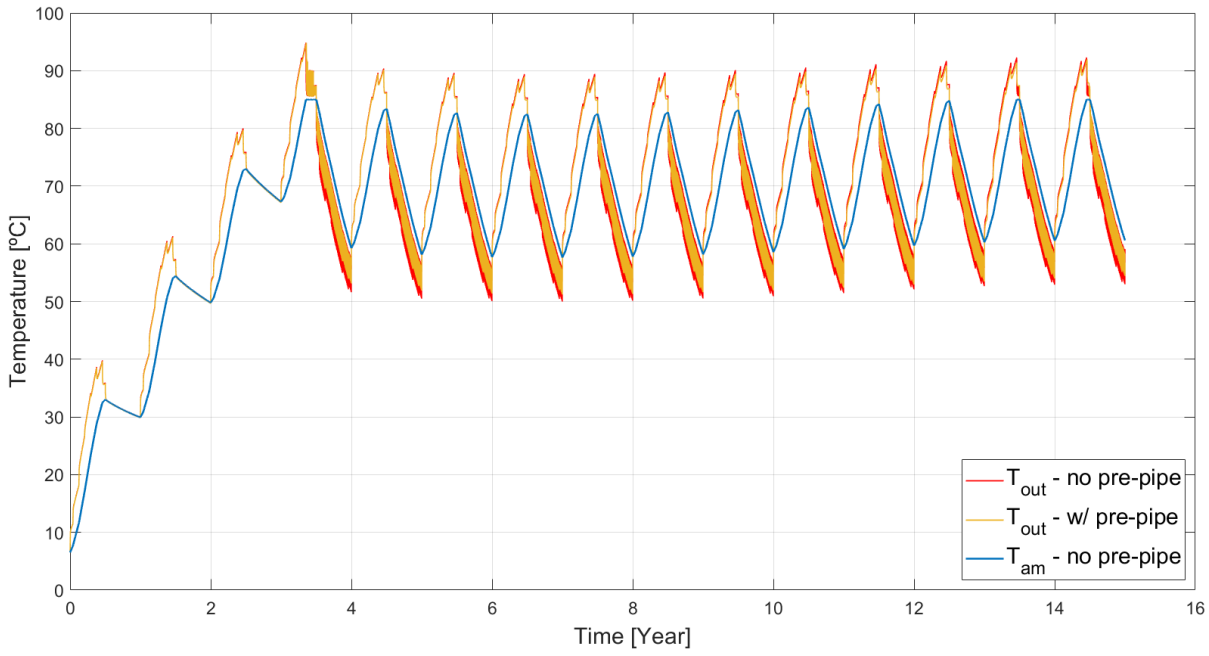

Figure 7.6: Resulting outgoing temperature and average storage temperature for case 1. Simulation load cycle is without nightboosting.

Table 7.1: Injected and extracted annual energy [GWh] for case 1 without nightboosting.

	Preheating Phase	**Operational Phase**
E_{in}	7.5	7.5
E_{out}	0	5.49

Figure 7.7 shows the resulting temperature developments for case 2. The maximum storage temperature in case 2 is 82.5°C and is achieved after the preheating phase in year 10. T_{out} goes below 60°C already in mid-December for the model without pre-pipe and 1/3 into January for the results with pre-pie. The heating demand of the LT-DH network can therefore only be supplied directly for less than half of the heating period by the HT-BTES in case 2. For case 2, only three charging seasons are required during the preheating phase before the HT-BTES can be discharged. The annual charged and discharged energy amounts for the preheating phase and operational phase are listed in table 7.2.

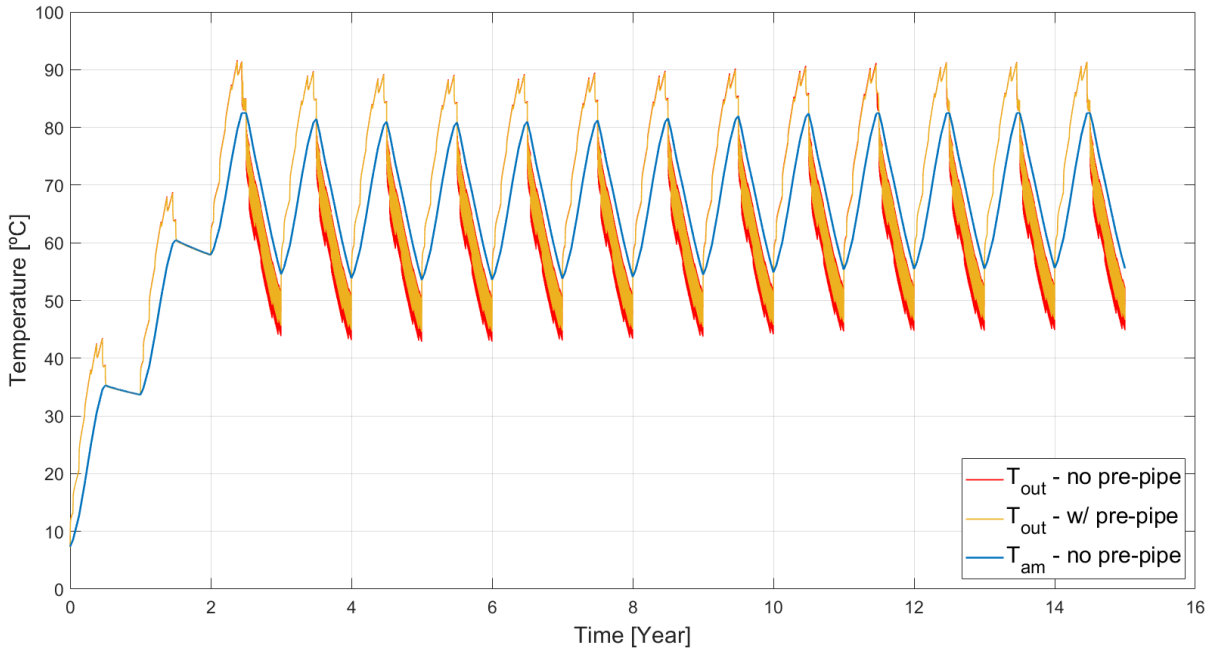

Figure 7.7: Resulting outgoing temperature and average storage temperature for case 2. Simulation load cycle is without nightboosting.

Table 7.2: Injected and extracted annual energy [GWh] for case 2 without nightboosting.

	Preheating Phase	**Operational Phase**
E_{in}	60	60
E_{out}	0	53.07

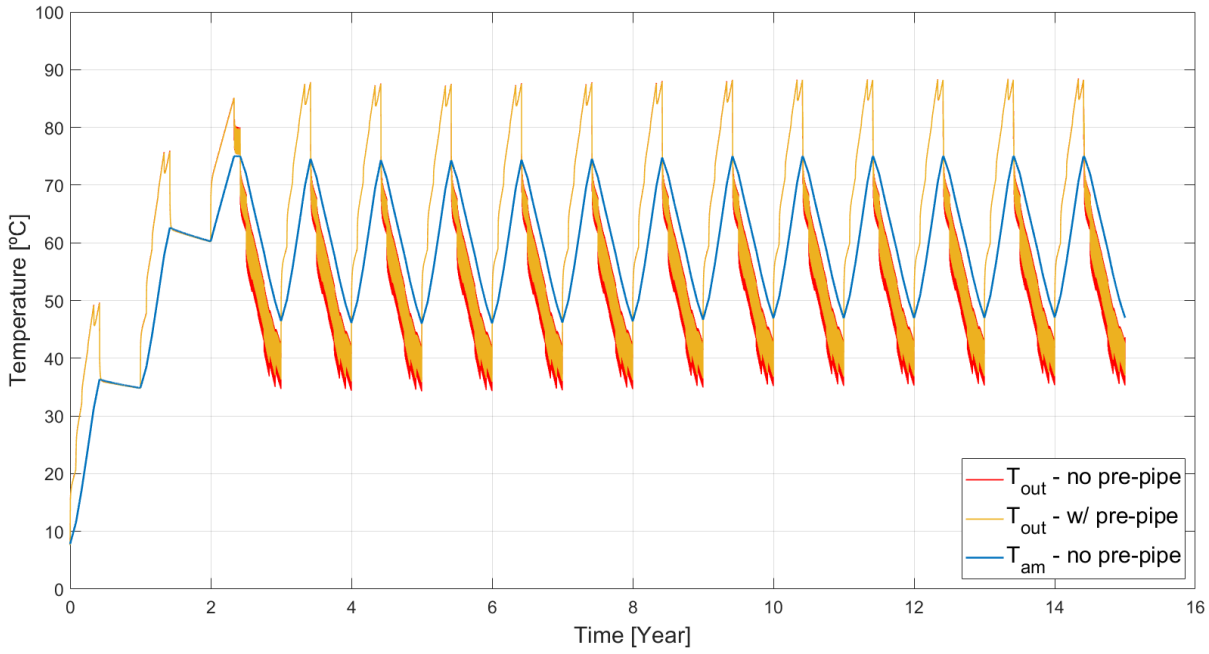

Figure 7.8: Resulting outgoing temperature and average storage temperature for case 3. Simulation load cycle is without nightboosting.

Table 7.3: Injected and extracted annual energy [GWh] for case 3 without nightboosting.

	Preheating Phase	**Operational Phase**
E_{in}	125	125
E_{out}	0	115.86

The resulting temperature developments for case 3 are presented in figure 7.8. The maximum average storage temperature in case 3 is 75°C and is reached after the preheating phase in year 9. A consequence of the significantly lower maximum storage temperature is that T_{out} drops below 60°C at the beginning of November, for the results with and without pre-pipe. Approximately only 1/6 of the heating demand of the LT-DH network can therefore be supplied directly from the HT-BTES in case 3. The annual charged and discharged energy amounts for the preheating phase and operational phase are listed in table 7.3. Case 3 requires three charging seasons in the preheating phase before discharging of the HT-BTES, and less energy is required during the third charging season.

When comparing figure 7.6 - 7.8 it is observed that the maximum average storage temperature declines from case 1 to 3. The decline is a consequence of increasing rates q (W/m) for increasing storage capacities. With higher rates, a greater difference between T_f and T_{am} will be required in order to transfer the desired amount of heat. The temperature difference will consequently limit the maximum average storage temperature if the required T_f is higher than the temperature rating of the BHE material. Since

case 1 has the highest maximum average storage temperature, it also requires one more charging season than case 2 and 3 during the preheating phase. Figure 7.6 - 7.8 also show that steady-state operation is reached sooner for increasing storage capacity, which is most likely a consequence of lower maximum average storage temperature. None of the HT-BTES cases were able to supply a LT-DH network directly for the entire heating season. Increasing storage capacity and consequently lower maximum T_{am} therefore trends to reduce the amount of time the heating demand can be supplied directly by the HT-BTES.

7.2.2 Load cycle with nightboosting

Temperature results for case 1, 2 and 3 with nightboosting are presented in figure 7.9 - 7.11. The results show that the temperature difference between the maximum and minimum average storage temperature is significantly reduced. This reduction has consequently also increased the outlet temperature of the HT-BTES. Since nightboosting also is used during the preheating phase, the preheating time has been reduced by one year for case 1. For cases 2 and 3, three charging seasons remain necessary for both cases, but the injected energy during the last year of the preheating phase is reduced. Table 7.4, 7.5 and 7.6 shows the injected and extracted energy for case 1, 2 and 3 respectively. The tables also show that a significant amount of energy is injected to each HT-BTES by nightboosting.

Since the outlet temperature is significantly increased, the time for which the three cases could supply the heating demand of the LT-DH network directly increased. For case 1, the entire heating demand during all discharging years can be supplied directly (see fig.7.9). With nightboosting the injected energy (E_{in}) during the charging season is lower than the available amount of excess heat. This extra excess heat could be used to reach the maximum storage temperature for all operation years before the steady-state operation.

Table 7.4: Injected and extracted annual energy [GWh] for case 1 with nightboosting.

	Preheating Phase	**Operational Phase**
E_{in}	7.5	4.93
E_{NB}	2.57	2.57
E_{out}	0	5.49

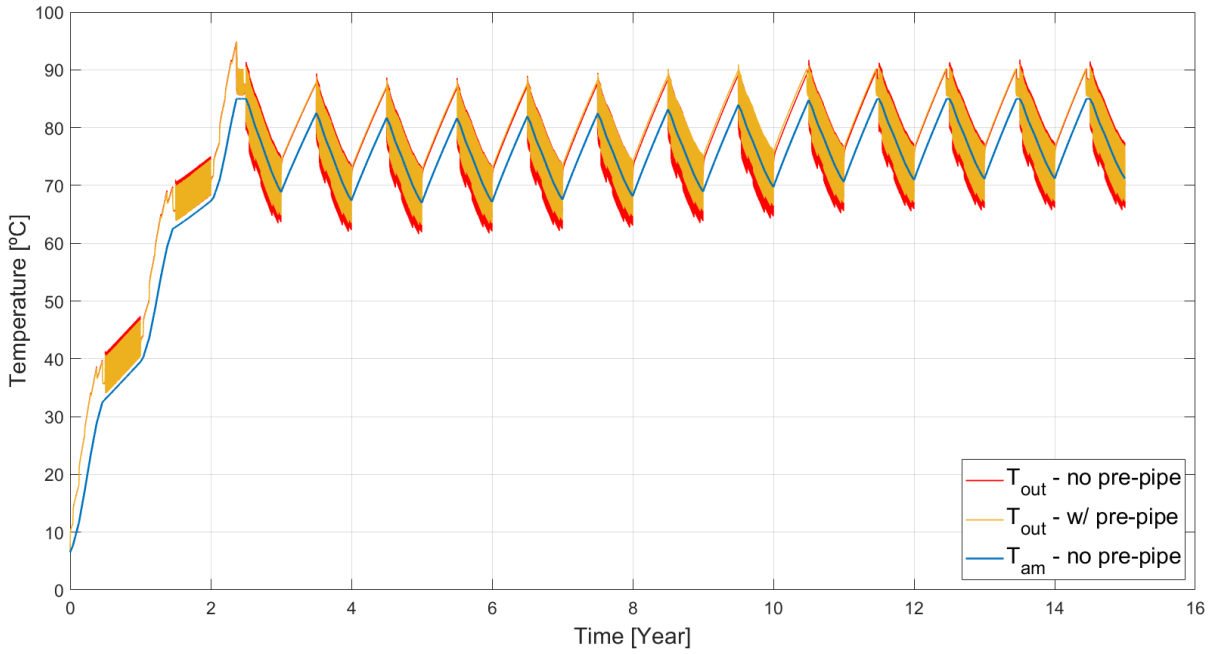

Figure 7.9: Resulting outgoing temperature and average storage temperature for case 1. Simulation load cycle is with nightboosting.

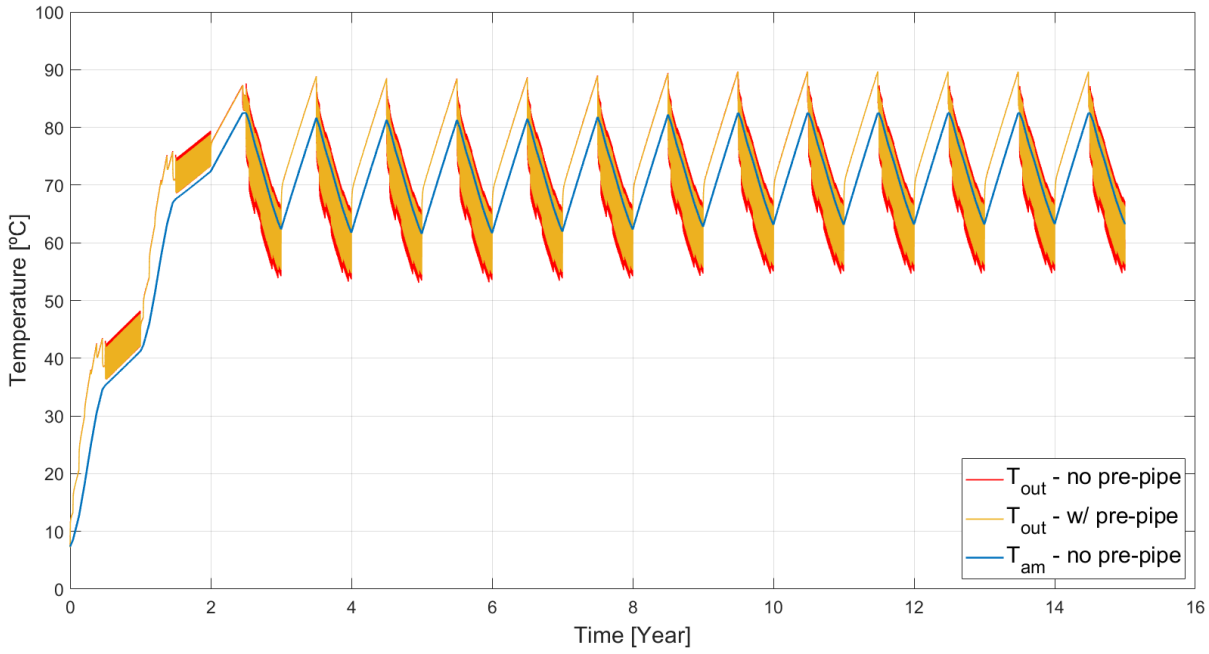

Figure 7.10: Resulting outgoing temperature and average storage temperature for case 2. Simulation load cycle is with nightboosting.

Table 7.5: Injected and extracted annual energy [GWh] for case 2 with nightboosting.

	Preheating Phase	**Operational Phase**
E_{in}	60	44.24
E_{NB}	15.76	15.76
E_{out}	0	53.07

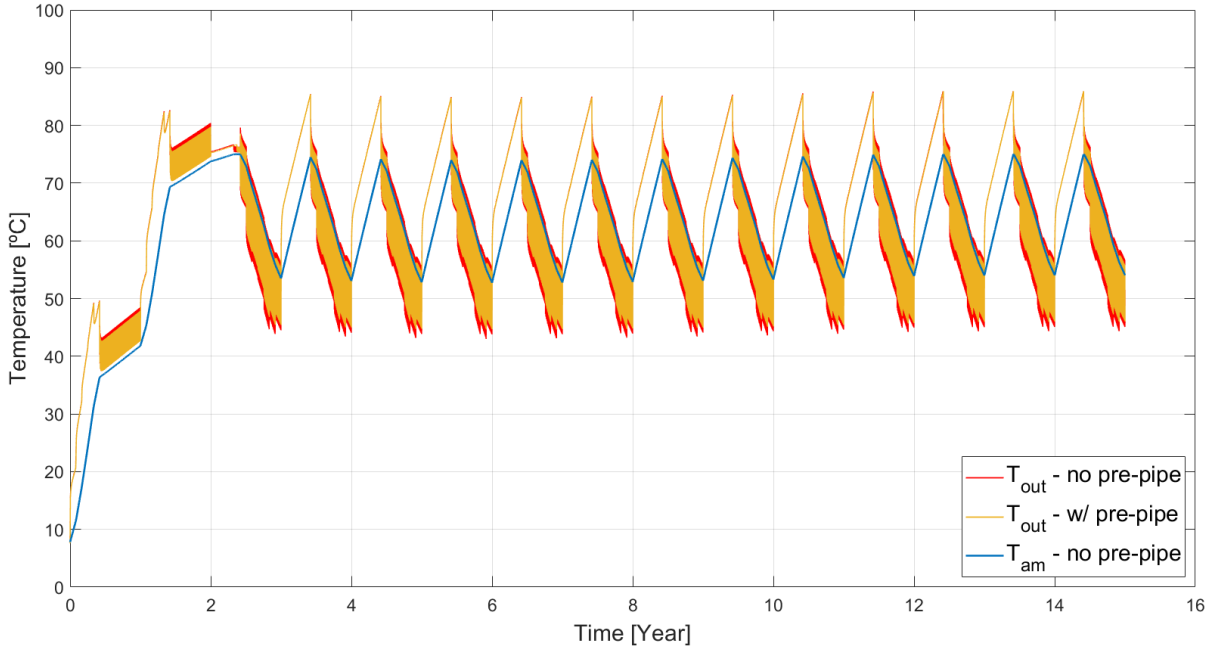

Figure 7.11: Resulting outgoing temperature and average storage temperature for case 2. Simulation load cycle is with nightboosting.

Table 7.6: Injected and extracted annual energy [GWh] for case 3 with nightboosting.

	Preheating Phase	**Operational Phase**
E_{in}	125	94.78
E_{NB}	30.22	30.22
E_{out}	0	115.86

Figure 7.12 shows the development of the annual average storage temperature for cases 1,2 and 3 for with and without nightboosting. The increase as a consequence of nightboosting is substantial in all three cases, but the effect is descending with increasing storage capacity. This is observed by comparing ΔT for each case in table 7.7. It is observed less reduction of ΔT due to nightboosting for increasing storage capacity. The reductions in ΔT due to nightboosting are 43.4%, 28.3% and 24.9% for case 1,2 og 3 respectively.

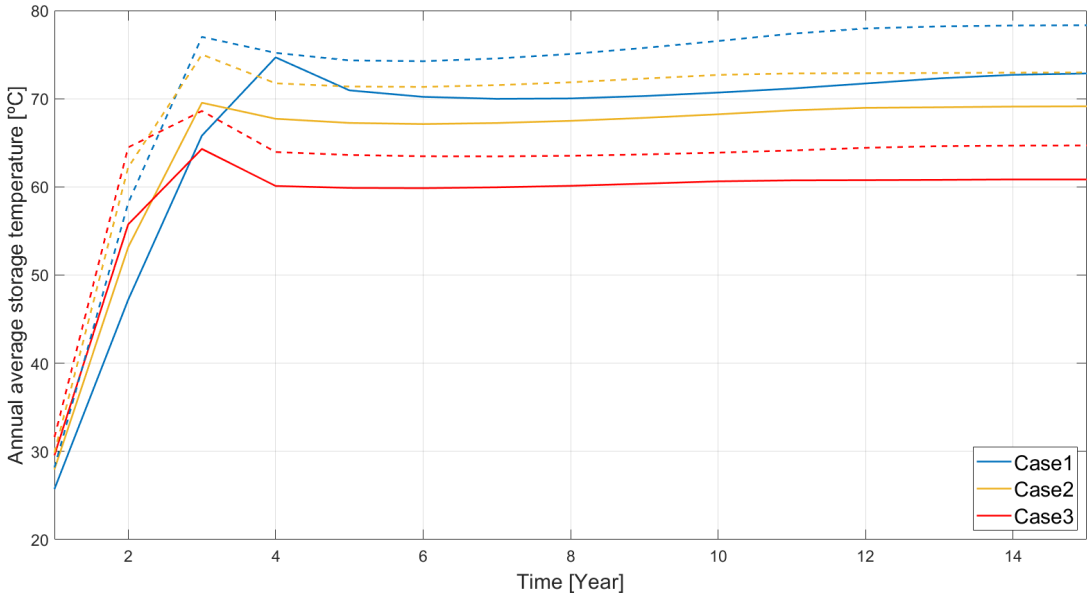

Figure 7.12: Annual average storage temperature for case 1, 2 and 3 with and without night-boosting. Dotted graphs are with nightboosting.

Table 7.7: Average storage temperature specifications during year 15 for case 1, 2 and 3 with and without nightboosting. $\Delta T = T_{am-max}$ - T_{am-min}

Case	$\overline{T_{am}}$ [°C]	**ΔT** [°C]	$\mathbf{T}_{am-max}$ [°C]	$\mathbf{T}_{am-min}$ [°C]
Case 1 - No NB	72.98	24.45	85	60.55
Case 1 - w/ NB	78.33	13.83	85	71.17
Case 2 - No NB	69.14	26.88	82.5	55.62
Case 2 - w/ NB	72.98	19.26	82.5	63.24
Case 3 - No NB	60.84	27.93	75	47.07
Case 3 - w/ NB	64.70	20.98	75	54.02

7.2.3 Heat pump performance

When investigating the performance of the HP installation in each case, the average SCOP, lowest COP and % operation time were analyzed. The average SCOP is the total average value, the lowest COP is the lowest calculated value throughout all discharging seasons, while % operation time represents both the average seasonal and total HP operation time. The heat pump performance results for case 1, 2 and 3 are presented in table 7.8, 7.9 and 7.10 respectively.

Table 7.8: Heat pump overall performance for case 1. Results are without and with nightboosting as well as without and with a pre-pipe. NB = nightboosting, PP = pre-pipe.

Scenario	Average SCOP	Lowest COP	% HP operation time
No NB & no PP	23.84	12.96	37.34
No NB & with PP	23.41	14.11	37.90
With NB & no PP	n/a	n/a	0
With NB & with PP	n/a	n/a	0

Table 7.9: Heat pump overall performance for case 2. Results are without and with nightboosting as well as without and with a pre-pipe. NB = nightboosting, PP = pre-pipe.

Scenario	Average SCOP	Lowest COP	% HP operation time
No NB & no PP	16.87	8.69	58.21
No NB & with PP	17.04	9.46	57.06
With NB & no PP	27.20	16.40	36.00
With NB & with PP	27.95	18.59	31.90

Table 7.10: Heat pump overall performance for case 3. Results are without and with nightboosting as well as without and with a pre-pipe. NB = nightboosting, PP = pre-pipe.

Scenario	Average SCOP	Lowest COP	% HP operation time
No NB & no PP	12.93	6.21	84.49
No NB & with PP	13.20	6.55	83.55
With NB & no PP	16.94	8.76	77.70
With NB & with PP	17.30	9.47	74.46

The results presented in table 7.8, 7.9 and 7.10 show that nightboosting has a substantial effect on the heat pump performance. A difference is also occurring due to the pre-pipe component. Tables 7.8 - 7.10 shows that the effect on the HP performance parameters due to nightboosting is descending from case 1 to 3. For case 1, only the lowest COP value was improved as a consequence of the pre-pipe component. This is thought to be because of the sensitivity of the calculated COP results as the trend is different for case 2 and 3.

The results presented in figure 7.13 and 7.14 will be better understood when viewed in combination with the temperature development of case 3 in figure 7.1. Results without the pre-pipe greatly underestimate the temperature of the outgoing heat carrier fluid during the peak load. This effect is increased with nightboosting which is observed by comparing figure 7.13 and 7.14 during the peak loads. Based on the coherence of the COP during the base load, the difference between results with and without pre-pipe presented in table 7.8 - 7.10 are mainly a result of the difference occurring during peak loads.

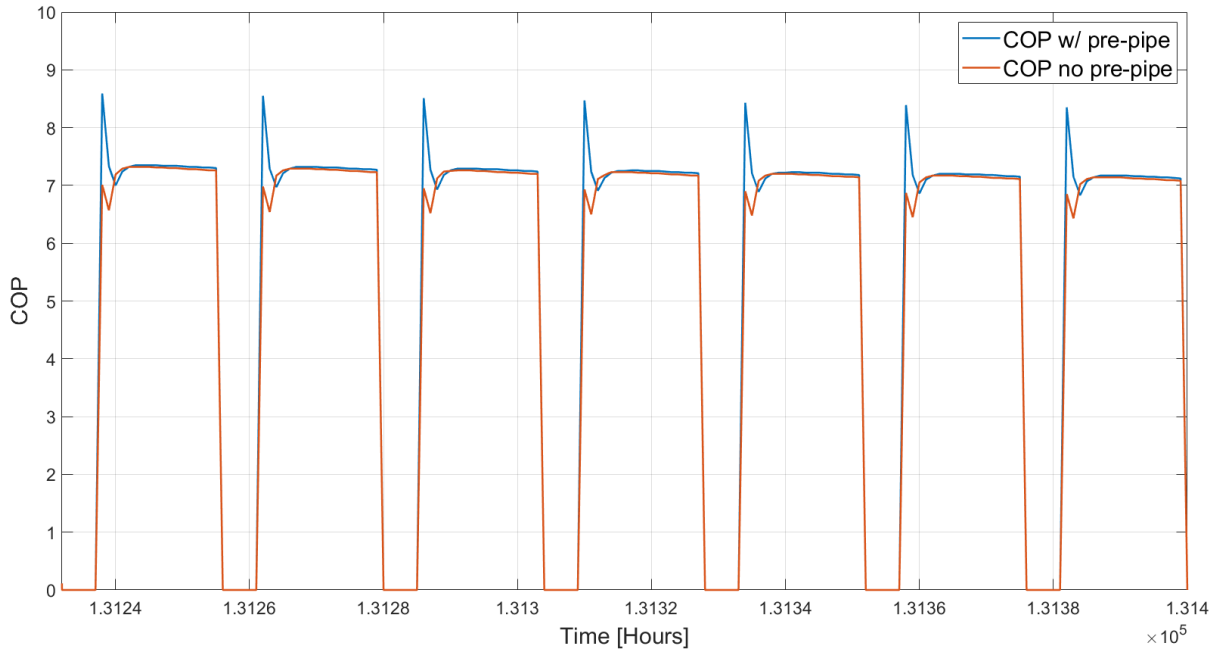

Figure 7.13: Heat pump COP value during the last week of the discharging period in year 15 for case 3 without nightboosting.

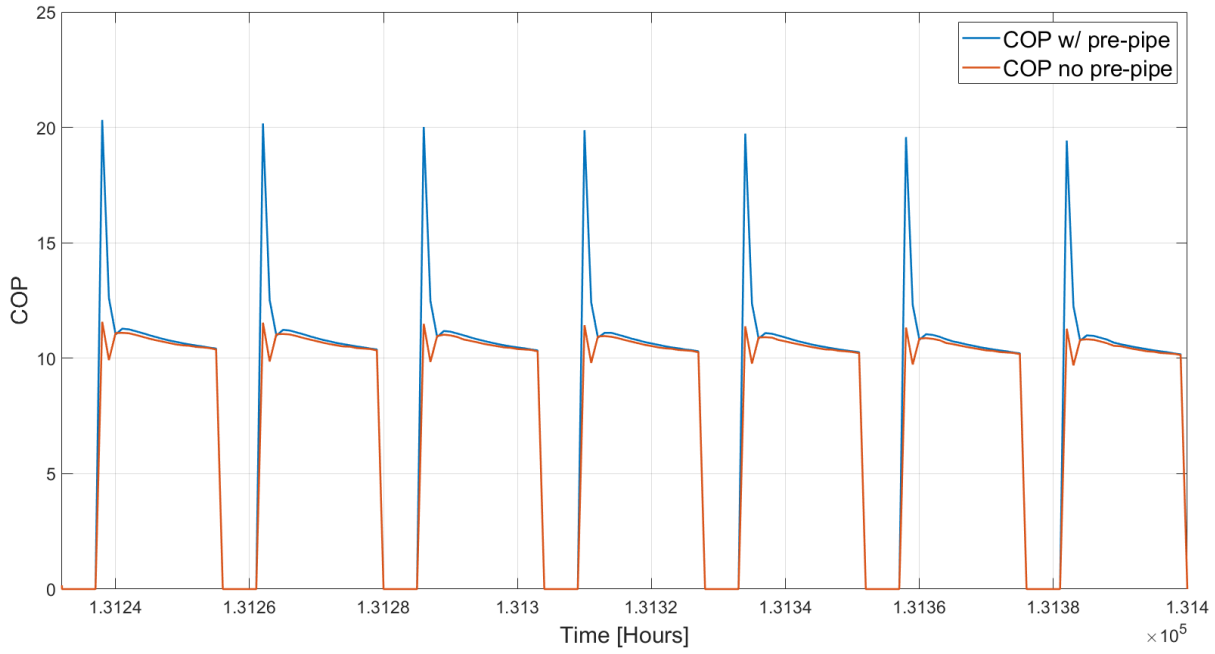

Figure 7.14: Heat pump COP value during the last week of the discharging period in year 15 for case 3 with nightboosting.

7.3 Sensitivity Analysis - Case 2

Parameters investigated in the sensitivity analysis are top surface insulation, thermal stratification, header depth and ground conductivity. Their influence on the average storage temperature development will be the main focus of the analysis. The results presented are therefore only for simulations without the pre-pipe component. This is because the deviation between T_{am} for results with and without pre-pipe was observed to be minimal in the pre-pipe analysis. The load cycle without nightboosting is used for the simulations performed in the sensitivity analysis.

7.3.1 Top surface insulation

Different top surface insulation scenarios for case 2 are presented in figure 7.15. The figure shows that the annual average storage temperature will be elevated by insulating the top surface. The load cycle assumes a BTES efficiency of approximately 0.88, which can only be achieved with a lower annual average storage temperature for the non-insulated and 0.1m insulated scenario. The temperature difference between the annual average storage temperature in year 15 between the perfectly and non-insulated scenario is measured to be 15.60K. Figure 7.15 also presents that the effect of the top surface insulation declines with increasing insulation thickness. It is important to point out that the insulation effect and thickness of the top surface insulation are very dependant on the thermal conductivity of the insulation material.

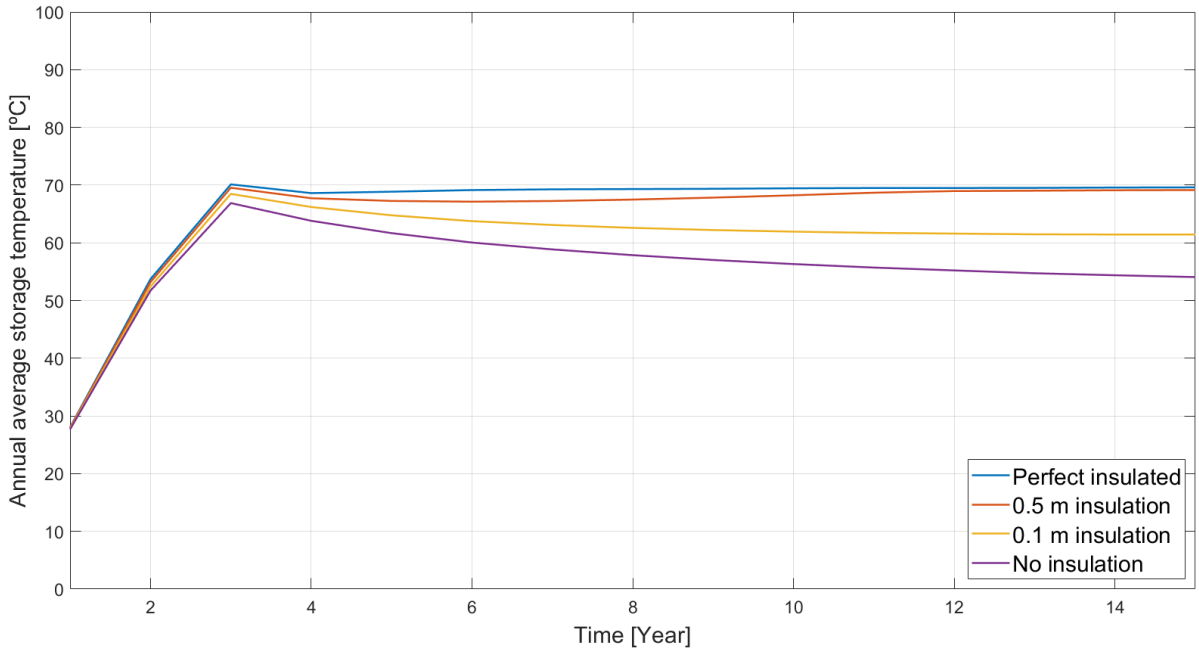

Figure 7.15: Annual average storage temperature development for different top surface insulation scenarios. Horizontal $D_i/H = 0.1$ and Insulation conductivity = 0.11 W/mK

An associated parameter with the top surface insulation is the insulation height fraction (D_i/H). The extra insulation D_i, can either be placed horizontally or vertically at the edge of the HT-BTES. These two placements were simulated with D_i/H = 0.1 and compared with results where $D_i = 0$. The insulation thickness was 0.5m in all simulations. The results showed that the insulation height fraction had a minimal effect on the development of the average annual storage temperature. The maximum increase in T_{am} was 1% and was achieved with vertical placement. The horizontal placement achieved a maximum increase in T_{am} of 0.75%.

7.3.2 Thermal stratification

The effect of thermal stratification inside the storage was analyzed by varying the number of boreholes connected in series. The resulting annual average storage temperature development for each scenario is plotted in figure 7.16. The results show that the effect of thermal stratification in case 2 is minimal and that the same steady-state annual T_{am} is reached. Results for 9 boreholes connected in series are plotted on top of the results for 3 boreholes in series since they are close to equal. The effect of thermal stratification is therefore most notable with 5 boreholes connected in series for case 2.

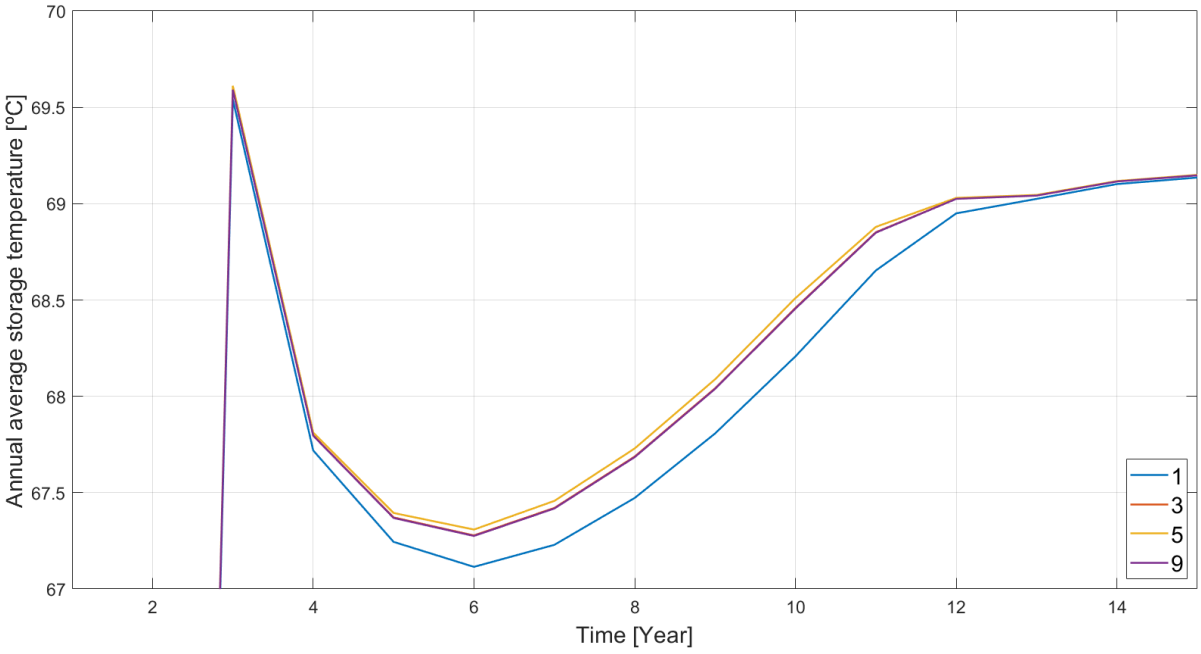

Figure 7.16: Annual average storage temperature development for different number of boreholes in series.

Another consequence of connecting boreholes in series is that the mass flow through each BHE increases. The effect of increasing mass flow is described in subsection 5.3.5 and shows that the required temperature difference between T_{in} and T_{out} is reduced. This will consequently reduce T_{in} and increase T_{out}. T_{out} were therefore analyzed for 1 borehole and 5 boreholes connected in series. This was done by calculating the average outlet temperature during the discharging seasons. The most substantial difference was calculated during the discharging season in year six and found to be 0.46K. After this, it was reduced towards a constant value of 0.20K. The difference of 0.46K was observed when the annual average storage temperature deviated the most from the steady-state value.

7.3.3 Header depth

Header depth is the depth below the surface where the top of the U-tube BHE is located. The depth gives an insulating layer in the soil or rock with a thickness equal to the header depth. Different header depths are simulated for case 2 and the results are shown in figure 7.17. The results show that increasing header depth decreases the time before case 2 reaches the steady-state value of the annual average storage temperature. Increasing header depth also slightly increases the steady-state annual average storage temperature, which is observed in year 15 in figure 7.17. The results also show that the effect of the header depth decreases as header depth increases.

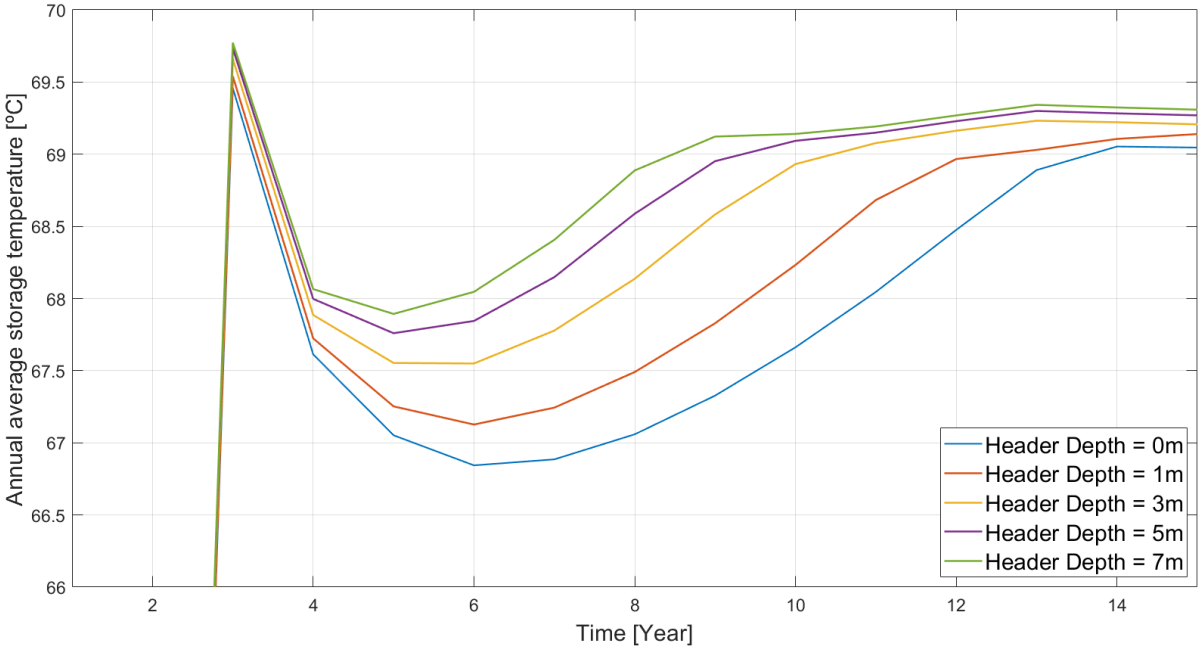

Figure 7.17: Annual average storage temperature in case 2 for different header depths.

7.3.4 Ground conductivity

The conductivity of the ground is an important parameter as it directly impacts the resistance of the ground. A high value for ground conductivity results in low ground resistance and low ground conductivity results in high ground resistance. Figure 7.18 shows the effect on the annual average storage temperature. The results show that the steady-state temperature is slightly higher and achieved earlier with lower ground conductivity. This is a result of lower heat loss to the surrounding ground for lower ground conductivity values.

The results in figure 7.19 shows that the outgoing temperature from the HT-BTES is higher for increasing ground conductivity values. T_{out} is reasonably higher, although the annual average storage temperature is slightly lower for higher ground conductivity values. Higher values for T_{out} is a result of lower ground thermal resistance which is a direct consequence of higher ground thermal conductivity values.

Another consequence of lower ground conductivity values, is that the heat carrier temperature has to be higher during charging in order to transfer the same amount of heat to the HT-BTES (see fig.7.19). This is also a consequence of higher ground thermal resistance. The increased required heat carrier temperature could become a limitation due to the temperature restrictions in the BHE material. The limitation could consequently result in lower maximum average storage temperature for lower ground conductivity values.

Figure 7.18 and 7.19 also show that the impact of increasing ground conductivity is declining for both T_{am} and T_{out}. This is because the thermal resistance in the ground is of less significance in the total thermal resistance when the ground conductivity increases, and the ground thermal resistance consequently decreases. The difference between T_{am} and T_{out} for varying ground conductivity is therefore most substantial between results for $k_g = 2$ W/mK and $k_g = 3$ W/mK.

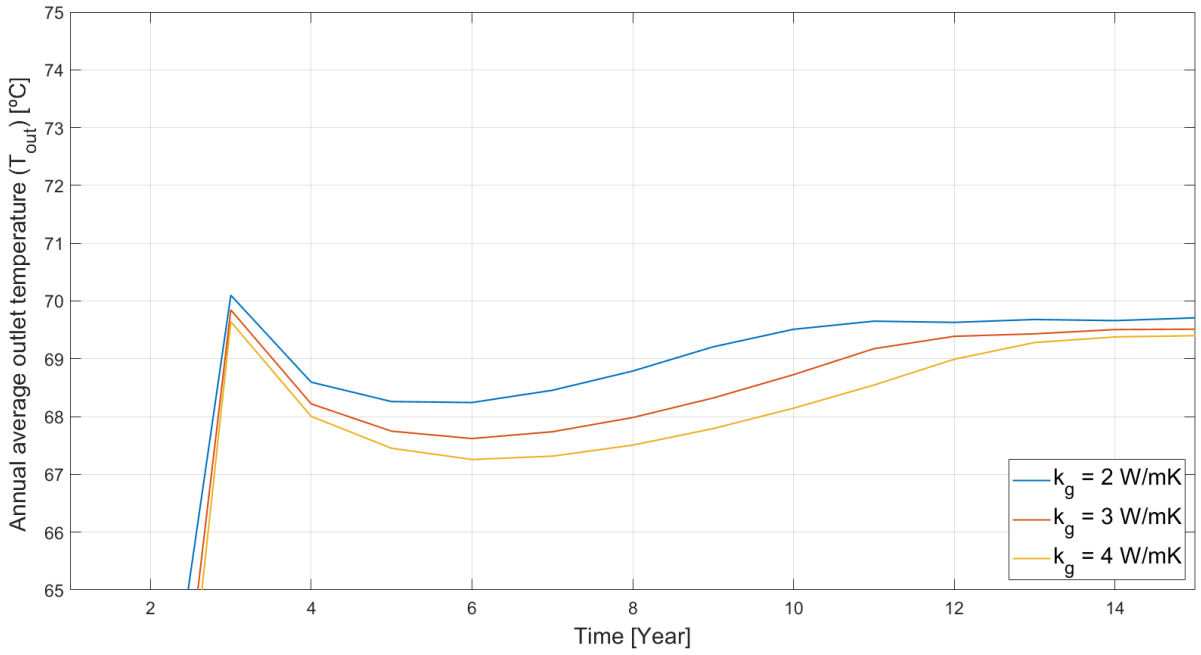

Figure 7.18: Annual average storage temperature in case 2 for different ground conductivity.

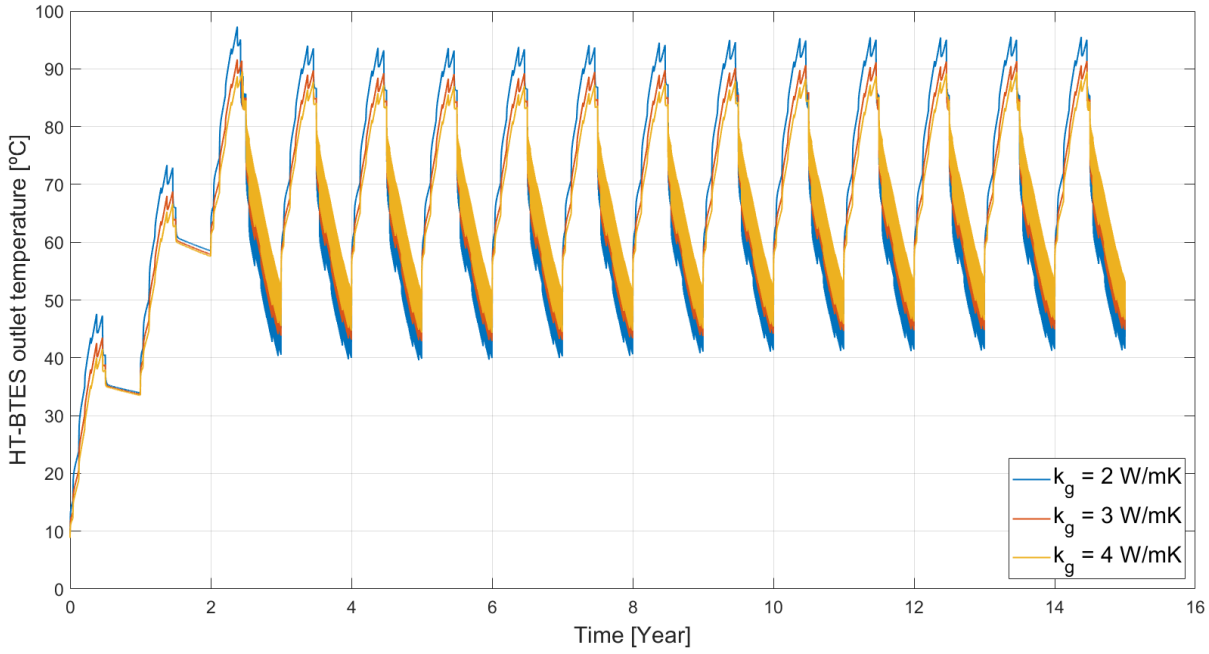

Figure 7.19: HT-BTES outlet temperature development for different ground conductivity.

Chapter 8

Discussion

The non-grouted MATLAB model developed by Holmberg (2016) was slightly modified in order to be used for the evaluation of a HT-borehole. The modified model was only validated by comparing low-temperature results with the unmodified model. This causes some uncertainty in the results presented in the thermal analysis chapter. An improvement in the validity of the results would therefore be to compare results from the modified MATLAB model with measured data from a TRT. The results in the thermal analysis were simulated over a maximum time period of one week in order to avoid the effect of thermal interaction between adjacent boreholes. The time before thermal interaction will vary, depending on local conditions and the design of the HT-BTES. Simulations results with only one HT-borehole over a maximum time period of one week should therefore not be viewed as conclusive, but as guidelines.

The results from the thermal analysis show that a notable increase in T_{out} is achieved due to nightboosting. The lasting temperature effect is however most significant for the first peak load during the 24-hour load cycle. This indicates that nightboosting has a smaller temperature effect on the heat carrier fluid during the second daily peak load. In the nightboosting evaluation, the value of the charging rate (W/m) shows to have the most significant impact on the heat carrier temperature. The value of the nightboosting rates used in the thermal analysis is however only assumed, and will in reality, depend on the amount of available heat. For the TRNSYS model, the type 31 pipe was used to simulate the borehole thermal capacity. This component was used due to its availability and the results could possibly be further improved with the recommended pipe - type 604. The calculated and evaluated pre-pipe diameters in this thesis should not be directly replicated. New diameters should be calculated and further evaluated for the individual analysis. The results should preferably be evaluated with measured data from a TRT.

The design of the three cases in the case analysis is based on certain assumptions in order to calculate the required HT-BTES parameters. Other design parameters are also based on empirical data presented in the graphical summary. The designs are therefore not optimized and are base cases that can be further optimized for each of the three

HT-BTES cases. The load cycles are created based on the monthly information acquired in the feasibility study in chapter four. The daily load cycles are therefore made equal over the duration of one month, and daily variations in the heating load are consequently not accounted for. This was however seen as adequate for the case analysis since daily variations were not of main interest.

Simplifications were made for the heat pump model and modeling of the LT-DH network in the case analysis simulation models. Part load operation and the practical implications of variable source temperature to the heat pump were therefore not accounted for. The efficiency of the heat exchangers and heat loss in the LT-DH network is also not accounted for. These assumptions idealize the discharging of the HT-BTES, and the real heating loads could therefore be higher. The results presented for the heat pump performance should be viewed in terms of their trend and not exact value due to the assumptions made. The mass flow in the simulation models is assumed to be constant. Mass flow control and variation is therefore an improvement which could enhance the presented results.

The temperature results from the pre-pipe evaluation in the case analysis had a similar temperature development as in the thermal analysis evaluation. The assessment in the case analysis did however show that increasing heat transfer rates q(W/m) and decreasing T_{am} both increased the deviation between results with and without pre-pipe. The impact of increasing storage capacity is however uncertain. The effect of capacity is unsure because no direct comparison was possible to make, and since the same percentage of borehole thermal capacity is accounted for regardless of storage capacity. It is therefore seen as reasonable to assume the influence of increasing storage capacity on the temperature deviation as minimal or not present. The pre-pipe component becomes of less significance when the duration of the heating load increases. However since the time length of nightboosting will be short due to its short-time availability, it is therefore seen as necessary to include the pre-pipe component when analyzing nightboosting. For simulations without nightboosting the peak load duration could be increased or the values re-calculated into daily averaged values. This would decrease the effect of the borehole thermal capacity and consequently make it possible to avoid the pre-pipe component.

Table 6.7 and 6.6 shows that both charging and discharging rates q(W/m) increased with increasing storage capacity. The importance of the fluid to ground thermal resistance will therefore become greater with increasing storage capacity. The same constant fluid to ground thermal resistance is however used in all three cases and could therefore cause some uncertainty in temperature results. Measures to decrease the fluid to ground thermal resistance or the heating rates were not evaluated. Decreasing the heat transfer rates q can be achieved by reducing the borehole spacing or increasing the borehole depth.

These measures would however also increase the drilling cost of the HT-BTES construction. The fluid to ground thermal resistance could also be slightly reduced by using a double U-tube BHE instead of a single. Both of the mentioned changes would result in higher values for T_{out}, which would increase the amount of heat supplied directly to the LT-DH network. The impact of nightboosting is evaluated as significant for both the temperature development of the storage and the heat carrier fluid. The charging rate of 60 W/m is however only assumed, and it is not validated that this rate would be possible. A lower charging rate would have the same trend as observed in the case analysis, but with a reduced impact.

The sensitivity analysis of case 2 shows that some of the investigated parameters have a minimal effect on the heat loss and T_{am} of the HT-BTES in case 2. It is however essential to specify that case 2 has a relatively high storage capacity of 60 GWh, which is significantly higher than for existing HT-BTES projects. With a lower storage capacity, the impact of the steady-state heat loss becomes of more significance. It can therefore be thought that heat loss reduction measures will have a more significant impact on HT-BTES with smaller storage capacities. The effect of the ground thermal conductivity is notable for case 2, and points out the importance of a geological investigation of the construction site. Groundwater flow was assumed not to be present in the simulations performed, which is an assumption beneficial for the heat loss of the storage. Large groundwater flows could significantly impact the heat loss and consequently, also the performance of the HT-BTES.

An evaluation where heat is delivered to the existing DH-network was not performed. The need for a heat pump or other auxiliary heater would then be present for all three cases, both with and without nightboosting. Nightboosting is however thought to give the same resulting trends in terms of temperature development and heat pump performance, if heat is delivered back to the existing DH network. For heat delivery to a LT-DH network, nightboosting removed the need for a heat pump in case 1 and reduced the operation time in case 2 and 3. A consequence of reduced operation time is that the payback time of the heat pump installation would increase. The payback time increase could be reduced by having other appliances for the heat pump in addition to delivering heat to the LT-DH network. This was however not evaluated in the case analysis since economical aspects were not of focus in this master thesis.

Chapter 9

Conclusion

The goal of this master thesis was to gather knowledge regarding the potential of HT-BTES systems, analyze the thermal process in HT-boreholes and to apply this in a HT-BTES case analysis. Knowledge was obtained through theory, empirical data and a feasibility study targeting waste-to-energy DH plants. A further understanding was acquired by analyzing the thermal process in non-grouted HT-boreholes. This knowledge was then applied in a case analysis evaluating three HT-BTES cases with a storage capacity of 7.5 GWh, 60 GWh and 125 GWh, respectively.

The comparison between design and measured values showed considerable deviations in both BTES efficiency and extracted energy in the graphical summary on existing HT-BTES projects. Measured BTES efficiency was in average 17.42% lower and extracted energy 25.66%, both without including the HT-BTES in Emmaboda. The summary highlights the importance of monitoring, evaluating and altering the operation of HT-BTES systems, as well as the significance of reliable operation. The feasibility study found a total excess heat production of 560 GWh/year, which can be supplied at a temperature of at least 95°C. The potential for HT-BTES in the waste-to-energy DH sector in Norway is therefore present.

The thermal analysis on HT-boreholes found a significant potential with the use of nightboosting as a dynamic operational strategy. Nightboosting was seen possible from 00.00 - 06.00 due to low heating demand at this time of day. With a charging rate of 80 W/m the temperature of the outgoing heat carrier fluid was 10K higher after 150 hours and 4.32K after the following peak load. The results in the thermal analysis showed that the effect of nightboosting declined over the daily load cycle and therefore was most profound for the morning peak load (06.00 - 08.00). The annual impact of nightboosting could not be concluded with based on the results from the thermal analysis.

The effect of the borehole thermal capacity was found to be of importance during short-time charging and discharging. The thermal capacity of the borehole was therefore accounted for in TRNSYS by a pre-pipe component. The best resemblance to the results

from the MATLAB model was achieved with a pre-pipe diameter that consequently accounted for 50% of the borehole thermal capacity. A further pre-pipe investigation was performed in the case analysis to highlight possible annual effects. The pre-pipe results in the case analysis found deviations in the order of 5-22% for T_{out} and only small deviations up to 0.5% for T_{am}. Differences increased with increasing heat transfer rates q(W/m) and declining average storage temperature. Based on the results from both the thermal analysis and case analysis evaluation the borehole thermal capacity should be accounted for when short-time charging or discharging loads are present.

Increasing storage capacity was found to have a notable impact on the HT-BTES systems in the case analysis. Heating rates q (W/m) increased with increasing storage capacity which consequently resulted in maximum T_{am} of 85°C, 82.5°C and 75°C for case 1, 2 and 3. None of the HT-BTES cases were able to supply the LT-DH network directly for the entire heating season when operating without nightboosting. Operation with nightboosting resulted in a significant impact on T_{am} and T_{out}. The temperature difference between the maximum and minimum average storage temperature was decreased with 43.4%, 28.3% and 24.9% for cases 1, 2 and 3. Case 1 was therefore able to supply the entire heating demand directly, while the average SCOP for cases 2 and 3 increased by 64% and 31% respectively, for the results with pre-pipe. The effect of nightboosting can therefore be concluded as significant for all three cases, but with decreasing effect for increasing storage capacity.

In the sensitivity analysis of case 2, top surface insulation and ground thermal conductivity were found to have the most significant impact on the HT-BTES. By removing the 0.5m of insulation on the top surface, the annual average storage temperature declined with 15.44K. Lower ground thermal conductivity decreased heat loss but also increased the ground thermal resistance. A greater temperature difference between the heat carrier fluid and ground temperature is therefore required, which also results in a lower outgoing temperature during discharging. The effect of thermal stratification and header depth was present, but not evaluated significant for the performance of the HT-BTES system in case 2.

A potential for HT-BTES systems was found in the waste-to-energy DH sector in Norway, and simulation shows that storage temperatures up to 85°C can be achieved. The annual average storage temperature can also be further increased with a more dynamic operation of the HT-BTES. Assumptions and simplifications are made throughout the design of the HT-BTES cases and in the simulation models. The presented results should therefore be viewed as guidelines and reviewed with caution. The results still underline the potential and trends of HT-BTES system solutions.

Chapter 10

Future Work

In the feasibility study in this master thesis, excess heat production was in focus and requested by the relevant district heating plants. A continuation of this feasibility study should be to acquire more information from the district heating plants regarding the relevance of a LT-DH network and what other desired system solutions might be. The feasibility study should also address nightboosting and gather information regarding the amount of available energy and consequently the value of possible nightboosting rates.

Future work should also be to establish cooperation with one or more of the relevant district heating plants. The partnership could enable more detailed and actual measured input data to be used in the design of a HT-BTES system solution. This data would result in a more realistic and practical approach in a case analysis. A more practical approach could also encourage a higher interest in HT-BTES system solutions for the district heating sector.

The simulation models developed in TRNSYS for this master thesis were mostly focused on the HT-BTES system. Future work with the simulation model should therefore focus on improving both the heat pump model and the modeling of the district heating network. This improvement would also increase the possibility of analyzing more data within the total system solution. Depending on the necessity of a pre-pipe component other options than the type31 pipe should also be evaluated.

In this master thesis, three HT-BTES base cases are analyzed. All three cases are a base case design and not an optimized design. If more realistic data can be acquired and with an improved simulation model, a focus on optimization of the HT-BTES design based on specific key performance indicators should be performed. A more in depth sensitivity analysis on nightboosting and dynamic operation of a HT-BTES is also of interest to acquire more information and knowledge on the subject. The focus of this master thesis was mainly technical. An economic evaluation is therefore also suggested as future work in order to evaluate and present key economic aspects in the realization of a HT-BTES system solution.

Appendix A

Additional graphs

A.1 Additional graphs litterature review

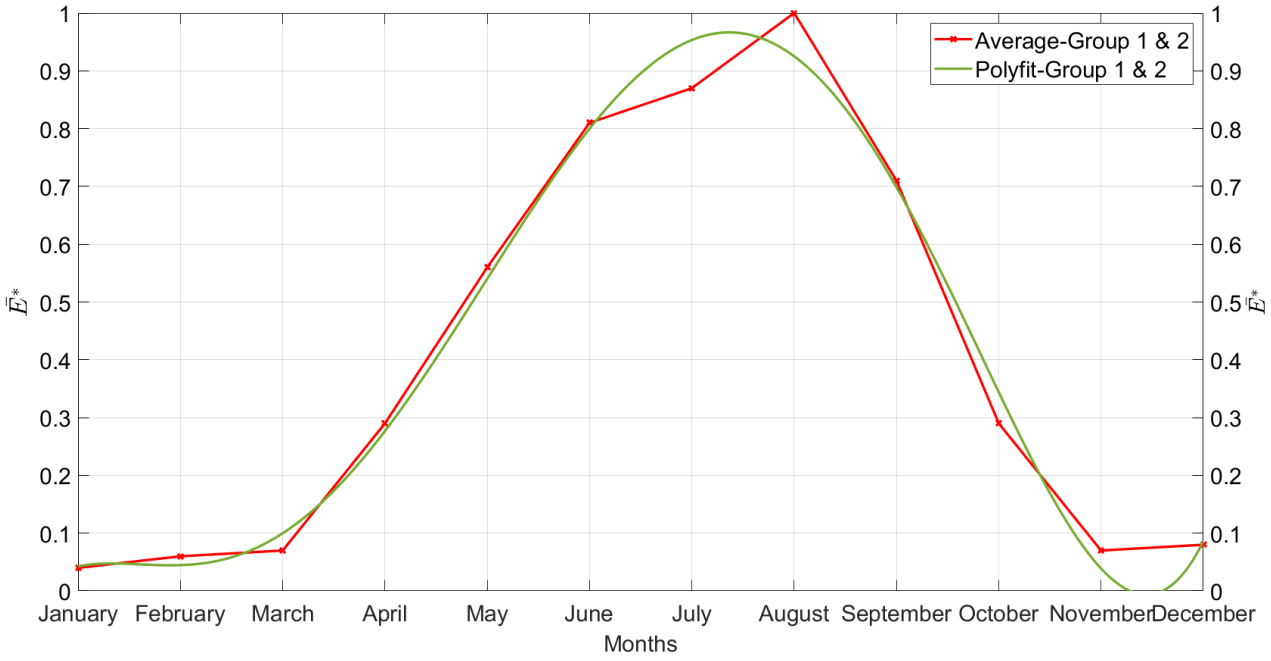

Figure A.1: Polynomial fitted curve and respective plot of the average normalized monthly surplus heat production values for all DH plants

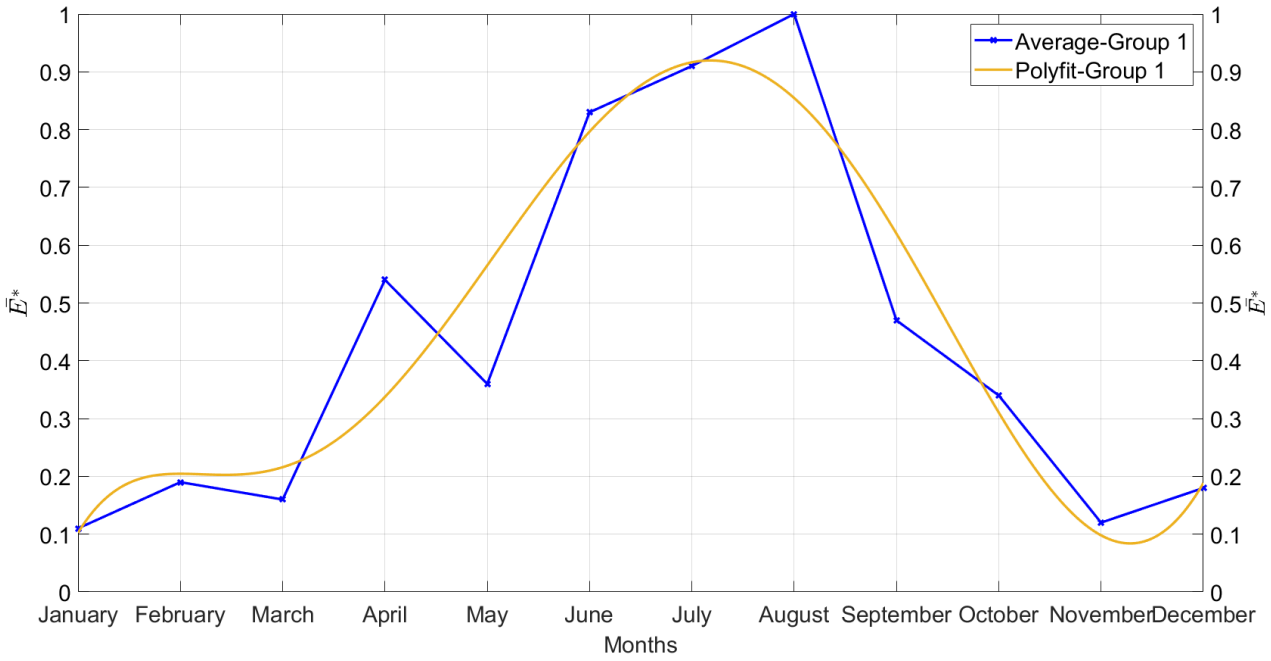

Figure A.2: Polynomial fitted curve and respective plot of the average normalized monthly surplus heat production values for Group 1 DH plants

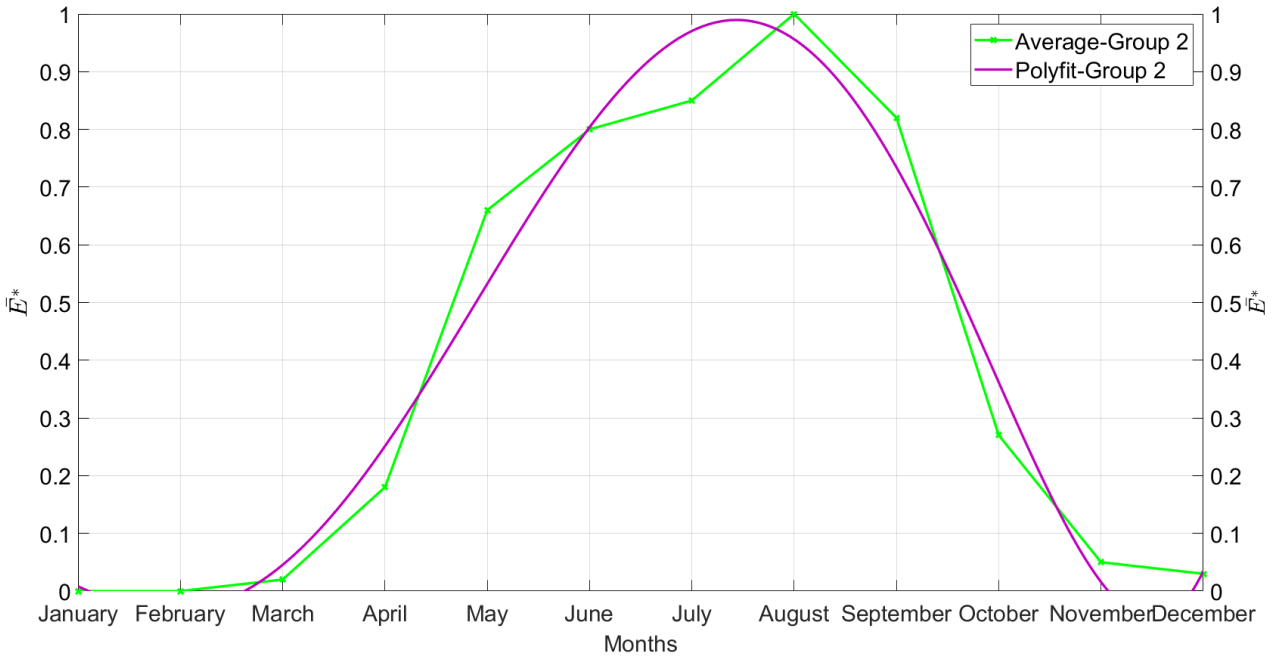

Figure A.3: Polynomial fitted curve and respective plot of the average normalized monthly surplus heat production values for Group 2 DH plants

Bibliography

Bertram, E. (2015). "Heat pump systems with vertical ground heat exchangers and uncovered solar thermal collectors". PhD thesis. Hannover: Gottfried Wilhelm Leibniz Universität Hannover.

Brand, M. et al. (2014). *Heating and Domestic hot water Systems in Buildings Supplied by low-Temperature District heating*. Technical University of Denmark, Department of Civil Engineering.

CoolPack (1999). *CoolPack–Simulation tools for refrigeration systems*.

Dalla-Rosa, A. et al. (2014). *Annex X Final report: Toward 4th Generation District Heating: Experience and Potential of Low-Temperature District Heating*.

Gadd, H. and Werner, S. (2014). "Achieving low return temperatures from district heating substations". In: *Applied energy* 136, pp. 59–67.

Gehlin, S. (2002). "Thermal response test: method development and evaluation". PhD thesis. Luleå tekniska universitet.

— (2016). "Borehole thermal energy storage". In: *Advances in Ground-Source Heat Pump Systems*. Elsevier, pp. 295–327.

Gehlin, S., Spitler, J., and Hellström, G. (2016). "Deep boreholes for ground source heat pump systems—scandinavian experience and future prospects". In: *ASHRAE Winter Meeting, Orlando, Florida*, pp. 23–27.

Hellström, G. (1989). "Duct ground heat storage model, manual for computer code". In: *Department of Mathematical Physics, University of Lund, Sweden*.

— (1991). *Ground heat storage: Thermal analyses of duct storage systems*.

Holmberg, H. (2016). "Transient Heat Transfer in Boreholes with Application to Non-Grouted Borehole Heat Exchangers and Closed Loop Engineered Geothermal Systems". PhD thesis. Norwegian University of Science and Technology (NTNU).

Lund, H. et al. (2014). "4th Generation District Heating (4GDH): Integrating smart thermal grids into future sustainable energy systems". In: *Energy* 68, pp. 1–11.

Lundh, M. and Dalenbäck, J. (2008). "Swedish solar heated residential area with seasonal storage in rock: Initial evaluation". In: *Renewable Energy* 33.4, pp. 703–711.

Malmberg, M. (2017). *Transient modeling of a high temperature borehole thermal energy storage coupled with a combined heat and power plant*.

Malmberg, M. et al. (2018). *High temperature borehole thermal energy storage - A case study*.

Mesquita, L. et al. (2017). "Drake Landing Solar Community: 10 years of operation". In: *ISES Solar World Congress*.

Miedaner, O., Mangold, D., and Sørensen, P. (2015). "Borehole thermal energy storage systems in Germany and Denmark-Construction and operation experiences". In: *The 13th International Conference on Energy Storage*, pp. 1–8.

Miljødirektoratet (2019). *Deponering av avfall*. URL: https://miljostatus.miljodirektoratet.no/tema/avfall/avfallshandtering/deponering-av-avfall/ (visited on Feb. 3, 2020).

NGU (1858a). *Nasjonal berggrunnsdatabase*. URL: http://geo.ngu.no/kart/berggrunn_mobil/ (visited on Mar. 4, 2020).

— (1858b). *Nasjonal Løsmassedatabase*. URL: http://geo.ngu.no/kart/losmasse/ (visited on Mar. 4, 2020).

Nord, N. et al. (2018). "Challenges and potentials for low-temperature district heating implementation in Norway". In: *Energy* 151, pp. 889–902.

Nordell, B. (1994). "Borehole heat store design optimization". PhD thesis. Luleå tekniska universitet.

Nordell, B. et al. (2016). *Long-term Long Term Evaluation of Operation and Design of the Emmaboda BTES.: Operation and Experiences 2010-2015*. Luleå tekniska universitet.

Norsk Fjernvarme (2019a). *Fjernvarme - Nasjonale tall*. URL: https://www.fjernkontrollen.no/ (visited on Apr. 5, 2020).

— (2019b). *Om energikildene*. URL: https://www.fjernkontrollen.no/content/om-energikildene/ (visited on Mar. 22, 2020).

Nussbicker, J., Heidemann, W., and Mueller-Steinhagen, H. (2006). "Monitoring results and operational experiences for a central solar district heating system with borehole thermal energy store in Neckarsulm (Germany)". In: *10th International Conference on Thermal Energy Storage, Richard Stockton College of New Jersey*. Vol. 31. 02.06.

Olsen, P. et al. (2014). "Guidelines for low-temperature district heating". In: *EUDP–DEA. Denmark*.

Pachauri, R. et al. (2014). *Climate change 2014: synthesis report. Contribution of Working Groups I, II and III to the fifth assessment report of the Intergovernmental Panel on Climate Change*. Ipcc.

Pärisch, P. et al. (2015). "Short-term experiments with borehole heat exchangers and model validation in TRNSYS". In: *Renewable Energy* 74, pp. 471–477.

Plan Energi (2013). *Boreholes in Brædstrup*. URL: http://planenergi.dk/wp-content/uploads/2018/05/15-10496-Slutrapport-Boreholes-in-Br%5C%C3%5C%A6dstrup.pdf (visited on Feb. 10, 2020).

Reuss, M. (2015). "The use of borehole thermal energy storage (BTES) systems". In: *Advances in Thermal Energy Storage Systems*. Elsevier, pp. 117–147.

Schmidt, F. (2019). *Large scale heat storage*.

Sibbitt, B. and McClenahan, D. (2014). "Seasonal Borehole Thermal Energy Storage – Guidelines for design & construction". In: *IEA-SHC TECH SHEET 45.B.3.1*, pp. 1–15.

Skarphagen, H. et al. (2019). "Design Considerations for Borehole Thermal Energy Storage (BTES): A Review with Emphasis on Convective Heat Transfer". In: *Geofluids* 2019.

SSB (2019). *Avfallsregnskapet*. URL: https://www.ssb.no/natur-og-miljo/statistikker/avfregno (visited on Feb. 3, 2020).

Standard Norge (2014). *Beregning av bygningers energiytelse - Metode og data*. NS 3031:2014.

Stene, J. (2019). *Lecture slides from TEP4246 - Working Fluids*.

Thorén, Å. (2016). *Practical evaluation of borehole heat exchanger models in TRNSYS*.

TRNSYS (2020a). *TRNSYS*. URL: http://www.trnsys.com/ (visited on Apr. 20, 2020).

— (2020b). *TRNSYS TESS-Libraries*. URL: http://www.trnsys.com/tess-libraries/ (visited on Apr. 20, 2020).

Underground Energy (2009). *BTES – Borehole Thermal Energy Storage*. URL: https://undergroundenergy.com/our-technology/btes/#how-does-btes-work (visited on Jan. 26, 2020).

Fredrik Schmidt

Large scale heat storage for district heating

NTNU
Norwegian University of
Science and Technology